A spatially-resolved transcriptional atlas of the murine dorsal pons at single-cell resolution

Stefano Nardone[1,2], Roberto De Luca[3,#], Antonino Zito[4,a,b,#], Nataliya Klymko[5,#], Dimitris Nicoloutsopoulos[6], Oren Amsalem[1], Cory Brannigan[7], Jon M. Resch[8,9], Christopher L. Jacobs[1,2], Deepti Pant[1], Molly Veregge[1], Harini Srinivasan[1,2], Ryan M. Grippo[1], Zongfang Yang[1], Mark L. Zeidel[5], Mark L. Andermann[1], Kenneth D. Harris[6], Linus T. Tsai[1,2], Elda Arrigoni[3], Anne M. J. Verstegen[5,##,$], Clifford B. Saper[3,##,$], Bradford B. Lowell[1,##,$]

[1]Department of Medicine, Division of Endocrinology, Diabetes and Metabolism, Beth Israel Deaconess Medical Center and Harvard Medical School, Boston, MA, USA.
[2]Broad Institute of MIT and Harvard, Cambridge, MA, USA.
[3]Department of Neurology, Division of Sleep Medicine, Beth Israel Deaconess Medical Center and Harvard Medical School, Boston, MA, 02215, USA.
[4]Department of Twin Research & Genetic Epidemiology, King's College London, London, UK.
[5]Division of Nephrology, Department of Medicine, Beth Israel Deaconess Medical Center, Harvard Medical School, 330 Brookline Ave., Boston, MA 02215, USA.
[6]UCL Queen Square Institute of Neurology, University College London, London, UK.
[7]HEAVY.AI, 100 Montgomery St Fl 5, San Francisco, California, 94104, USA.
[8] Department of Neuroscience and Pharmacology, University of Iowa, Iowa City, IA, USA.
[9]Fraternal Order of Eagles Diabetes Research Center. University of Iowa Carver College of Medicine, Iowa City, IA 52242.

[#]Contributed equally.
[##]Contributed equally.
[$]Corresponding author.
Current address: [a]Department of Molecular Biology, Massachusetts General Hospital, Boston, MA, USA. [b]Department of Genetics, The Blavatnik Institute, Harvard Medical School, Boston, MA, USA.

ABSTRACT

The “dorsal pons”, or “dorsal pontine tegmentum” (dPnTg), is part of the brainstem. It is a complex, densely packed region whose nuclei are involved in regulating many vital functions. Notable among them are the parabrachial nucleus, the Kölliker Fuse, the Barrington nucleus, the locus coeruleus, and the dorsal, laterodorsal, and ventral tegmental nuclei. In this study, we applied single-nucleus RNA-seq (snRNA-seq) to resolve neuronal subtypes based on their unique transcriptional profiles and then used multiplexed error robust fluorescence in situ hybridization (MERFISH) to map them spatially. We sampled ~1 million cells across the dPnTg and defined the spatial distribution of over 120 neuronal subtypes. Our analysis identified an unpredicted high transcriptional diversity in this region and pinpointed many neuronal subtypes' unique marker genes. We also demonstrated that many neuronal subtypes are transcriptionally similar between humans and mice, enhancing this study's translational value. Finally, we developed a freely accessible, GPU and CPU-powered dashboard (http://harvard.heavy.ai:6273/) that combines interactive visual analytics and hardware-accelerated SQL into a data science framework to allow the scientific community to query and gain insights into the data.

INTRODUCTION

The pons consists of two main divisions: the “pontine tegmentum”, which represents its dorsal part, and the “basis pontis”, which is its ventral part. This study focuses on the dorsal portion of the pontine tegmentum (dPnTg). The dPnTg plays a pivotal role in the functioning of the autonomic nervous system, but it also represents a strategic hub for integrating many vital processes. It harbors many anatomically-defined subnuclei (Table 1) that perform a wide range of functions, including the PB and pre-LC, which have been implicated in receiving ascending visceral sensory and pain inputs from the spinal cord and medulla, and integrating them with forebrain cognitive, arousal, and emotional inputs to direct behavior, autonomic, and endocrine functions. In addition, specific neuronal populations residing in this area have been reported to be involved in respiration[1,2], arousal[3,4,5] sleep-wake regulation[6], pain[7,8], reward processing and reinforcement[9,10,11], movement[12,13], memory formation[14,] feeding[15,16], micturition[17,18], aversive behaviors[19], thermoregulation[20], cardiovascular regulation[21], itch[22] , and other behaviors. To facilitate future mechanistic investigations of how this brain region controls these processes, it is of great interest to catalog, at a transcriptional level, all the neuron subtypes that populate this area.

Here, we applied single-nucleus and spatial transcriptomics to unravel the neuronal complexity of the dPnTg[23,24]. To accomplish this, we first performed snRNA-seq on cells from this region. The purpose of this first step was two-fold: to identify highly informative marker genes specifying each neuronal subtype, which we would later use for spatial localization, and to obtain a complete transcriptomic inventory of genes expressed by the different neuronal subtypes. Then, MERFISH was performed using 315 informative genes to spatially locate each neuronal subtype within the dPnTg.

RESULTS

Single-nucleus transcriptional profiling identifies distinct cell types in the dPnTg

To profile the single-nuclei whole transcriptome of the dPnTg, we employed two snRNA-seq approaches: DroNc-seq[23] and 10X (Fig 1a). DroNc-seq data were generated by this study using tissue biopsies restricted to dPnTg, whereas the 10X data were retrieved from the Allen Brain Atlas (ABA) effort that used tissue biopsies representing the entire pons[25,26]. To dissect the dPnTg with high precision, in the DroNc-seq dataset we marked the PB and Bar, two brain nuclei that help define its extent, and used their fluorescent signal to guide the dissection (Fig 1b; methods), whereas in the 10X dataset of the pons, we used the anatomical annotation available for each nucleus, imputed from MERFISH data, to select only nuclei belonging to the

dPnTg. After pre-processing and quality control steps, a merged dataset of 222,592 nuclei x 34,457 genes was analyzed using a pipeline that includes Seurat v.3.2.3 and Harmony v.1.1 packages[27,28,29,30] (SFig 1a-b; methods). Our analysis identified 63 clusters comprising 12 major cell types (Fig 1c-d; SFig 2a). Each cell type was characterized by uniquely expressed genes (i.e., markers), of which many have been previously reported in the literature (Fig 1e; SFig 2b; STable 1). Neurons encompassed 32 clusters, accounting for ~40% of all nuclei. The glial/ non-neuronal cells encompassed 31 clusters, accounting for the remaining 60% of all nuclei (Fig 1c-d; SFig 2a). We identified 11 major glial/ non-neuronal cell types: oligodendrocytes, astrocytes, oligodendrocyte precursor cells (OPCs), immature oligodendrocytes, perivascular macrophages (PVMs), microglia, vascular smooth muscle cells (VSMCs), pericytes, vascular and leptomeningeal cells (VLMCs type I and II), choroid plexus epithelial cells (CPE) and ependymocytes (Fig 1c-e; SFig 2a-b; STable 1).

To disentangle the neuronal diversity of the dPnTg, we first selected all neurons, excluding neurons outside our region of interest (ROI) and glial/ non-neuronal cells, and then we categorized them into two main groups for re-clustering (methods). The first group, called "excitatory neurons," included 47,756 nuclei divided into 71 clusters. They expressed *Slc17a6*, *Slc17a7,* or *Slc17a8* (glutamatergic neurons), and in some cases, they expressed *Th*/*Slc18a2* (noradrenergic neurons), *Tph2*/*Slc6a4* (serotoninergic neurons), *Chat*/*Slc5a7* (cholinergic neurons) or *Slc17a6*/*Slc32a1* ("hybrid neurons")[24] (Fig 1f, h). The second group, "inhibitory neurons", included 30,771 nuclei divided into 57 clusters. All neurons in this group expressed *Slc32a1* (GABAergic neurons), and at the same time, some also expressed *Slc6a5* (glycinergic neurons) (Fig 1g, i). Each cluster was defined by the expression of one or a combination of marker genes (Fig 1g-i; STable 2-3). Albeit to a different extent, every covariate contributed to each neuronal cluster (% of cells), confirming the mitigation of the batch effect (SFig 2c-i). Our analysis pinpointed many novel neuronal types and confirmed several already documented in the literature, identifying even rare populations accounting for <1% of cells in the dataset.

MERFISH allows the identification and localization of distinct cell types in the dPnTg

We employed MERFISH to spatially resolve the transcriptional neuronal organization of the dPnTg (Fig 2a). Specifically, we investigated the spatial patterns of 315 genes that include 1) marker genes from differential expression (DE) analysis of the snRNAseq dataset, 2) canonical glial, non-neuronal, and neuronal markers; and 3) transcriptional factors, neuropeptides, and receptors (STable 4; methods). We profiled ~5.5 million cells across 46 coronal sections from 7 mice spanning, at intervals of 80-90 µm, a brain region corresponding to -4.7 to -5.8 bregma level in the Franklin-Paxinos atlas[31]. For each MERFISH section, we manually defined the boundaries of the ROI, i.e., dPnTg. The dorsal boundary at rostral levels was defined by the inferior colliculus and more caudally by the dorsal surface of the pons; the ventral boundary was the dorsal part of the motor trigeminal nucleus (Mo5). Then, we used the boundaries' pixel cartesian coordinates to subset each gene counts matrix to include only cells (*polygons*) and transcripts (*spots*) inside the ROI. After removing low-quality and external-to-ROI cells, 685,289 cells were retained for downstream analyses (methods). Throughout the manuscript, all mention of rostral to caudal bregma levels refers to sections approximated to the best matched in the Franklin-Paxinos atlas[31]. We also used the nomenclature from that atlas to identify nuclei and areas.

Our analysis of all cells from the ROI identified 44 clusters grouped into nine transcriptionally distinct cell types. Neurons encompassed 24 clusters, accounting for 50% of all cells in the dataset (Fig 2b-c; SFig 7a; STable 5). Each cell type was characterized by uniquely expressed genes (Fig 2d; SFig 7b). Afterward, we selected only the neurons, discarded the glial/ non-neuronal clusters, and, as before, divided them into two main groups for re-clustering. The first

group, called "excitatory neurons", included 231,103 cells divided into 45 clusters (Fig 2e). The second group, called "inhibitory neurons", included 110,332 cells divided into 45 clusters (Fig 2f). Each cluster was defined by the expression of one or a combination of marker genes (Fig 2g-h; STable 6-7). Cells from different MERFISH slides belonging approximately to the same rostrocaudal level contributed equally to the same neuronal clusters (% of cells), confirming the reproducibility between independent series of sections (SFig 7c-d). Both genders were equally represented among the clusters (SFig 7e). Supplementary Tables 8 ("excitatory neurons") and 9 ("inhibitory neurons") comprehensively list the neuronal MERFISH clusters, their marker genes, and spatial location. Finally, to provide transcriptional resolution on a spatial scale that is of specific interest to investigators and achieve better cluster granularity, we re-clustered the MERFISH-profiled neurons according to four anatomically defined subregions that include the following brain nuclei: 1) KF; 2) LPB and MPB; 3) MTN, pre-LC, LC, and Bar; and 4) LDTgV, LDTg, VTg, DTgC, DTgP, PDTg, CGA, CGB, Sph, O, and CGPn (Table 1). In this study, we excluded from downstream analyses brain nuclei that were only partially represented within the ROI in our sections (e.g., DR, PPTg, SPTg). To avoid ambiguity in the cluster nomenclature, we prepended a prefix to each cluster ID for each subregion (as identified above): "at1_", "at2_", "at3_", and "at4_", respectively.

MERFISH-resolved atlas of the KF

The KF, along with the LPB and MPB, is one of the three subdivisions of the parabrachial complex and is predominantly located in sections just rostral to the LPB and MPB[32,33]. To build a transcriptional atlas of the KF, first, we bilaterally traced its boundaries on MERFISH coronal sections spanning from -4.8 to -4.9 bregma level, and then, we used their pixel cartesian coordinates to subset each gene counts matrix to include only cells and transcripts inside the defined boundaries. A final dataset of 4,554 neurons was analyzed using our bioinformatic pipeline (methods). This analysis pinpointed 19 clusters characterized by unique marker genes, which we classified into five groups based on shared gene expression profiles (Fig 3a-c, f). Briefly, group 1 includes *Tfap2b*+ clusters at1_0, at1_1, at1_6, at1_8, at1_14, and at1_17; group 2 includes *Calca*+/*Onecut3*+ clusters at1_10 and at1_11; group 3, the only GABAergic/ glycinergic group, includes *Pax2*+ clusters at1_4 and at1_13, group 4 includes clusters at1_7 (*Nos1*+/*Lhx9*+) and at1_15 (*Nps*+/*Qrfpr*+)[34], both located outside the KF along the margin of the nucleus of the lateral lemniscus (NLL); lastly, the miscellaneous group includes clusters at1_2, at1_3, at1_5, at1_9, at1_12, at1_16, and at1_18, of which cluster at1_3 is located outside the KF (Fig 3b-d; STable 10). Next, to visualize neuronal clusters in space, we plotted the cartesian pixel coordinates of each cell as Voronoi plots and computed the cell frequency (cluster trajectory) across three bregma levels, from -4.80 to -4.9 (Fig 3b, e). Interestingly, the four KF groups displayed distinct spatial distributions.

Then, we focused on *Calca*+ neurons, a well-known population of the LPBE[19,35,36], and hypothesized that *Calca*+ clusters at1_10 and at1_11 in the KF could be a more rostral continuation of that cell group. To test for this assumption, we assessed the transcriptional similarity by performing a Pearson's *r* correlation among the average expression of 315 genes across all neurons of KF clusters at1_10, at1_11, and at1_6 (negative control, *Calca*-) and the PB cluster at2_2. Strikingly, the KF cluster at1_10 exhibited the highest correlation score (r= 84.8%) with PB cluster at2_2 compared to KF clusters at1_11 (r= 59.6%) and at1_6 (r= 33.3%) (Fig 3g). While cluster at1_11 is scattered, cluster at1_10 is focally concentrated in the ventral part of the KF and could represent a rostral continuation of the main *Calca*+ LPBE population (Fig 3i-j). To discover genetic markers that allow selective access to these neuronal subtypes, we performed a DE analysis between the PB cluster at2_2, all PB clusters except at2_2, and KF clusters at1_6, at1_10, and at1_11. *Calca* was expressed in KF clusters at1_10, at1_11, and PB cluster at2_2. *Onecut3* emerged as the most selective marker for KF *Calca*+ clusters at1_10

and at1_11 versus LPBE cluster at2_2. In addition, the genes *Ebf2* and *Chst9* selectively marked the KF cluster at1_11 (Fig 3h; STable 11). Anatomically, the KF clusters at1_10 and at1_11 mingle along their caudal edge with the most rostral neurons of the LPBE cluster at2_2. However, in the MERFISH assay, the KF *Calca*+ neurons express lower levels of *Calca* transcript and are smaller. In addition, using mice expressing Cre recombinase under the Calca promoter, *Calca* neurons in the PB complex have been found to project to the forebrain but also to the ventrolateral medulla[37]. Because LPBE neurons do not project to the medulla, but KF neurons do, this latter projection likely comes from the KF neurons of clusters at1_10 or at1_11, a hypothesis that can now be tested as identifying distinct genetic markers will allow selective genetic access to these populations. Furthermore, we confirmed *Calca*+ neuron types of the KF/ PB and their markers in an independent scRNAseq atlas of the same region[38], and tested the correspondence of its clusters with clusters of MERFISH atlases 1-2 (KF/ PB) by using MetaNeighbor, an unsupervised replication framework that employs neighbor voting to quantify the degree of cluster similarity across datasets (SFig 8a-e; STable 12-13; methods)[39,40]. Specifically, scRNA-seq clusters 15 and 16 matched with our MERFISH clusters at2_2 (AUROC= 0.94) and at1_11 (AUROC= 0.87) and were distinguished by the same genes previously identified by our analysis (Fig 3h; SFig 8d-g; STable 11, 14).

MERFISH-resolved atlas of the PB

The other two divisions of the parabrachial complex are LPB and MPB[32]. To build a transcriptional atlas of the PB, first, we bilaterally traced its boundaries on MERFISH coronal sections spanning from -4.95 to -5.75 bregma level, and then we clustered the 79,413 neurons located within the PB boundaries (methods). The analysis identified 43 clusters, of which 36 belong to the PB. Each cluster was defined by unique gene expression and spatial patterns (Fig 4a-d; STable 15).

Next, we aimed to compare PB neuron types identified by this study with those described in the literature. We observed four different scenarios. 1) Neuron types whose location and marker gene have a correlate in our data: these would include cluster at2_2, *Calca*+/*Il20ra+,* which corresponds with the well-studied CGRP neurons in the LPBE, involved in the response to aversive stimuli[19]; cluster at2_5, *Foxp2*+/*Pdyn*+, which corresponds with dynorphin neurons located in the LPBD, involved in thermoregulation[20]; cluster at2_42, *Nps*+/*Scn5a*+[34]; and cluster at2_13, *Satb2*+/*Col14a1*+, which correspond to *Satb2* neurons located predominantly in the MPB, involved in taste perception[41]. 2) Neuron types with identified location but whose marker gene has not been identified yet: these would include the correspondence of the *Foxp2*+/*Slc32a1*+ population in the MPBE[42] with GABAergic cluster at2_11, which also expresses *Foxp2* but is marked more selectively by *Skor2* and *Gm47757.* This cluster differs substantially from another GABAergic population, cluster at2_16, which is *Foxp2-* and it is marked by *Slc6a5* and *Pax2,* which are expressed at high levels exclusively in the KF and at low levels in the MPBE (Fig 3f; SFig 9a-d; STable 16). Another case is cluster at2_9, *Rxfp1*+/*Runx1*+, which likely corresponds to *Cck*+ neurons in the LPBS projecting to the ventromedial nucleus of the hypothalamus (VMH) and that are responsible for the control of counterregulatory responses to hypoglycemia[43]. 3) Neuron types reported in the literature but with no correlate in our study: these would include *Oxtr*+ cells, which regulate fluid intake[44]; *Tacr1*+ cells, which regulate pain[8,7]; a *Pdyn*+ population, which relays visceral and mechanosensory signals essential for meal termination[16] and a *Foxp2*+/*Pdyn*- cluster, located in an area that Geerling and colleagues called the rostral-to-external Lateral PB subnucleus (PBreL) that is activated at 4°C, as opposed to a *Foxp2*+/*Pdyn*+ population of the LPBD (cluster at2_5) that is activated at 36°C[20,45]. Because these genes have been chosen for their correlation with a physiologically activated population of neurons, they might be co-expressed by more than one cluster rather than defining a single neuron type. 4) Neuron types and their marker genes that haven't previously been described in the literature: these would include neurons located in

the LPB but especially in the MPB, where only a *Satb2*+ neuron type was previously characterized (SFig 9e-f; STable 17)[41]. As assay validation and an example of an uncharacterized population, we confirmed the spatial distribution of cluster at2_26 using RNA-scope staining (SFig 10a-c; STable 18-19). Its neurons express *Foxp2*/*Gpr101* (and *Trhr*) and are located in the part of the PB complex where Kaur et al. have found *Foxp2*+/*Calca*- neurons expressing *cFos* after animals are exposed to high CO_2 and that project to respiratory areas of the medulla[46]. This population, located adjacent to cluster at2_2 (*Calca*+/*Il20ra*+), possibly corresponds to cluster at2_26. Identifying *Gpr101* and *Trhr* as markers for these neurons will permit genetic access to them for future investigation.

Finally, we asked if a large population, such as cluster at2_2 (*Calca*+/*Il20ra*+), could harbor transcriptionally-defined subpopulations. To test this hypothesis, we isolated all 4,504 neurons from cluster at2_2, reran them through the same bioinformatic pipeline, and plotted the resulting cells using Voronoi plots. Interestingly, each of the ten *Calca*+ clusters was distinguished by different markers and had a specific spatial pattern (Fig 4e-h; STable 20). Clusters 4 (*Slc6a2*+) and 8 (*Qrfpr*+) were notable: the first is located in the dorsal part of the main cluster at2_2, whereas the second is in its ventral part (Fig. 4i-j). Given the unique transcriptional profiles and spatial localizations of different subsets of *Calca* neurons, it is interesting to speculate whether these subsets subserve different functions and/ or have different afferent and efferent connectivities. For example, in rats, the respiratory parts of the nucleus of the solitary tract project to the rostral ventral portion of the *Calca* territory, gustatory inputs of the caudal ventral part, and gastrointestinal inputs to the middle, dorsal portion[47].

MERFISH-resolved atlas of the MTN, pre-LC, LC, and Bar

To build a transcriptional atlas of an ROI that includes MTN, LC, pre-LC, and Bar, first, we bilaterally traced its boundaries on MERFISH coronal sections spanning from -5.2 to -5.8 bregma level, and then we clustered the 22,358 neurons within the ROI boundaries (methods). Overall, we detected 32 clusters, of which only 27 correspond to neurons of this ROI. Each cluster was characterized by unique gene expression and spatial patterns (Fig 5a-d; STable 21). The MTN is a paired structure located at the mesopontine junction, which consists of two populations of primary proprioceptive trigeminal sensory neurons that ipsilaterally innervate spindles in the jaw-closing muscles (*first population*; 80–90% of all MTN neurons) or periodontal pressure receptors (*second population*; 10–20% of all MTN neurons)[48]. We identified clusters at3_8 and at3_24 as MTN neurons because of their unique spatial organization and the expression of *Prph*, *Slc17a7*, and *Pvalb* (Fig 5e)[13]. Most probably, cluster at3_8 (79% of all MTN neurons) corresponds to the jaw muscle population, whereas cluster at3_24 (21% of all MTN neurons) to the periodontal one. We also identified unique marker genes for cluster at3_8 versus at3_24 (adj. p-value <0.01*)* (Fig 5e; STable 22) that will allow studying their different properties.

The LC is the primary source of noradrenergic innervation of the cerebral cortex and cerebellum, and it is located in the dorsolateral PnTg on the lateral floor of the fourth ventricle[3]. It receives input from widespread brain regions and projects throughout the forebrain, brainstem, cerebellum, and spinal cord[3]. Recently, it has been demonstrated that the modular input-output organization of the LC can enable temporary, task-specific modulation of different brain regions[3]. However, whether this modularity corresponds to transcriptionally defined groups of noradrenergic neurons is still undetermined. To this end, we isolated 4,074 noradrenergic neurons from cluster at3_0 and reran them through the same bioinformatic pipeline. Each cluster was distinguished by different markers and had a specific spatial pattern (Fig 5g-j; STable 23): clusters 0, 1, 4, and 5 were distributed across the LC, whereas clusters 2

(*Col18a1*+/*Gpr101*+) and 3 (*Tacr3*+/*Ecel1*+) were located in the dorsal portion of the caudal LC and the ventral part of the rostral LC, respectively (Fig 5g, i). As cortical projections arise mainly from the dorsal LC and spinal projections from the ventral LC, it would be interesting to determine whether these populations have different targets[49,50]. In addition, we report two LC non-noradrenergic populations: a low-expressing *Slc17a6/Slc32a1* population likely corresponding to cluster at3_10 and a population of *Penk* neurons that is part of cluster at3_1 (Fig 5d).

The term "pre-locus coeruleus" broadly refers to a small region that lies on both sides of the LC, approximately from bregma levels -5.3 to -5.7. It was initially coined by Geerling and colleagues to identify a neuronal population located ventromedial to the rostral LC that receives excitatory inputs from aldosterone-sensing HSD2 neurons of the NTS[51,52], expresses *Foxp2* and *Pdyn* genes[53], and has elevated levels of *cFos* during dietary sodium deprivation[54]. Our analysis detected six clusters restricted to the pre-LC (group 1 except clusters at3_0, at3_8, and at3_24) and another seven whose cells were shared with medial regions (group 3) (Fig 5a-b). Based upon their gene expression, these neurons discovered by Geerling and colleagues could correspond to cluster at3_30, *Tnc+/Rxfp2*+. Notably, cluster at2_5 from the PB also expresses *Foxp2, Pdyn,* and *Th,* and its cells project to the preoptic area (PoA) and hypothalamus[53,55]. DE analysis identified the top 5 (adj. p-value <0.01) marker genes for cluster at3_30. Of note, none of the genes in our MERFISH panel was a marker for PB cluster at2_5 (Fig 5f; STable 24).

The Bar is a small nucleus located between the LC and the LDTg and is critical for bladder voiding[56]. Bar neurons send long-range projections to the lumbosacral level of the spinal cord, where bladder- and external urethral sphincter-innervating motor neurons reside[18,57]. While more than half of the Bar neurons express *Crh*[58] and stimulation of Bar^{Crh} neurons promotes bladder contractions[18], the genetic and functional identity of other Bar neurons remains elusive. Our analysis detected nine clusters in the "medial region" (group 2). Crh-expressing cluster at3_2 is the main glutamatergic population (Fig 5a-c). Other glutamatergic clusters in or near Bar include at3_9 (*Lhx4*+/*Vsx2*+), at3_26 (*Vglut3*+), and at3_1 (*Penk*+/*Mc4r*+) (Fig 5a-d). It was recently shown that photo-inhibition of Bar^{Esr1} neurons terminates ongoing urethral sphincter relaxation and stops voiding[59]. We detected *Esr1* transcript in cluster at3_2 (*Crh+)* and, to a lesser extent, in neurons of other Bar clusters (SFig 9d). Among the GABAergic populations, clusters at3_12 (*Crhbp+/Glp1r*+) and at3_7 (*Lhx1+/Gm47757*+) are intermingled with the Crh+ neurons of Bar, and GABAergic clusters at3_25, at3_27, at3_28, and at3_31 surround the nucleus. These inhibitory populations could represent neurons in the CGPn or local interneurons that influence Bar's neuronal activity[60]. Furthermore, Bar neurons have extensive dendritic arbors[18], and cholinergic neurons in LDTg (cluster at3_29) are likely in close contact with the *Crh*+ neurites[61].

MERFISH-resolved atlas of the brain nuclei of the medial part of the dPnTg

To investigate a ROI that includes LDTg, VTg, DTg, CGA, CGB, Sph, O, and CGPn, we first traced its boundaries on MERFISH coronal sections spanning from bregma level -4.7 to -5.8, and then we clustered the resulting 120,182 neurons within the ROI boundaries (methods). Overall, we detected 46 clusters, of which only 38 corresponded to neuronal types within this ROI. Each cluster was characterized by unique gene expression and spatial patterns (Fig 6a-d; STable 25).

The LDTg borders the LC and the DTg through some of its course from bregma level -4.7 to -5.6[62]. To decipher its spatial organization, we first computed the contribution of each cluster to the LDTg/ LDTgV region and then its trajectory across 11 rostrocaudal levels (Fig 7b-c, h). The analysis detected 27 LDTg/ LDTgV neuronal clusters, of which 17 (55%) are GABAergic, 8 (32%) glutamatergic, and 2 (13%) cholinergic (Fig 7b). Strikingly, similar ratios were

documented by Luquin E. et al. in rats (Fig 7d, left side)[63]. In our analysis, the well-characterized cholinergic population of the LDTg corresponded to clusters at4_1 and at4_39. These neurons are active during wakefulness and REM sleep[64], and cannot release glutamate or GABA[63], lacking *Slc17a6* and *Slc32a1* expression (Fig 6d). Glutamatergic neurons of the LDTg region are mainly represented by *Shox*2+ clusters at4_0 and at4_7 (also *Lhx4*+), whose cells are uniformly distributed from rostral to caudal, where they gradually replace the cholinergic neurons. The remaining glutamatergic clusters are primarily rostral (Fig 7b-c). Among them, cluster at4_28 (*Tnc*+) is only found in the LDTgV, representing a potential marker to study its specific function[65] (Fig 7a). Conversely, GABAergic clusters showed a more specific spatial distribution along the rostrocaudal axis (Fig 7b-c). Finally, previous work has identified a population of *Glp1r*+ neurons in the LDTg that play a role in attenuating cocaine-seeking behavior by projecting to the ventral tegmental area (VTA)[66]. In our dataset, *Glp1r*+ neurons of the LDTg corresponded to GABAergic clusters at4_21 and at4_38 (~68%) and the glutamatergic cluster at4_22 (~32%) (Fig 7d, right side)[66].

Gudden's tegmental nuclei comprise the VTg and DTg. In the rat, both divisions send heavy projections to the mamillary bodies: the VTg innervates the medial mammillary nucleus, supporting spatial learning, whereas the DTg innervates the lateral mammillary nucleus, supporting spatial navigation[67]. The VTg is located near the midline from -4.7 to -5.2 bregma level and is a purely GABAergic nucleus (Fig 7e-f). In fact, >90% of its neurons belong to GABAergic cluster at4_6 (*Satb1*+), while the remaining are from clusters at4_4 (*Tacr1*+), at4_38 (*Robo3*+) and at4_40 (*Calca*+) (Fig 7f). The DTg is also located near the midline, from -5 to -5.8 bregma level, and it is composed of three divisions: the DTgP, DTgC, and PDTg (Fig 7h). Its primary function is in landmark and directional navigation, and its cells, referred to as head direction (HD) cells, fire in response to changes in head velocity and direction (i.e., left, right)[12]. To decrypt its spatial organization, we first computed the overall contribution of each cluster to the DTg and then its trajectory across ten sequential rostrocaudal levels (Fig 7g, i). Our analysis identified 21 clusters divided into GABAergic (17/21 clusters, representing 88.5% of DTg neurons) and glutamatergic (4/21 clusters, representing 11.5% of DTg neurons) (Fig 7g). Next, we investigated their spatial location with respect to their anatomical organization. The DTgP extends from bregma level -5 to -5.6 (Fig 7h). The rostral-central part of the DTgP is mainly characterized by GABAergic clusters at4_3 (*Vmn1r209*+), at4_5 (*Gpr39*+), at4_12 (*Nts*+), and at4_16 (*Onecut1*+) (Fig 7i, k). In contrast, its caudal part is mostly glutamatergic; it harbors cluster at4_0 (*Shox2*+) and a small GABAergic *Npy*+ population corresponding to cluster at4_36 (Fig 7i, k). The DTgC borders the DTgP for all its extend, except in its rostral part (Fig 7h). The rostral-central part of the DTgC is populated exclusively by the GABAergic cluster at4_4 (*Tacr1*+) that ends in the caudal region, intermingled with the glutamatergic cluster at4_25 (*Lhx9*+) (Fig 7k). Finally, the PDTg occupies the very caudal portion of the DTg, from -5.70 to -5.80 bregma level (Fig 7h); it represents a point where VTg, DTgP, DTgC, and the Sph, which is dorsal to the DTgP from -5.4 to -5.55 bregma level, converge into one structure. (Fig 7k). Our analyses indicated that the Sph is composed of >90% of GABAergic neurons belonging to clusters at4_18 (*Ebf2*+) and at4_41 (*Rxfp1*+) (Fig 7j).

Finally, we examined the nucleus O (also known as nucleus incertus (NI)), CGA, and CGB. The NI extends from -5.30 to -5.6 bregma level and consists of a midline, bilateral cluster of large, multipolar neurons in the central grey[68] (Fig 7h; SFig 11 c). Recent evidence suggests its involvement in modulating arousal, feeding, stress responses, anxiety, addiction, attention, and memory by projecting to high-order structures of the forebrain[4,5,14]. Despite its main GABAergic population being known to express *Rln3*, the genetic makeup of the other neuronal subtypes is unknown. As before, we first computed the overall contribution of each cluster to the NI, CGA, and CGB brain nuclei and then its trajectory across five sequential rostrocaudal levels (SFig

11a-c). Our analysis identified 24 neuronal clusters, of which 16 (58.2%) are GABAergic and 8 (41.8%) are glutamatergic (SFig 11a). None of these neuron types was previously documented.

Correspondence between MERFISH and snRNA-seq neuronal clusters of the dPnTg allows whole transcriptome imputation

Given the limited number of genes profiled by MERFISH, we sought to determine the degree to which neuronal clusters identified by MERFISH in the 4 subregions corresponded to snRNA-seq clusters. This would allow the transfer of transcriptional and spatial information between the two datasets. To this end, we applied MetaNeighbor[39,40] (methods). We found that 94/114 MERFISH-identified clusters corresponded to 82/127 snRNA-seq-identified clusters, and this correspondence was reciprocal in 50/122 instances (AUROC >0.85; Fig 8a-b; STable 26; methods). While only for "mutual" matches, i.e., those having 1:1 correspondence, it is possible to directly infer the expression of genes not probed by MERFISH from the snRNAseq dataset, "non-mutual" correspondences are still useful because they help restrict the field of investigation. Of note, "non-mutual" or missing matches between clusters of the two datasets could stem from the difference in technology sensitivity, number of neurons profiled, features used, and difference in contamination from neighboring regions due to precision in dissecting the ROI.

Comparison between mouse and human neuronal subtypes reveals a high degree of transcriptional similarity

A recent publication[69] made snRNA-seq data from the human pons accessible. We retrieved and pooled together all the nuclei from two dissection biopsies: the first including the pontine reticular formation (PnRF) and the PB; the second, the DTg and all other medial nuclei of the dPnTg. A pre-filtered dataset of 50,250 high-quality nuclei x 37,165 genes was analyzed by using our bioinformatic pipeline (methods)[27,28,29,30]. The analysis identified 32 clusters that we grouped into 10 main cell types (SFig 12a-b; SFig 13a-b, e; STable 27). Next, we isolated only the neurons, excluding the glial/ non-neuronal clusters, and divided them into two main groups for re-clustering. The "excitatory neurons" group included 17,995 nuclei divided into 38 clusters, whereas the second group, "inhibitory neurons", included 11,871 nuclei divided into 29 clusters (SFig 13c-d). Each cluster was defined by the expression of one or a combination of marker genes (SFig 13f-g; STables 28-29). Albeit to a different extent, every covariate contributed to each neuronal cluster (% of cells), confirming the mitigation of the batch effect (SFig 12c-g).

Next, given the extensive use of *Mus musculus* as a model to study neuronal circuits, we employed MetaNeighbor to evaluate the interspecies degree of transcriptional similarity (methods). Interestingly, 50/67 human snRNA-seq clusters corresponded to 52/127 mouse snRNA-seq clusters, and this correspondence was mutual in 23/64 instances, indicating a medium-high interspecies transcriptional similarity (SFig 13h; STable 30). This fact could underlie an evolutionarily conserved function of this brain region. Finally, to gain more insights into the functional relationships of genes driving cell-type replicability, we applied a supervised version of MetaNeighbor that uses clusters with "reciprocal' matches and tests a list of gene sets. We used the *Mus musculus* gene ontology (GO) (methods) as gene sets. The top-scoring average AUROCs pinpointed GO terms related to neurotransmitters/ synaptic functions and neuropeptides, meaning these GO gene sets are moderately conserved functional gene ensembles contributing to cell-type replicability between the two species (SFig 14e-f; STable 31).

Finally, we decided to focus on the PB because it has shared anatomy between humans and mice and because scRNA-seq data from PB are publicly available for both species[38,69]. After discarding GABAergic, cholinergic, serotoninergic, and noradrenergic clusters to limit the contamination from neighboring areas, a dataset of 6,638 putative human PB glutamatergic

neuronal nuclei was re-clustered. The analysis identified 36 clusters specified by distinct marker genes (SFig 14a-b; STable 32). MetaNeighbor analysis run between mouse PB scRNA-seq atlas[38] versus human snRNA-seq PB atlas revealed many clusters had a high degree of transcriptional similarity between the two species. 29/36 human snRNA-seq clusters. corresponded to 20/21 mouse scRNA-seq clusters, and this correspondence was mutual in 15/33 instances (SFig 14c-d; STable 33). Of note, the anatomy of human clusters 14 (*CALCA*+/ *CALCB*+) and 21 (*NPS+/ FOXP2*+) have also been confirmed by immunohistochemistry in sections of human post-mortem brain tissue to be homologous to those in rodents[70,71]. For cluster 4, the human *CGRP* cell group is in the exact relative location as the LPB *Calca* neurons in mice, and *CGRP* terminals were found in the same forebrain areas targeted by *CGRP* neurons in rodents[35,70].

DISCUSSION

To gain selective access and mechanistically investigate the neuronal subtypes within the dPnTg, it is necessary to identify their spatial location and transcriptional identity, particularly their marker genes. While the field presently has characterized some genetic markers for this region, the transcriptional identity of most neuronal subtypes has remained elusive. By combining snRNA-seq and MERFISH, we generated a spatially-resolved transcriptional atlas of the dPnTg at a single-cell resolution. This study analyzed ~1 million cells and identified over 120 neuronal clusters across four anatomical subregions of the dPnTg, confirming the remarkable degree of transcriptional diversity in this region[25,26,69]. To accomplish this, we employed an unsupervised approach, snRNA-seq, to identify the most informative genes and then a supervised approach, MERFISH, relying on a subset of 315 genes, to spatially resolve the neuronal clusters. Finally, we applied MetaNeighbor, an unsupervised replication framework that employs neighbor voting to quantify the degree of cluster similarity across MERFISH and snRNA-seq datasets while preserving the dataset independence[39,40]. Mapping the correspondence between clusters using MetaNeighbor allows the transfer of transcriptional and spatial information from one dataset to another.

To our knowledge, this is the first study to spatially characterize the transcriptome of the mouse dPnTg at single-cell resolution. For the first time, we identified the neuronal subtypes populating this region, spatially located them and provided the marker genes that specify each subtype. In addition, we related this information to the scientific literature to reconcile our findings with the field's current state of knowledge. Our spatially-resolved transcriptional atlas should greatly facilitate future mechanistic investigations of neural circuits in this region. For example, knowing the genetic markers allows for generating recombinase-driver mice that can be used to access specific neuronal populations to perform behavioral, neuronal tracing, and activity mapping experiments[72]. Furthermore, to grant the scientific community easy access to this resource, we developed a GPU-powered visualizer (http://harvard.heavy.ai:6273/) to query the dPnTg MERFISH-resolved datasets, which includes a representative series of 12 sequential coronal sections cut at intervals of 80-90 µm that span bregma levels from -4.7 to -5.8.
By leveraging these two molecular techniques, we built a spatially-resolved transcriptomic atlas of the dPnTg at single-cell resolution and made the dataset accessible and interactive. This will allow future studies to shed light on the function of the many neuronal subtypes populating this region.

ONLINE METHODS

Mouse strains and brain dissections

DroNc-seq and MERFISH experiments were performed on C57BL/6J background mice purchased from the Jackson Laboratory (JAX). Mice were housed at 25°C, ~55% humidity, on a 12:12-h light/dark cycle. Animal experiments were approved by the Beth Israel Deaconess Medical Center's Institutional Animal Care and Use Committee (IACUC) (protocol no. 047-2022). A total of 9 and 8 batches (3-5 mice each) of male and female mice, respectively, 8-10 weeks old, were used for DroNc-seq. To obtain a more precise dissection of the dPnTg and minimize the contamination from neighboring areas, such as the cerebellum, we labeled two nuclei that define its extension: the PB and the Bar.

To visualize the PB, we exploited the fact that the PB receives extensive synaptic inputs from the NTS[73]. A Cre-expressing adeno-associated virus, AAV1-hSyn-Cre (*pENN-AAV1-hSyn-Cre-WPRE-hGH*; titer ≥ 1×10^{13} vg/mL; Addgene, 105553), was injected into the NTS of an Ai14 mouse. The Ai14 mouse (JAX, stock no. #007914, Gt(ROSA)26Sor$^{tm14(CAG-tdTomato)Hze}$) has a Cre reporter allele with a loxP-flanked STOP cassette preventing transcription of a CAG promoter-driven red fluorescent protein variant (tdTomato), all inserted into the Gt(ROSA)26Sor locus. Injection of AAV-Cre into the NTS results in the expression of tdTomato, which travels through the projections from the NTS to label the PB specifically. Two weeks after the AAV injection, mice were decapitated for brain dissection. To visualize the Bar, we exploited the highly selective expression of *Crh* in this brain nucleus[18]. Crh-IRES-Cre mice (JAX, stock no. #012704, B6(Cg)-Crh$^{tm1(cre)Zjh/J}$) were crossed with EGFP-L10a (JAX, stock no. #024750, B6;129S4-Gt(ROSA)26Sor$^{tm9(EGFP/Rpl10a)Amc/J}$) to obtain Crh-IRES-Cre::EGFP-L10a mice whose *Crh*-expressing neurons were selectively labeled with GFP.

In both approaches, mice were sacrificed between 10 am -1 pm. To avoid any stress-related transcriptional changes, mice were decapitated immediately after removal from home cages. After decapitation, the brain was removed from the skull, chilled for 3 min in an ice-cold DMEM/F12, no phenol red (Thermo Fisher Scientific) media slush, and placed ventral surface up in an ice-cold stainless steel brain matrix (Roboz Surgical Instrument Co). A 1 mm thick coronal slice was cut, and the area of interest was dissected bilaterally using a micro dissecting knife (Roboz Surgical Instrument Co.) under the fluorescent stereotactic microscope (Zeiss Discovery V8). Dissections were flash-frozen in dry ice and stored at -80°C.

Stereotactic injection into the NTS

Stereotaxic AAV injections into the NTS were performed in seven- to ten-week-old male/female mice under ketamine (100 mg/kg) and xylazine (10 mg/kg) anesthesia. Mice were placed into a stereotaxic apparatus (David Kopf model 940) with the head angled down at approximately 60 degrees. An incision was made at the level of the cisterna magna, and skin and muscle were retracted to expose the dura mater covering the 4th ventricle. A 28-gauge needle was used to cut through the dura and allow access to the brainstem. Subsequently, a pulled glass micropipette (20-40 mm diameter tip) was used to inject AAV1-hSyn-Cre into the NTS. Stereotaxic coordinates were anterior 0.3 mm, lateral ± 0.15 mm, and ventral 0.3 mm from calamus scriptorius. The virus was injected (200 nl) by an air pressure system using picoliter air puffs through a solenoid valve (Clippard EV 24VDC) pulsed by a Grass S48 stimulator to control injection speed (40 nl/min). The pipette was removed 3 min post-injection, followed by wound closure using absorbable suture for muscle and silk suture for the skin. Subcutaneous injection of sustained-release Meloxicam (4 mg/kg) was provided as postoperative care.

Nuclei isolation

5-6 bilateral tissue dissections were placed in a dounce homogenizer with 1 mL cold (4°C) Lysis Buffer containing 10 mM trisHCl pH 8 (Sigma-Aldrich), 250 mM Sucrose (Sigma-Aldrich), 25 mM KCl, 5mM $MgCl_2$ (Sigma-Aldrich), 0.1% Triton x100 (Sigma-Aldrich), 0.5% RNasin Plus

RNase Inhibitor (Promega), 0.1 mM Dithiothreitol (DTT) (Sigma-Aldrich) in UltraPure™ DNase/RNase-Free Distilled Water (Thermo Fisher Scientific). After douncing for 20 times, the solution was filtered through a sterile 20 µm Cell Strainer (pluriSelect), collected in 1.5 mL DNA LoBind® Tubes (Eppendorf), and centrifuged for 10 min at 900 g (rcf) at 4 C. The "slow sedimenting" component (debris and membranes) was aspirated and discarded while the "fast sedimenting" component (nuclear fraction) was gently resuspended in a 1 mL of Working Solution containing 1X pH 7.4 RNase free PBS (Thermo Fisher Scientific), 0.01% Albumin Bovine Serum (BSA) (Sigma-Aldrich), 0.5% RNasin Plus RNase inhibitor (Promega) in UltraPure™ DNase/RNase-Free Distilled Water (Thermo Fisher Scientific). Nuclei were kept on ice while transferred to the BNORC Functional Genomics and Bioinformatics (FGB) Core for DroNc-seq assay.

DroNc-seq assay, library preparation, and sequencing

DroNc-seq-seq was performed as per Habib et al., with minor modifications[23]. Briefly, nuclei stained with Hoechst 33342 (ThermoFisher, cat. R37605) were counted on a hemocytometer and diluted in NSB to ~250,000 nuclei/ml. Barcoded beads (Chemgenes, Cat # Macosko-2011-10) were size-selected using a 40 µm strainer, diluted to 350,000 per ml, and loaded onto 70 µm wide and 75 µm deep microfluidic device (Nanoshift). The nuclei and barcoded bead suspensions were loaded and run at 35 ml/hr each, along with carrier oil (BioRad Sciences, Cat # 186-4006) at 200 ul/min, to co-encapsulate single nuclei and beads in ~75 µm drops (vol. ~200 pl) at 4,500 drops/sec and double Poisson loading concentrations. The microfluidic emulsion was collected into 50 ml Falcon tubes for 10-25 min each and placed on ice 2h before droplet disruption. Individual 200µl reverse transcription (RT) reactions were performed on up to 90K beads. After further exonuclease digestion, aliquots of 800-5K beads were PCR amplified for 10 cycles, and PCR products were pooled in batches of 4 wells or 16 wells for library construction. Purified cDNA was quantified, and 550 pg of each sample was fragmented, tagged, and amplified in each Nextera reaction. Libraries were sequenced on the Illumina NextSeq500 using between 1.6–1.7 pM and 0.3 µM Read1CustSeqB (GCCTGTCCGCGGAAGCAGTGGTATCAACGCAGAGTAC) using a 20 × 8 × 60 read structure to a depth of 60,000 reads/nucleus.

DroNc-seq read alignment and gene expression quantification

Raw sequencing reads were demultiplexed to FASTQ format files using bcl2fastq (Illumina; version 2.20.0). Digital expression matrices (DGE) were generated using the Drop-Seq tools pipeline (https://github.com/broadinstitute/Drop-seq, version 2.4.0) as follows. Cell and UMI barcodes were extracted from read 1 and tagged onto read 2 -- barcodes with any base quality score <10 were filtered out. Subsequently, reads were trimmed at the 5′ end to remove any TSO sequence and at the 3′ end to remove poly(A) tails and/or (reverse complemented) barcodes and adapters. Tagged and trimmed reads were aligned with STAR (version 2.7.3) against the GRCm38 genome assembly using the GENCODE M20 primary assembly genomic annotation, pre-filtered to remove pseudogenes. Gene counts were obtained on a per-barcode basis by summarizing the unique read alignments across exons and introns, collapsing UMI barcodes at hamming distance 1.

Mouse dPnTg snRNA-seq data analysis

72 DGEs from DroNc-seq (42 from the PB-centered and 30 from Bar-centered dissections) sampling the dPnTg were imported into RStudio (R v 4.2.3) and converted into single Seurat objects; metadata were assigned to each object before merging them. An additional dataset sampling the entire Pons (that includes the dPnTg) was publicly available from the ABA effort to profile the whole mouse brain transcriptome at single-cell resolution using snRNA-seq (10X v3) and MERFISH techniques[25,26]. An AnnData file containing a single snRNA-seq DGE matrix and

relative metadata representing the entire Pons was imported into RStudio and converted into a Seurat object using the *Convert()* and *LoadH5Seurat()* functions. Using the metadata annotation, which also includes the spatial localization from each snRNA-seq nuclei (imputed from MERFISH data), the Seurat object was subsetted to include only nuclei belonging to the dPnTg. Finally, the resulting object was merged with the DroNc-seq object. Nuclei with 1) mitochondrial gene expression detection rate >10%; 2) hemoglobin gene expression detection rate >5%; 3) <400 or >10000 unique gene features, possibly representing empty droplets /low-quality nuclei or cell doublets, respectively, were removed. A post-filtered dataset of 222,592 nuclei x 34,457 genes was inputted into Seurat v3.2.3 + Harmony v1.1 pipeline[27,28,29,30]. Downstream processing was performed using functionalities available in the Seurat R package. Data were first log-normalized using *NormalizeData(),* and then *CellCycleScoring()* was used to infer G2M and S cell cycle scores. This function classifies each cell into one of the 3 phases, G1, G2/M, and S, based on the expression of known G2/M and S phase marker genes[74]. Count data were then processed using *SCTransform()*, which performs a negative binomial-based normalization, identifies the top 3,000 variable features, and regresses out covariates. Regressed covariates included sex, feeding schedule (fasted, re-fed, and ad libitum), CO2 treatment, mitochondrial gene detection rate, inferred cell cycle scores, experimental batch, library batch, mouse genotype, and anatomical dissection (PB-, Bar- and Pons-centered). Principal Component Analysis (PCA) was performed on the 3,000 most variable features using the *runPCA()* function. *RunHarmony()* was subsequently used to harmonize the two technologies (snRNA-seq and DroNc-seq) gene expression profiles. Downstream analyses were conducted on the harmonized dataset. Distinct cell clusters were determined via Shared Nearest Neighbor (SNN) and k-Nearest Neighbor (KNN) analyses. For SNN analysis, resolution parameters of 0.4 for “all nuclei” and 0.6 for the neurons of the “excitatory” and “inhibitory” groups were used. T-distributed stochastic neighbor embedding (t-SNE) was performed on the first 50 PCs to visualize cell clusters. Finally, DE analysis between clusters was performed using the non-parametric Wilcoxon Rank Sum test implemented in *FindAllMarkers()* and *FindMarkers()* functions. A gene was defined as differentially expressed if the absolute average log fold-change (avg_logFC) was >0.25 and the Bonferroni-adjusted p-value <0.01. Cell types were assigned to each cell cluster based on the expression of specific marker genes. Glia/non-neuronal cell types were removed. The remaining neuronal clusters were categorized into "excitatory" and "inhibitory" (see results). Expression datasets representing “excitatory” and “inhibitory” groups were re-processed the same way as described above. Descriptive statistics relative to the abovementioned datasets are presented in SFig 1a-i.

Data analysis of the mouse PB scRNA-seq dataset from Pauli et al

scRNA-seq data were retrieved from the Pauli et al. manuscript that classifies the PB neuronal types by their transcriptional profile and axonal projections[38]. 4 DGEs representing 4 experimental batches were obtained from the NCBI Gene Expression Omnibus (GEO) portal (ID GSE207708) and imported into RStudio. A Seurat object, including only PB neurons, was generated and used for cluster analysis. DE between clusters was performed using the non-parametric Wilcoxon Rank Sum statistics implemented in *FindAllMarkers()* and *FindMarkers()* functions. A gene was defined differentially expressed if absolute logFC was >0.25 and Bonferroni-adjusted p-value <0.01.

MERFISH gene panel selection

MERFISH assay was performed by Vizgen, Inc. (Cambridge, MA, USA). (Vizgen, #10400003). A MERSCOPE panel of 315 genes meeting at least one of the following criteria was assembled: 1- highly variable genes obtained from DE analysis of the snRNA-seq dataset (adj. p-value <0.01; Av. logFC >0.25); 2- canonical glial, non-neuronal, and neuronal markers; 3- transcriptional factors, neuropeptides, and receptors – including those which could be potential

pharmacological targets. For each gene, a panel of 30 encoding probes was designed by Vizgen using a proprietary algorithm, except for 11 genes where the targetable regions were <30 (STable 4). Each MERFISH encoding probe contains a targeting region complementary to the RNA of interest and a series of Vizgen's proprietary readout sequences that encode the specific barcode assigned to each RNA. In addition, 70 scrambled probes (*blanks*) to which have been assigned a specific binary barcode were added to the library as a negative control.

MERFISH sample preparation

A total of 7 C57BL/6J mice (4 males and 3 females) 8-10 week-old from JAX were used for the MERFISH experiment. Mice were housed and sacrificed as described above. After decapitation, the brain was removed from the skull, chilled for 3 min in an ice-cold DMEM/F12, no phenol red (Thermo Fisher Scientific) media slush, and placed ventral surface up in an ice-cold stainless steel brain matrix (Roboz Surgical Instrument Co.). A 2 mm-thick coronal section containing the entire pons-medulla region was cut, placed in a square mold (S22, Kisker Biotech), embedded in OCT (Tissue-Tek® O.C.T. Compound, Sakura), and stored at -80°C. Afterward, the brain block embedded in OCT was incubated for 1 hour at -20°C in a cryostat (LEICA CM1510 S CRYOSTAT), and 10 µm thick coronal sections were cut. To ensure the inclusion of our ROI, we cut from each mouse 10 sections at intervals of 80-90 µm starting approximately from -4.70 to -5.80 bregma level in the Franklin-Paxinos atlas[31]. Two sections at the time were mounted on a warm, functionalized, bead-coated MERSCOPE slide (Vizgen, #20400001) within the boundaries drawn using a 1cm^2 hexagonal gasket (Vizgen). Tissue sections were then placed face-up in a 60 mm petri dish (VWR, 25382-687) and stored at -20°C. Subsequently, 4 ml of Fixation Buffer (4% PFA; EMS, 15714) in buffered 1X PBS (ThermoFisher, AM9625) was added to each petri dish, and sections were incubated for 15 min at room T in a fume hood. After 15 minutes, the Fixation Solution was discarded, and the sections were washed 3 times, 5 minutes each, with a Washing Solution (1X PBS, ThermoFisher, AM9625) at room T. Then, 5 mL of 70% Ethanol (Sigma-Aldrich) was added to the petri dish, and sections were incubated for 5 minutes at room T. Finally, sections were transferred in a Polytube bag, 4 mm thickness (Vizgen) with 10 ml of 75% Ethanol (Sigma-Aldrich), sealed, and stored in the dark at 4°C before shipping to Vizgen facility. After washing with 5 ml Sample Preparation Wash Buffer (Vizgen, #20300001) for 5 minutes and 5 ml Formamide Wash Buffer (Vizgen, #20300002) for 30 minutes at 37°C, the sample was hybridized with the MERSCOPE Gene Panel Mix at 37°C in an incubator for 36-48 hours. The tissue slices were then washed twice with 5 ml Formamide Wash Buffer at 47°C for 30 minutes and embedded into a hydrogel using the Gel Embedding Premix (Vizgen, #20300004), ammonium persulfate (Sigma, 09913-100G), and TEMED (N,N,N',N'-tetramethylethylenediamine) (Sigma, T7024-25ML) from the MERSCOPE Sample Prep Kit (Vizgen, #0400012). After the gel embedding solution polymerized, the sample was incubated with a Clearing Solution consisting of 50 ul of Protease K (NEB, P8107S) and 5 ml of Clearing Premix (Vizgen, #20300003) at 37°C overnight. Then, the sample was washed with 5 ml Sample Preparation Wash Buffer and imaged on the MERSCOPE system (Vizgen 10000001). A fully detailed, step-by-step instruction on the MERFISH sample prep is available at: https://vizgen.com/resources/fresh-and-fixed-frozen-tissue-sample-preparation/. Full Instrumentation protocol is available at: https://vizgen.com/resources/merscope-instrument/.

MERFISH imaging and cell segmentation

After image acquisition, the data were analyzed through the merlin pipeline through Vizgen's MERSCOPE Analysis Computer by selecting the watershed cell segmentation algorithm. The output files for each coronal brain section consisted of 1) **cell_by_gene.csv** - A matrix where each row corresponds to a cell and each column to a gene. The matrix is not filtered for segmentation artifacts. Before analyses, cells with <15 gene counts were removed; 2) **detected_transcripts.csv** -DataFrame of all detected transcripts in a coronal section where

each row is a detected transcript. The columns are "barcode_id" – 315 internally used gene IDs that identify each gene univocally; "global_x, global_y" - the global micron x and y coordinates of each transcript; "global_z" - the index of the z-stack in the section where the transcript was detected. To note that 7 z-stacks per section were acquired at an interval of ~1.5 µm; "x, y" - the pixel coordinates of a transcript within the field of view (FOV); "fov" - the index of the FOV where the transcript was detected; "gene" - the gene name of the detected transcript; 3) **cell_metadata.csv** - Spatial metadata of detected cells. Each row corresponds to a cell. The columns are: "fov" - the field of view containing the cell; "volume" - the volume of the cell in μm^3; "center_x" - the x coordinate of the center of the cell in global micron coordinates; "center_y" - the y coordinate of the center of the cell in global micron coordinates; "min_x, max_x" - the x minimum and maximum of the bounding box containing the cell in global micron coordinates; "min_y, max_y" – the y minimum and maximum of the bounding box containing the cell in global micron coordinates; 4) **cell_boundaries.hdf5** - Polygon boundaries relative to cells identified in a single FOV. Each file refers to a FOV. Boundaries are stored in .hdf5 format indexed by the unique cell ID; 5) **images** – Folder containing 7 mosaic_DAPI.tiff and 7 mosaic_PolyT.tiff images. These represent stitched DAPI or PolyT staining images acquired from a 10 µm thick MERFISH coronal section at ~1.5 µm intervals; micron_to_mosaic_pixel_transform.csv - contains the transformation matrix used to convert micron into pixel coordinates; manifest.json – contains the metadata of the stacked image.

Mouse dPnTg MERFISH data analysis

46 mosaic DAPI images, one per coronal section, were imported into Adobe Illustrator v26.5. Using the lasso tool, the dPnTg's boundaries were manually defined for each image. The cartesian pixel coordinates defining each image's boundaries were extracted using a custom script (STable 34). Then, 46 gene count matrices (cell_by_gene.csv) related to the 46 DAPI images were imported into Python v3.8. Using the cartesian pixel coordinates defined by the lasso tool, the count matrices were subsetted to include only data relative to features (genes) and barcodes (cells) located within the defined boundaries. 46 subsetted matrices were imported into RStudio and converted into Seurat objects; metadata were assigned to each object before merging them[27,29,30]. Cells with <15 gene counts were filtered out. A post-filtered dataset of 685,289 cells x 315 genes was inputted into Seurat v3.2.3 + Harmony v1.1 pipeline[27,28,29,30]. Data were analyzed using the same bioinformatic pipeline employed for snRNA-seq with a few modifications. Briefly, count data were processed using *SCTransform()*. Regressed covariates included only mouse gender. PCA was performed on the 315 features using the *runPCA()* function. Harmony was subsequently used to harmonize the gene expression profiles across the sections. Downstream analyses were conducted on the harmonized dataset. Distinct cell clusters were determined via SNN and KNN analyses. SNN analysis was based on resolution parameters of 0.4 for “all cells”, 0.8 and 0.6 for the neurons of the “excitatory” and “inhibitory” groups, respectively, 0.4 for the subregion-specific atlas_1 and 0.8 for atlases 1-3 (see results). T-SNE was used on the first 50 PCs to visualize cell clusters. Finally, DE analysis between clusters was performed using the non-parametric Wilcoxon Rank Sum statistics implemented in *FindAllMarkers()* and *FindMarkers()* functions. A gene was defined as differentially expressed if the absolute average log fold-change (avg_logFC) was >0.25 and the Bonferroni-adjusted p-value <0.01. As in snRNA-seq analysis, after assigning all the clusters to a cell type, clusters corresponding to glial/ non-neuronal cell types were discarded. The remaining neuronal clusters were divided into "excitatory" and "inhibitory". They underwent the same analyses as described above. Descriptive statistics relative to the abovementioned datasets are in SFig 6a-h. Next, raw and normalized gene count matrices, metadata, and cartesian pixel coordinates of each polygon were extracted from the three Seurat objects containing “all cells”, “excitatory”, and “inhibitory” neurons and imported into GIOTTO

v1.1.2 package for data visualization[75]. The function *createGiottoObject()* was used to create a single GIOTTO object, which included dPnTg cells and transcripts across 46 sections. *subsetGiottoLocs()* was employed to subset the gene count matrices based on spatial coordinates to generate the 4 anatomical subregions that were then analyzed using the Seurat v3.2.3 + Harmony v1.1 pipeline described above.

Estimation of clusters' replicability using MetaNeighbor

The R package MetaNeighbor version 1.14.0[39,40] was employed to assess cluster replicability across technologies (i.e., MERFISH, snRNA-seq(10X), DroNc-seq, scRNA-seq (10X)) and species (i.e., homo sapiens, mus musculus). Four main comparisons were made using MetaNeighbor: 1) across technologies, between MERFISH and snRNA-seq neuronal datasets of the mouse dPnTg and 2) between MERFISH and scRNA-seq neuronal datasets (Pauli et al.)[38] of the mouse PB; 3) across species, between the mouse and the human (Siletti et al.)[69] snRNA-seq neuronal datasets of the dPnTg and 4) between the mouse scRNA-seq (Pauli et al.)[38] and human snRNA-seq (Siletti et al.)[69] of the PB. For the cross-species analyses (points 3-4), gene symbols were converted between species using a manifest file ("gene_orthologs.gz") listing gene symbol correspondences across species as available at NCBI (https://ftp.ncbi.nlm.nih.gov/gene/DATA/).

Briefly, unique IDs were assigned to neuronal clusters of the two datasets. Seurat objects were converted into SingleCellExperiment objects using the function *as.SingleCellExperiment().* The two objects were then merged using the *mergeSCE()* function from the MetaNeighbor package. The function selects only genes, assays, and metadata columns shared by the two objects. The function *variableGenes()* was used to select genes with high variance in both datasets. In the comparison between MERFISH and snRNA-seq/ scRNAseq (points 1-2), the 315-panel genes were set as highly variable genes. The unsupervised *MetaNeighborUS()* function with the "fast_version" parameter set to TRUE and the "symmetric_output" parameter set to FALSE was used to assess cell type homology. In brief, cells from the reference dataset (e.g., MERFISH) vote for their closest neighbors in the target dataset (e.g., snRNA-seq), effectively ranking these cells by similarity. Then, the cell-level ranking is aggregated at the cell-type level (i.e., clusters) in the target dataset as an area under the receiver operator characteristic curve (AUROC), which mirrors the proximity of a target cell type to the reference cell type. The same analysis is computed by reversing reference and target roles. The *topHitsByStudy()* function was used to select only matches with an AUROC >0.85 and/ or classified as "reciprocal" top hits.

Functional classification of gene sets driving cell type replicability

In cross-species analysis (point 3 in the above paragraph), we conducted gene ontology (GO) enrichment analysis of the gene sets driving the cluster replicability. A list of GO sets (*Mus Musculus*) comprising 22,546 GO terms categorized into the three main classes, Cellular Component (CC), Molecular Function (MF), and Biological Process (BP), was downloaded from https://figshare.com/articles/dataset/Protocol_data_R_version_/13020569/2[40]. The GO sets were filtered to (i) include only genes shared with our merged human-mouse dataset and (ii) be large enough to learn expression profiles (>10 genes) and small enough to enrich for GO terms (<100), as previously described[40]. Finally, the supervised *MetaNeighbor()* function was employed to construct a rank correlation network between cells for a GO gene set and predict cell type membership. The resulting AUROC, in this case, represents how well cells can be assigned to a cell type label using individual GO gene sets (how well a gene set contributes to each cell-type replicability). AUROC values of ~0.5–0.6 indicate random performance, AUROC values of ~0.7 suggest that they contribute moderately to replicability, while AUROC values >0.8 indicate high performance[40].

Estimation of clusters' replicability between snRNA-seq and the 4 MERFISH subregion atlases using CCA for spatial dashboard

To compare mouse neuronal clusters resolved by snRNA-seq versus those resolved by MERFISH, we applied a canonical correlation analysis (CCA) function built in Seurat 3 that operates at the single-cell level, and then we aggregated the results at the cluster level to calculate the cluster-to-cluster correspondence. The following functions built-in Seurat 3 were used: 1) *FindTransferAnchors()*, which performs a CCA on the reference (snRNA-seq) and query (MERFISH) and identify cell anchors which are used to transfer data from the reference to the query; 2)*TransferData()* to transfer labels across single-cell datasets. The function's output includes a *prediction score* for each MERFISH cell mapping onto each snRNA-seq cluster and a *max prediction score* with the respective *predicted ID*, i.e., the predicted snRNA-seq cluster for each MERFISH cell ID with the highest *prediction score*. We aggregated the results at the cluster level by considering only those matches with a number of cells mapped from snRNA-seq clusters onto MERFSH clusters and vice versa >0.25%, after normalizing for the cluster size.

Specificity, sensitivity, and reproducibility of MERFISH assay

MERFISH efficiency was evaluated by measuring the number of transcripts per FOV (FOV size = 200 x 200 µm). Only slices with >25,000 transcript counts per FOV were retained (SFig 3a). As a control for MERFISH specificity, for all the sections was demonstrated 1) a Pearson's *r* correlation coefficient >70% with a bulk RNA-seq dataset from the whole mouse brain (SFig 3b, 2f; STable 35-36) and 2) a difference of 15.5 folds from the non-specific signal (SFig 5a). For the MERFISH dataset, the average expression of the 315 genes was calculated across all cells and is reported as log10 raw counts (or log10 (raw counts+1)). For the bulk RNA-seq dataset, the average expression of the 315 genes was calculated across all samples and is reported as log10 FPKM (Fragments per kilobase of transcript per million mapped fragments). Pearson's *r* correlation between the average expression values of the 315 genes in MERFISH and bulk RNA-seq datasets was performed by matching the same isoform between the two sources (codebook STable 35-36). The bulk RNA-seq dataset from the whole mouse brain can be retrieved at https://www.ebi.ac.uk/arrayexpress/experiments/E-MTAB-6081/.
Experimental reproducibility was evaluated by computing the Pearson's *r* correlation coefficient of the average gene expression of 315 genes between sections of the same mouse (intra-batch reproducibility) and sections of different mice (inter-batch reproducibility) (SFig 4a-b). Sequential sections exhibited a higher pairwise correlation compared to non-sequential sections. (SFig 4a-b, 5c) In addition, the correlations between two coronal sections from the same or two different mice, representing approximately the same bregma level, were always extremely high (r>0.99, p=0) (SFig 5d-e). The difference in sensitivity between MERFISH and snRNA-seq was estimated by computing the fold change between the average expression levels of 315 genes across all cells in snRNA-seq versus MERFISH datasets. Average gene expression was 0.5 folds higher in MERFISH compared to the snRNA-seq dataset (SFig 5b), indicating a nearly identical sensitivity.

Interactive visualization of MERFISH and snRNA-seq data

The design and realization of a dashboard able to produce interactive visualization of spatial-transcriptomic data were done in partnership with HEAVY.AI. The dashboard hosts two viewers on two different pages: the first viewer, called "spatial cell viewer," displays a total of 14 full, 10 µm thick coronal sections and covers at an interval of 80-90 µm a region from -4.7 to -5.8 bregma level in the Franklin-Paxinos atlas[31], whereas the second viewer, called "subregion cell viewer", hosts the data relative to the four subsetted regions (see section " MERFISH data analysis"). The dashboard can be accessed at: http://harvard.heavy.ai:6273/. Complete documentation can be found at:
https://docs.heavy.ai/?_ga=2.207206352.2137306788.1595867219-1426127794.1594677732.

Transcriptomic data for the 3 snRNA-seq and 7 MERFISH datasets, all the raw and normalized count matrices, the cell metadata, and the t-SNE embeddings were uploaded on the single-cell BROAD portal. The study can be accessed at: https://singlecell.broadinstitute.org/single_cell/study/SCP1808. Complete documentation can be found at: https://singlecell.zendesk.com/hc/en-us.

Human dPnTg snRNA-seq dataset data analysis

snRNA-seq data were retrieved from a recent publication by Siletti et al., profiling the whole transcriptome of the entire adult human brain at a single-nucleus resolution[69]. A single .loom file containing a prefiltered DGE (for low-quality nuclei/ doublets) of over 3 million nuclei and relative metadata was imported into RStudio. *As.Seurat()* was employed to convert the .loom file into a Seurat object. The Seurat object was then subsetted to include only nuclei from anatomical dissections of 1) the pontine reticular formation (PnRF) and the PB or 2) other nuclei in the dPnTg and the DTg. A subsetted object of 50,250 high-quality nuclei x 37,165 genes was imported into R and processed using the Seurat v3.2.3 + Harmony v1.1 pipeline[36,37,38,39]. Data were analyzed using the same bioinformatic pipeline employed for snRNA-seq and MERFISH with a few modifications. Briefly, count data were processed using *SCTransform()*. Regressed covariates included age, cell cycle score, 10X chemistry, mitochondrial gene detection rate, donor label, and anatomical dissection. The data were derived from 3 male donors. PCA was performed on the 3,000 most variable features. *RunHarmony()* was subsequently used to harmonize the gene expression across different donors. Distinct cell clusters were determined via SNN and KNN analyses in Seurat. SNN analysis was based on resolution parameters of 0.4 for “all nuclei”, 0.8 for the neurons of the “excitatory”/ inhibitory“ groups, and for all PB neurons. T-SNE was used on the first 50 PCs to visualize cell clusters. DE analysis between clusters was performed using the non-parametric Wilcoxon Rank Sum statistics implemented in *FindAllMarkers()* and *FindMarkers()* functions. A gene was defined as differentially expressed if the absolute average log fold-change (avg_logFC) was >0.25 and the Bonferroni-adjusted p-value <0.01. Consistently with MERFISH and snRNA-seq analyses, all the clusters were assigned to a cell type. Clusters corresponding to glia/ non-neuronal cell types were discarded. The remaining neuronal clusters were divided into "excitatory" and "inhibitory". They underwent the same processing as described above.

RNA scope in situ hybridization

RNA Scope Multiplex Fluorescent Reagent Kit V2 (Advanced Cell Diagnostics, Hayward, CA; Cat. #323100) was used to perform RNA scope in situ hybridization for *Pdyn*, *Gpr101*, and *Foxp2* mRNA. Mice were, first, intracardially perfused with formalin (10% buffered solution) under deep anesthesia induced by isoflurane exposure (5% in O2), and then brains were removed from the skull and post-fixed in formalin (10% buffered solution) overnight. After incubating in 20% sucrose (for cryoprotection) for 24 h, the brains were cut into 30 µm-thick sections. Sections were treated with protease (40˚C; 30min; Protease IV, RNA scope) and incubated with RNA scope probes for *Pdyn*-C1 (RNA scope® Probe- Mm-Pdyn; Cat. #318771), *Gpr101*-C2 (RNA scope® Probe- Mm-*Gpr101*; Cat. #317281), and *Foxp2*-C3 (RNA scope® Probe-Mm-Foxp2; Cat. #428791; Advanced Cell Diagnostics) during the hybridization step (2 h; 40°C). After the hybridization step, we performed three amplification steps (40°C; AMP1-FL and AMP2-FL: 30 min each; AMP3-FL: 15 min), followed by horse radish peroxidase-C1 (HRP-C1) amplification (40°C for 15 min). Sections were then incubated in TSA plus Fluorescein (Perkin Elmer, Cat. #NEL744001KT) to visualize *Pdyn* mRNA (Channel 1 at 488nm) in green. This is followed by incubating the sections in HRP-C2 amplification step (40°C; 15 min). Sections were then incubated in TSA plus Cy3 (Perkin Elmer, Cat. #: NEL754001KT) fluorophore (1:1000; 30 min) to visualize *Gpr101* mRNA (Channel 2 at 550 nm) in red. In the last step of the process, sections were subjected to HRP-C3 amplification (40°C; 15 min) followed by TSA plus Cy5

incubation (40°C; 30 min; Perkin Elmer; Cat. #NEL754001KT) to visualize *Foxp2* mRNA (Channel 3 at 647 nm) in magenta. After each fluorophore step, sections were subjected to HRP blocking (40°C; 15 min). After each step in the protocol, the sections were washed two times with 1X wash buffer provided in the kit. The covered sections (Vectashield mounting medium; Vector Laboratories) were imaged and photographed with a confocal microscope (Leica Stellaris 5) at final magnification of 20X and 63X.

Graphics

All graphic representations were generated using R (v. 4.2.3) base functions or R packages. Bar plots, scatter plots, box plots, donut plots, staked area charts, line charts, and correlation matrix heatmaps were generated with R base functions or the ggplot2 package[76]. Sankey plots were generated with the networkD3 package. Dot plots, t-SNEs, and violin plots were generated using functions built in the Seurat v3.2.3 package[30]. Voronoi plots were generated using the functions built in the GIOTTO v1.1.2 package[75]. Human-mouse dot plots were generated using the function built in the MetaNeighbor package[39,40]. Schematics in Fig 1a and 2a were created with BioRender.com.

Statistics and reproducibility

No statistical method was used to predetermine the sample size. Our sample sizes for MERFISH and snRNA-seq are similar to or larger than those reported in the literature[24,77,78,79]. No randomization or blinding was performed for sample collection and data analysis. This was unrequired since we did not perform any comparison between different conditions or treatments. The criteria used to exclude data during the quality control process for mouse MERFISH, mouse snRNA-seq, and human snRNA-seq are documented in the “Mouse dPnTg MERFISH data analysis”, “Mouse dPnTg snRNA-seq data analysis”, and “Human dPnTg snRNA-seq data analysis” sections, respectively.

Acknowledgments

We thank Dr. Jiang He and Dr. George Emanuel from Vizgen for consenting us to enroll in the Vizgen early access program and granting us access to MERSCOPE before commercialization. We thank Mr. Tony Duarte from HEAVY.AI for his availability and collaboration in implementing our vision to use their HEAVY.AI proprietary GPU-accelerated technology to query single-cell spatial transcriptomic datasets in real-time. This project was funded by the NIH grants R01DK075632 (B.B.L), P01HL149630, NS072337 (C.B.S), R01-DK125708 (A.M.J.V.), R01-DK113030, P20-DK119789 (M.L.Z.), R01-NS091126 (E.A.), R00HL144923 (J.M.R), DP1-AT010971, R01-MH12343 (M.L.A.).

Author contributions

Project design: B.B.L., S.N. A.M.J.V. Project management: B.B.L., S.N., A.M.J.V, R.D.L. Data generation (snRNA-seq): S.N., A.M.J.V., N.K., R.D.L., J.M.R., D.P., M.V. Data generation (MERFISH): S.N., R.D.L., N.K. Data processing (snRNA-seq): C.L.J, H.S. Data processing (MERFISH): S.N., Data analysis (snRNA-seq): S.N., A.Z. Data analysis (MERFISH): S.N., A.Z. Data storage (snRNA-seq/ MERFISH): O.A., S.N. Spatial dashboard design: S.N., D.N., C.B. Animal experiments: A.M.J.V., N.K., Z.Y., R.M.G, S.N, R.D.L. In situ hybridization: R.D.L. Anatomic cluster annotation: S.N., R.D.L., C.B.S., A.M.J.V., N.K. Drafting of the manuscript and figure generation: S.N., R.D.L., E.A, A.M.J.V., N.K. Manuscript review and editing: S.N., B.B.L, A.M.J.V., C.B.S., A.Z., R.D.L., E.A., M.L.A., L.T., K.D.H., M.L.Z. Vizgen team contributed to MERFISH data generation and data processing. HEAVY.AI team contributed to the spatial design and implementation of the spatial viewer.

Data availability

Mouse DroNc-seq raw and processed data is accessible from the GEO portal (GSE226809). Mouse snRNA-seq raw and processed data from ABA[25,26] is accessible at https://knowledge.brain-map.org/data/LVDBJAW8BI5YSS1QUBG/collections. Mouse MERFISH raw and processed data are under the BIDMC repository: https://research.bidmc.harvard.edu/datashare/DataShareInfo.ASP?Submit=Display&ID=7. Mouse PB scRNA-seq raw and processed data from Pauli et al.[38] are accessible from the GEO portal (GSE207708). Human snRNA-seq processed data from Siletti et al.[69] are accessible at https://storage.cloud.google.com/linnarsson-lab-human.

Code availability

R code used to generate results in the manuscript are available on Zenodo: https://zenodo.org/records/10103722?token=eyJhbGciOiJIUzUxMiJ9.eyJpZCI6IjZkZThiYzhhLTQ3ZGQtNDYzMC1hYjcyLTg3ZmY0YmM0YWY3NSIsImRhdGEiOnt9LCJyYW5kb20iOiI3NmIyZDVhMmU4YjcwMmZhODM5NTM5MzY3NGVkMTAxNSJ9.ACwF0iRToyOYARYPXOBIC7YhVqK2kfmdFe9XzvLNzjfnpIkyqp1YvCCdEY9aLdYQyzxvI83xUO4E8aBh4ZD6Gw

Python code used to generate results in the manuscript are available on GitHub: https://emanuega.github.io/MERlin/index.html# and https://github.com/acycliq/merfish_python_pons.

Conflict of Interest

Cory Brannigan is a software architect at HEAVY.AI.

REFERENCES

1. Miller, J. R. *et al.* A Subregion of the Parabrachial Nucleus Partially Mediates Respiratory Rate Depression from Intravenous Remifentanil in Young and Adult Rabbits. *Anesthesiology* **127**, 502–514 (2017).
2. Kaur, S. & Saper, C. B. Neural Circuitry Underlying Waking Up to Hypercapnia. *Front. Neurosci.* **13**, 401 (2019).
3. Breton-Provencher, V., Drummond, G. T. & Sur, M. Locus Coeruleus Norepinephrine in Learned Behavior: Anatomical Modularity and Spatiotemporal Integration in Targets. *Front. Neural Circuits* **15**, 638007 (2021).

4. Ryan, P. J., Ma, S., Olucha-Bordonau, F. E. & Gundlach, A. L. Nucleus incertus—An emerging modulatory role in arousal, stress and memory. *Neurosci. Biobehav. Rev.* **35**, 1326–1341 (2011).
5. Lu, L. *et al.* Control of locomotor speed, arousal, and hippocampal theta rhythms by the nucleus incertus. *Nat. Commun.* **11**, 262 (2020).
6. Scammell, T. E., Arrigoni, E. & Lipton, J. O. Neural Circuitry of Wakefulness and Sleep. *Neuron* **93**, 747–765 (2017).
7. Deng, J. *et al.* The Parabrachial Nucleus Directly Channels Spinal Nociceptive Signals to the Intralaminar Thalamic Nuclei, but Not the Amygdala. *Neuron* **107**, 909-923.e6 (2020).
8. Barik, A. *et al.* A spinoparabrachial circuit defined by Tacr1 expression drives pain. *eLife* **10**, e61135 (2021).
9. Coimbra, B. *et al.* Role of laterodorsal tegmentum projections to nucleus accumbens in reward-related behaviors. *Nat. Commun.* **10**, 4138 (2019).
10. Hernandez, N. S. *et al.* GLP-1 receptor signaling in the laterodorsal tegmental nucleus attenuates cocaine seeking by activating GABAergic circuits that project to the VTA. *Mol. Psychiatry* **26**, 4394–4408 (2021).
11. Liu, Z. *et al.* Dorsal Raphe Neurons Signal Reward through 5-HT and Glutamate. *Neuron* **81**, 1360–1374 (2014).
12. Taube, J. S. The Head Direction Signal: Origins and Sensory-Motor Integration. *Annu. Rev. Neurosci.* **30**, 181–207 (2007).
13. Florez-Paz, D., Bali, K. K., Kuner, R. & Gomis, A. A critical role for Piezo2 channels in the mechanotransduction of mouse proprioceptive neurons. *Sci. Rep.* **6**, 25923 (2016).

14. Szőnyi, A. *et al.* Brainstem nucleus incertus controls contextual memory formation. *Science* **364**, eaaw0445 (2019).

15. Li, M. M. *et al.* The Paraventricular Hypothalamus Regulates Satiety and Prevents Obesity via Two Genetically Distinct Circuits. *Neuron* **102**, 653-667.e6 (2019).

16. Kim, D.-Y. *et al.* A neural circuit mechanism for mechanosensory feedback control of ingestion. *Nature* **580**, 376–380 (2020).

17. Fowler, C. J., Griffiths, D. & de Groat, W. C. The neural control of micturition. *Nat. Rev. Neurosci.* **9**, 453–466 (2008).

18. Verstegen, A. M. J., Vanderhorst, V., Gray, P. A., Zeidel, M. L. & Geerling, J. C. Barrington's nucleus: Neuroanatomic landscape of the mouse "pontine micturition center": VERSTEGEN et al. *J. Comp. Neurol.* **525**, 2287–2309 (2017).

19. Campos, C. A., Bowen, A. J., Roman, C. W. & Palmiter, R. D. Encoding of danger by parabrachial CGRP neurons. *Nature* **555**, 617–622 (2018).

20. Geerling, J. C. *et al.* Genetic identity of thermosensory relay neurons in the lateral parabrachial nucleus. *Am. J. Physiol.-Regul. Integr. Comp. Physiol.* **310**, R41–R54 (2016).

21. Davern, P. J. A role for the lateral parabrachial nucleus in cardiovascular function and fluid homeostasis. *Front. Physiol.* **5**, (2014).

22. Piyush Shah, D. & Barik, A. The Spino-Parabrachial Pathway for Itch. *Front. Neural Circuits* **16**, 805831 (2022).

23. Habib, N. *et al.* Massively parallel single-nucleus RNA-seq with DroNc-seq. *Nat. Methods* **14**, 955–958 (2017).

24. Moffitt, J. R. *et al.* Molecular, spatial, and functional single-cell profiling of the hypothalamic preoptic region. *Science* **362**, eaau5324 (2018).

25. Zizhen Yao *et al.* A high-resolution transcriptomic and spatial atlas of cell types in the whole mouse brain. *bioRxiv* 2023.03.06.531121 (2023) doi:10.1101/2023.03.06.531121.

26. Meng Zhang *et al.* A molecularly defined and spatially resolved cell atlas of the whole mouse brain. *bioRxiv* 2023.03.06.531348 (2023) doi:10.1101/2023.03.06.531348.

27. Butler, A., Hoffman, P., Smibert, P., Papalexi, E. & Satija, R. Integrating single-cell transcriptomic data across different conditions, technologies, and species. *Nat. Biotechnol.* **36**, 411–420 (2018).

28. Korsunsky, I. *et al.* Fast, sensitive and accurate integration of single-cell data with Harmony. *Nat. Methods* **16**, 1289–1296 (2019).

29. Hafemeister, C. & Satija, R. Normalization and variance stabilization of single-cell RNA-seq data using regularized negative binomial regression. *Genome Biol.* **20**, 296 (2019).

30. Stuart, T. *et al.* Comprehensive Integration of Single-Cell Data. *Cell* **177**, 1888-1902.e21 (2019).

31. Paxinos, G. & Franklin, K. B. J. The Mouse Brain in Stereotaxic Coordinates.

32. Olszewski, J. & Baxter, D. Cytoarchitecture of the human brainstem. By Jerzy Olszewski and Donald Baxter. Published and distributed in North America for S. Karger by J. B. Lippincott Company, Philadelphia and Montreal. 1954. 199 pages. Price $16.00 (Reviewed by Gerhardt von Bonin). *J. Comp. Neurol.* **101**, 825–825 (1954).

33. Varga, A. G., Maletz, S. N., Bateman, J. T., Reid, B. T. & Levitt, E. S. Neurochemistry of the Kölliker-Fuse nucleus from a respiratory perspective. *J. Neurochem.* **156**, 16–37 (2021).

34. Huang, D. *et al.* Neuropeptide S (NPS) neurons: Parabrachial identity and novel distributions. *J. Comp. Neurol.* **n/a**, (2022).

35. Kaur, S. *et al.* A Genetically Defined Circuit for Arousal from Sleep during Hypercapnia. *Neuron* **96**, 1153-1167.e5 (2017).

36. Kaur, S. *et al.* Role of serotonergic dorsal raphe neurons in hypercapnia-induced arousals. *Nat. Commun.* **11**, 2769 (2020).

37. Huang, D., Grady, F. S., Peltekian, L., Laing, J. J. & Geerling, J. C. Efferent projections of CGRP/Calca-expressing parabrachial neurons in mice. *J. Comp. Neurol.* **529**, 2911–2957 (2021).

38. Pauli, J. L. *et al.* Molecular and anatomical characterization of parabrachial neurons and their axonal projections. *eLife* **11**, e81868 (2022).

39. Crow, M., Paul, A., Ballouz, S., Huang, Z. J. & Gillis, J. Characterizing the replicability of cell types defined by single cell RNA-sequencing data using MetaNeighbor. *Nat. Commun.* **9**, 884 (2018).

40. Fischer, S., Crow, M., Harris, B. D. & Gillis, J. Scaling up reproducible research for single-cell transcriptomics using MetaNeighbor. *Nat. Protoc.* **16**, 4031–4067 (2021).

41. Jarvie, B. C., Chen, J. Y., King, H. O. & Palmiter, R. D. Satb2 neurons in the parabrachial nucleus mediate taste perception. *Nat. Commun.* **12**, 224 (2021).

42. Geerling, J. C., Yokota, S., Rukhadze, I., Roe, D. & Chamberlin, N. L. Kölliker-Fuse GABAergic and glutamatergic neurons project to distinct targets: GEERLING et al. *J. Comp. Neurol.* **525**, 1844–1860 (2017).

43. Garfield, A. S. *et al.* A Parabrachial-Hypothalamic Cholecystokinin Neurocircuit Controls Counterregulatory Responses to Hypoglycemia. *Cell Metab.* **20**, 1030–1037 (2014).

44. Ryan, P. J., Ross, S. I., Campos, C. A., Derkach, V. A. & Palmiter, R. D. Oxytocin-receptor-expressing neurons in the parabrachial nucleus regulate fluid intake. *Nat. Neurosci.* **20**, 1722–1733 (2017).

45. Norris, A. J., Shaker, J. R., Cone, A. L., Ndiokho, I. B. & Bruchas, M. R. Parabrachial opioidergic projections to preoptic hypothalamus mediate behavioral and physiological thermal defenses. *eLife* **10**, e60779 (2021).

46. Kaur, S. & Saper, C. FoxP2 cells in the lateral parabrachial area may drive respiratory responses to hypercapnia. *FASEB J.* **35**, (2021).

47. Moga, M. M. *et al.* Organization of cortical, basal forebrain, and hypothalamic afferents to the parabrachial nucleus in the rat. *J. Comp. Neurol.* **295**, 624–661 (1990).

48. Lazarov, N. E. Neurobiology of orofacial proprioception. *Brain Res. Rev.* **56**, 362–383 (2007).

49. Guyenet, P. G. The coeruleospinal noradrenergic neurons: Anatomical and electrophysiological studies in the rat. *Brain Res.* **189**, 121–133 (1980).

50. Loughlin, S. E., Foote, S. L. & Fallon, J. H. Locus coeruleus projections to cortex: Topography, morphology and collateralization. *Brain Res. Bull.* **9**, 287–294 (1982).

51. Gasparini, S. *et al.* Aldosterone-sensitive HSD2 neurons in mice. *Brain Struct. Funct.* **224**, 387–417 (2019).

52. Jarvie, B. C. & Palmiter, R. D. HSD2 neurons in the hindbrain drive sodium appetite. *Nat. Neurosci.* **20**, 167–169 (2017).

53. Gasparini, S., Resch, J. M., Gore, A. M., Peltekian, L. & Geerling, J. C. Pre-locus coeruleus neurons in rat and mouse. *Am. J. Physiol.-Regul. Integr. Comp. Physiol.* **320**, R342–R361 (2021).

54. Geerling, J. C. *et al.* FoxP2 expression defines dorsolateral pontine neurons activated by sodium deprivation. *Brain Res.* **1375**, 19–27 (2011).

55. Huang, D., Grady, F. S., Peltekian, L. & Geerling, J. C. Efferent projections of Vglut2, Foxp2, and Pdyn parabrachial neurons in mice. *J. Comp. Neurol.* **529**, 657–693 (2021).

56. Sakakibara, R. Chapter 15 - Lower urinary tract dysfunction in patients with brain lesions. in *Handbook of Clinical Neurology* (eds. Vodušek, D. B. & Boller, F.) vol. 130 269–287 (Elsevier, 2015).

57. Loewy, A. D., Saper, C. B. & Baker, R. P. Descending projections from the pontine micturition center. *Brain Res.* **172**, 533–538 (1979).

58. Valentino, R. J., Pavcovich, L. A. & Hirata, H. Evidence for corticotropin-releasing hormone projections from Barrington's nucleus to the periaqueductal gray and dorsal motor nucleus of the vagus in the rat. *J. Comp. Neurol.* **363**, 402–422 (1995).

59. Keller, J. A. *et al.* Voluntary urination control by brainstem neurons that relax the urethral sphincter. *Nat. Neurosci.* **21**, 1229–1238 (2018).

60. Mallory, B. S., Roppolo, J. R. & de Groat, W. C. Pharmacological modulation of the pontine micturition center. *Brain Res.* **546**, 310–320 (1991).

61. Kawatani, M. *et al.* Cholinergic modulation of CRH and non-CRH neurons in Barrington's nucleus of the mouse. *J. Neurophysiol.* **124**, 443–457 (2020).

62. Paxinos, G., Xu-Feng, H., Sengul, G. & Watson, C. Chapter 8 - Organization of Brainstem Nuclei. in *The Human Nervous System (Third Edition)* (eds. Mai, J. K. & Paxinos, G.) 260–327 (Academic Press, 2012). doi:10.1016/B978-0-12-374236-0.10008-2.

63. Luquin, E., Huerta, I., Aymerich, M. S. & Mengual, E. Stereological Estimates of Glutamatergic, GABAergic, and Cholinergic Neurons in the Pedunculopontine and Laterodorsal Tegmental Nuclei in the Rat. *Front. Neuroanat.* **12**, 34 (2018).

64. Boucetta, S., Cissé, Y., Mainville, L., Morales, M. & Jones, B. E. Discharge Profiles across the Sleep–Waking Cycle of Identified Cholinergic, GABAergic, and Glutamatergic Neurons in the Pontomesencephalic Tegmentum of the Rat. *J. Neurosci.* **34**, 4708–4727 (2014).

65. Lu, J., Sherman, D., Devor, M. & Saper, C. B. A putative flip–flop switch for control of REM sleep. *Nature* **441**, 589–594 (2006).

66. Hernandez, N. S. *et al.* GLP-1 receptor signaling in the laterodorsal tegmental nucleus attenuates cocaine seeking by activating GABAergic circuits that project to the VTA. *Mol. Psychiatry* **26**, 4394–4408 (2021).

67. Dillingham, C. M. *et al.* Calcium-binding protein immunoreactivity in Gudden's tegmental nuclei and the hippocampal formation: differential co-localization in neurons projecting to the mammillary bodies. *Front. Neuroanat.* **9**, (2015).

68. Ma, S. & Gundlach, A. L. Ascending Control of Arousal and Motivation: Role of Nucleus Incertus and its Peptide Neuromodulators in Behavioural Responses to Stress. *J. Neuroendocrinol.* **27**, 457–467 (2015).

69. Siletti, K. *et al.* Transcriptomic diversity of cell types across the adult human brain. *Science* **382**, eadd7046.

70. de Lacalle, S. & Saper, C. B. Calcitonin gene-related peptide-like immunoreactivity marks putative visceral sensory pathways in human brain. *Neuroscience* **100**, 115–130 (2000).

71. Adori, C. *et al.* Neuropeptide S- and Neuropeptide S receptor-expressing neuron populations in the human pons. *Front. Neuroanat.* **9**, (2015).

72. Daigle, T. L. *et al.* A Suite of Transgenic Driver and Reporter Mouse Lines with Enhanced Brain-Cell-Type Targeting and Functionality. *Cell* **174**, 465-480.e22 (2018).

73. Roman, C. W., Derkach, V. A. & Palmiter, R. D. Genetically and functionally defined NTS to PBN brain circuits mediating anorexia. *Nat. Commun.* **7**, 11905 (2016).

74. Kowalczyk, M. S. *et al.* Single-cell RNA-seq reveals changes in cell cycle and differentiation programs upon aging of hematopoietic stem cells. *Genome Res.* **25**, 1860–1872 (2015).

75. Dries, R. *et al*. Giotto: a toolbox for integrative analysis and visualization of spatial expression data. *Genome Biol.* **22**, 78 (2021).

76. Wickham, H. *ggplot2*. (Springer New York, 2009). doi:10.1007/978-0-387-98141-3.

77. Chen, R. *et al.* Decoding molecular and cellular heterogeneity of mouse nucleus accumbens. *Nat. Neurosci.* **24**, 1757–1771 (2021).

78. Zhang, M. *et al.* Spatially resolved cell atlas of the mouse primary motor cortex by MERFISH. *Nature* **598**, 137–143 (2021).

79. Hochgerner, H. *et al.* Neuronal types in the mouse amygdala and their transcriptional response to fear conditioning. *Nat. Neurosci.* (2023) doi:10.1038/s41593-023-01469-3.

SUPPLEMENTARY REFERENCES

abbreviation	brain nucleus	abbreviation	brain nucleus
Bar	Barrington's nucleus	LPBI	LPB, internal part
CGA	central gray, alpha part	LPBS	LPB, superior part
CGB	central gray, beta part	LPBV	LPB, ventral part
CGPn	central gray of the pons	Me5 or MTN	mesencephalic trigeminal nucleus
DR	dorsal raphe nucleus	MnR	median raphe nucleus
DTgC	dorsal tegmental nucleus, central part	MPB	medial parabrachial nucleus
DTgP	dorsal tegmental nucleus, pericentral part	MPBE	MPB, external part
KF	Kölliker-Fuse nucleus	O or NI	nucleus O or nucleus incertus
LC	locus coeruleus	PB	parabrachial nucleus
LDTg	laterodorsal tegmental nucleus	PBW	parabrachial nucleus, waist part
LDTgV	laterodorsal tegmental nucleus, ventral	PDTg	posterodorsal tegmental nucleus
LPB	lateral parabrachial nucleus	PPTg	pedunculopontine tegmental nucleus
LPBC	LPB, central part	pre-LC	pre locus coeruleus
LPBCr	LPB, crescent part	Sph	sphenoid nucleus
LPBD	LPB, dorsal part	SPTg	subpedencular tegmental nucleus
LPBE	LPB, external part	VTg	ventral tegmental nucleus

Table1

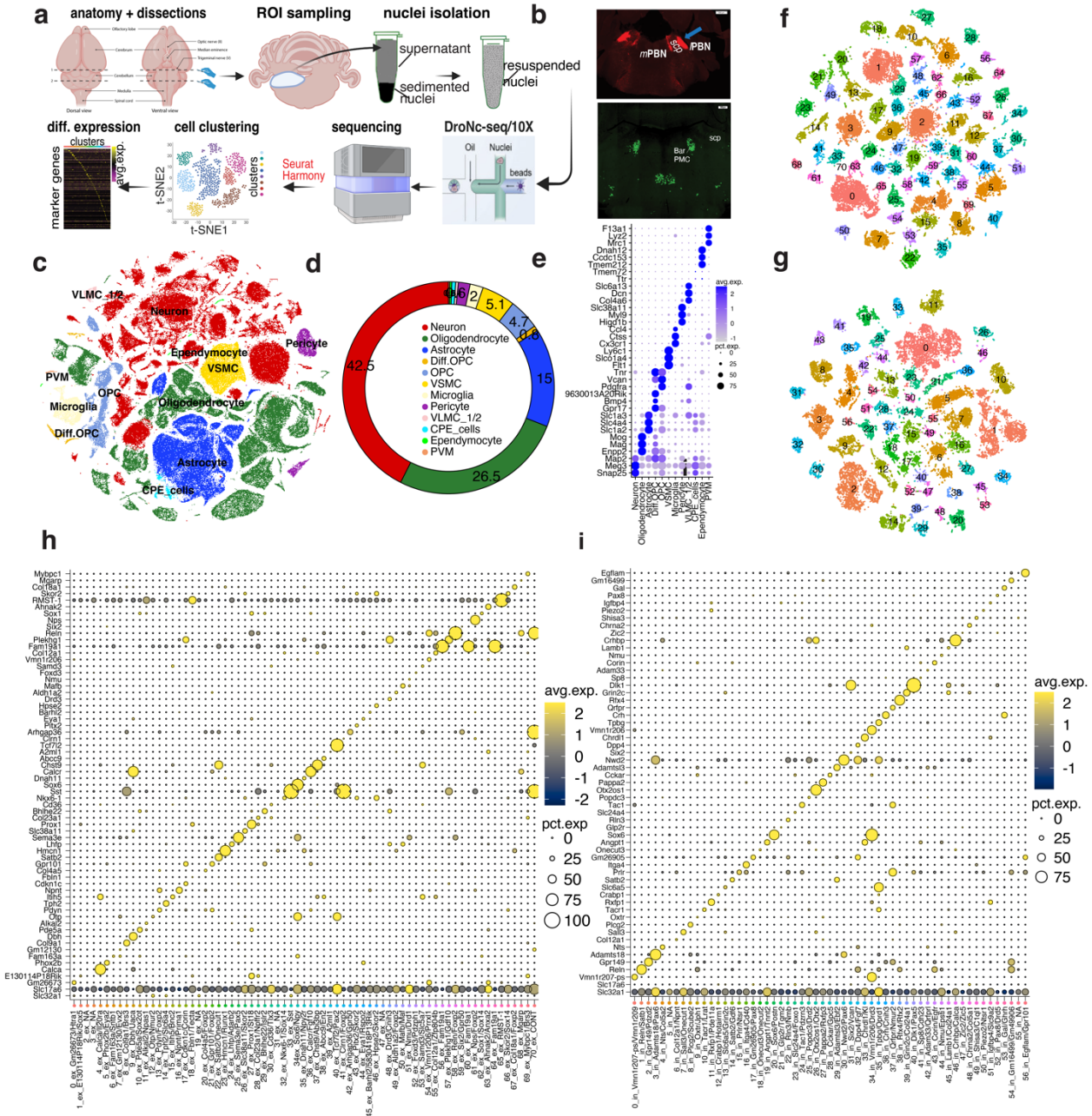
a
anatomy + dissections
ROI sampling
nuclei isolation
supernatant
sedimented nuclei
resuspended nuclei
diff. expression
cell clustering
sequencing
DroNc-seq/10X
clusters
marker genes
avg.exp.
t-SNE2
t-SNE1
Seurat
Harmony
Oil
Nuclei
beads
b
mPBN
LC
PBN
scp
Bar
PMC
c
VLMC_1/2
Neuron
Ependymocyte
VSMC
Pericyte
PVM
OPC
Microglia
Oligodendrocyte
Diff.OPC
Astrocyte
CPE_cells
d
42.5
26.5
15
4.7
2
5.1
Neuron
Oligodendrocyte
Astrocyte
Diff.OPC
OPC
VSMC
Microglia
Pericyte
VLMC_1/2
CPE_cells
Ependymocyte
PVM
e
avg.exp.
pct.exp.
f
g
h
avg.exp.
pct.exp
i
avg.exp.
pct.exp.

Figure 1

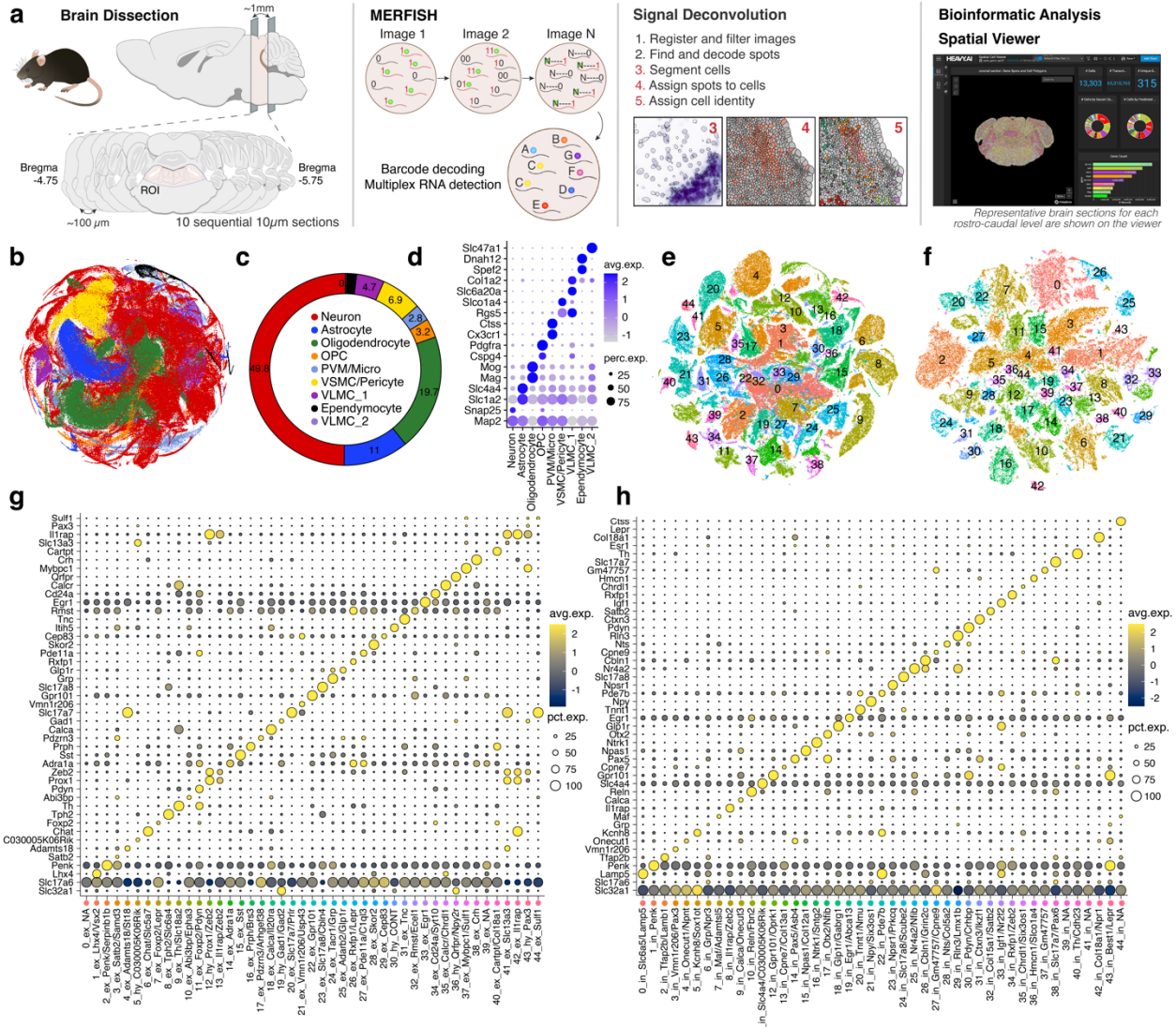
a
Brain Dissection
~1mm
Bregma -4.75
Bregma -5.75
ROI
~100 μm
10 sequential 10μm sections
MERFISH
Image 1
Image 2
Image N
Barcode decoding
Multiplex RNA detection
Signal Deconvolution
1. Register and filter images
2. Find and decode spots
3. Segment cells
4. Assign spots to cells
5. Assign cell identity
Bioinformatic Analysis
Spatial Viewer
Representative brain sections for each rostro-caudal level are shown on the viewer
b
c
Neuron
Astrocyte
Oligodendrocyte
OPC
PVM/Micro
VSMC/Pericyte
VLMC_1
Ependymocyte
VLMC_2
d
avg.exp.
perc.exp.
e
f
g
h
avg.exp.
pct.exp.

Figure 2

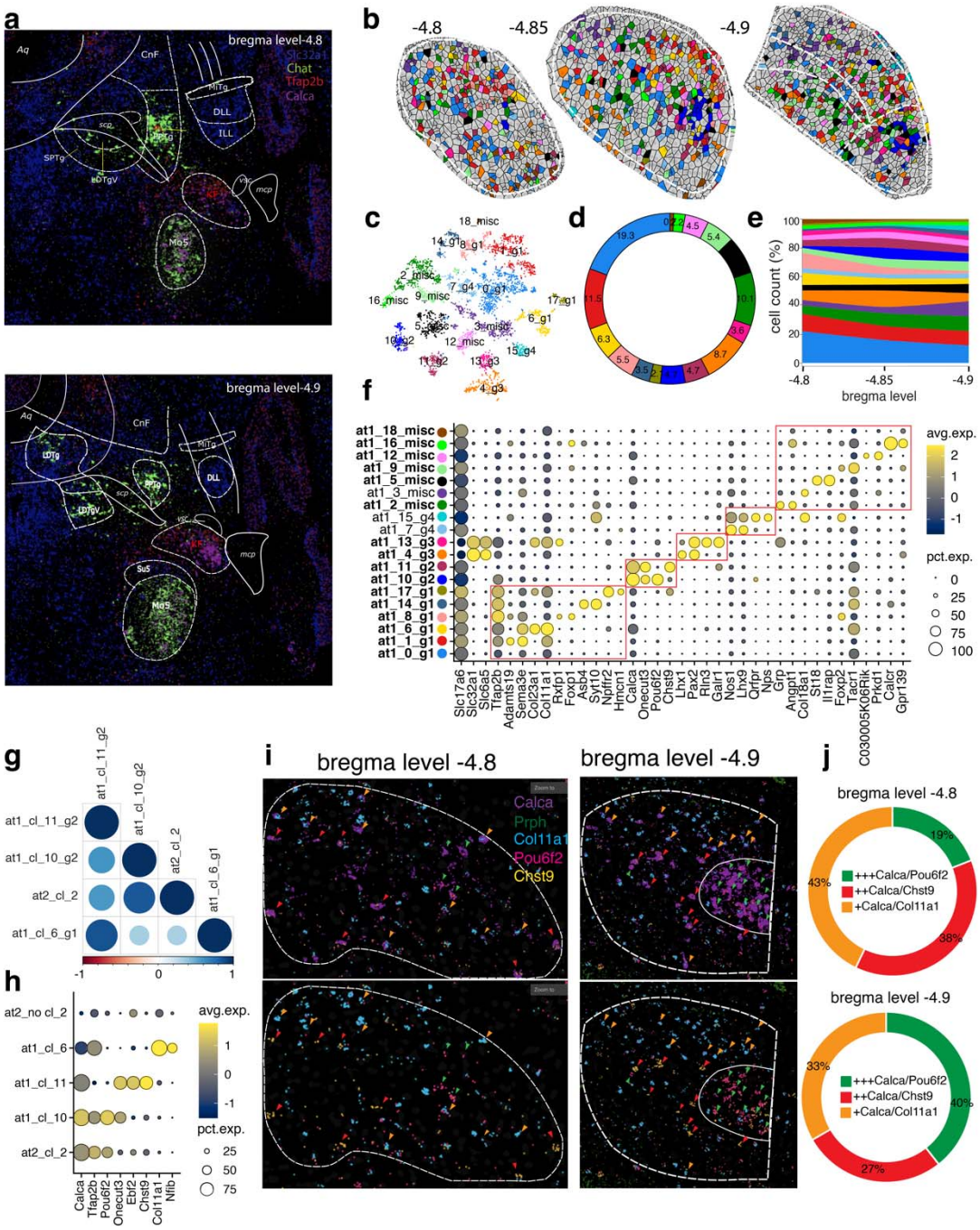
a
bregma level-4.8
Slc32a1
Chat
Tfap2b
Calca
bregma level-4.9
b
-4.8
-4.85
-4.9
c
d
e
cell count (%)
bregma level
f
avg.exp.
pct.exp.
g
h
avg.exp.
pct.exp.
i
bregma level -4.8
bregma level -4.9
Calca
Prph
Col11a1
Pou6f2
Chst9
j
bregma level -4.8
+++Calca/Pou6f2
++Calca/Chst9
+Calca/Col11a1
19%
43%
38%
bregma level -4.9
+++Calca/Pou6f2
++Calca/Chst9
+Calca/Col11a1
33%
40%
27%

Figure 3

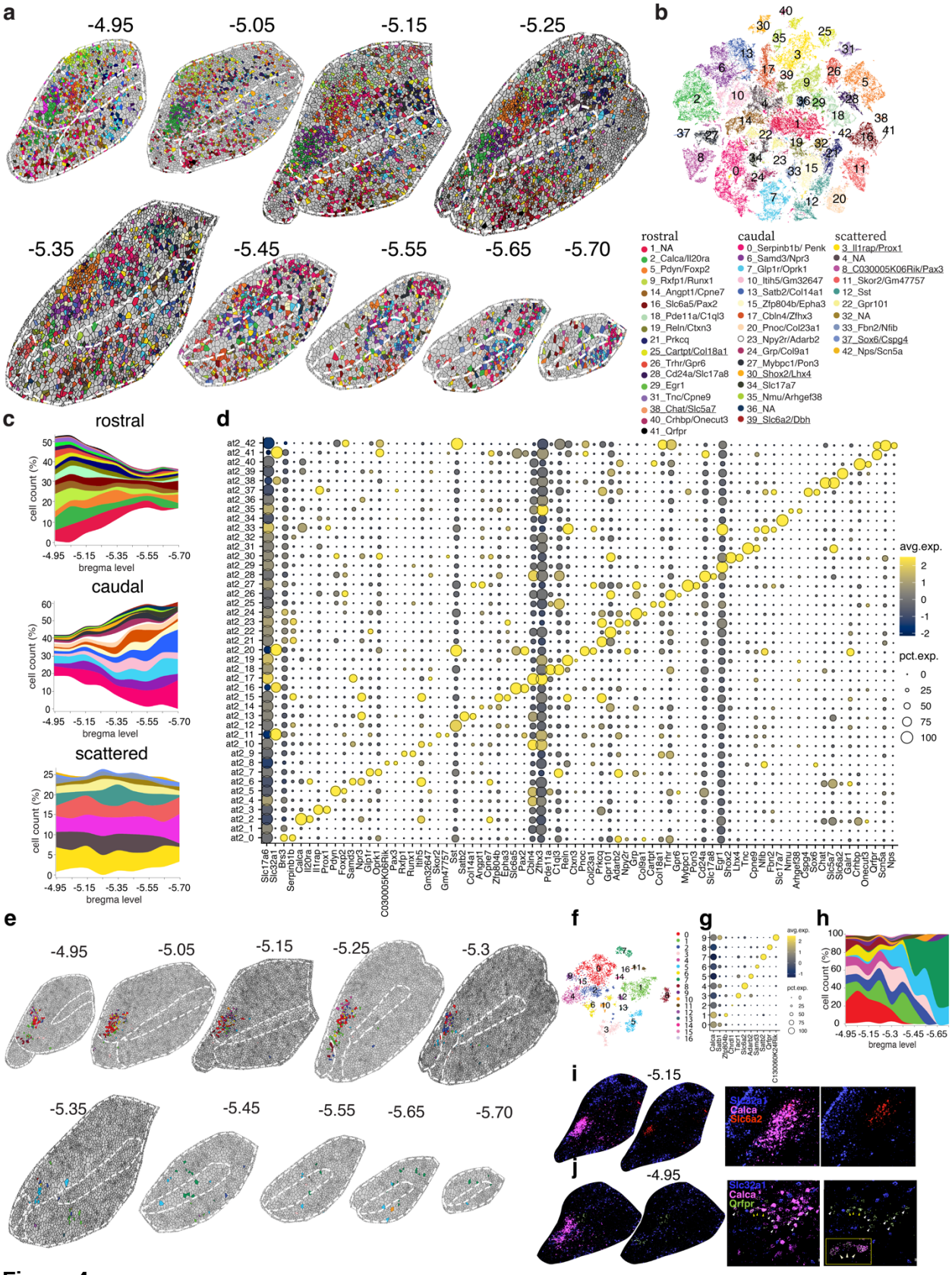
a
-4.95
-5.05
-5.15
-5.25
-5.35
-5.45
-5.55
-5.65
-5.70
b
rostral
1_NA
2_Calca/Il20ra
5_Pdyn/Foxp2
9_Rxfp1/Runx1
14_Angpt1/Cpne7
16_Slc6a5/Pax2
18_Pde11a/C1ql3
19_Reln/Ctxn3
21_Prkcq
25_Cartpt/Col18a1
26_Trhr/Gpr6
28_Cd24a/Slc17a8
29_Egr1
31_Tnc/Cpne9
38_Chat/Slc5a7
40_Crhbp/Onecut3
41_Qrfpr
caudal
0_Serpinb1b/ Penk
6_Samd3/Npr3
7_Glp1r/Oprk1
10_Itih5/Gm32647
13_Satb2/Col14a1
15_Zfp804b/Epha3
17_Cbln4/Zfhx3
20_Pnoc/Col23a1
23_Npy2r/Adarb2
24_Grp/Col9a1
27_Mybpc1/Pon3
30_Shox2/Lhx4
34_Slc17a7
35_Nmu/Arhgef38
36_NA
39_Slc6a2/Dbh
scattered
3_Il1rap/Prox1
4_NA
8_C030005K06Rik/Pax3
11_Skor2/Gm47757
12_Sst
22_Gpr101
32_NA
33_Fbn2/Nfib
37_Sox6/Cspg4
42_Nps/Scn5a
c
rostral
caudal
scattered
cell count (%)
bregma level
d
avg.exp.
pct.exp.
e
f
g
h
i
j
Slc32a1
Calca
Slc6a2
Qrfpr

Figure 4

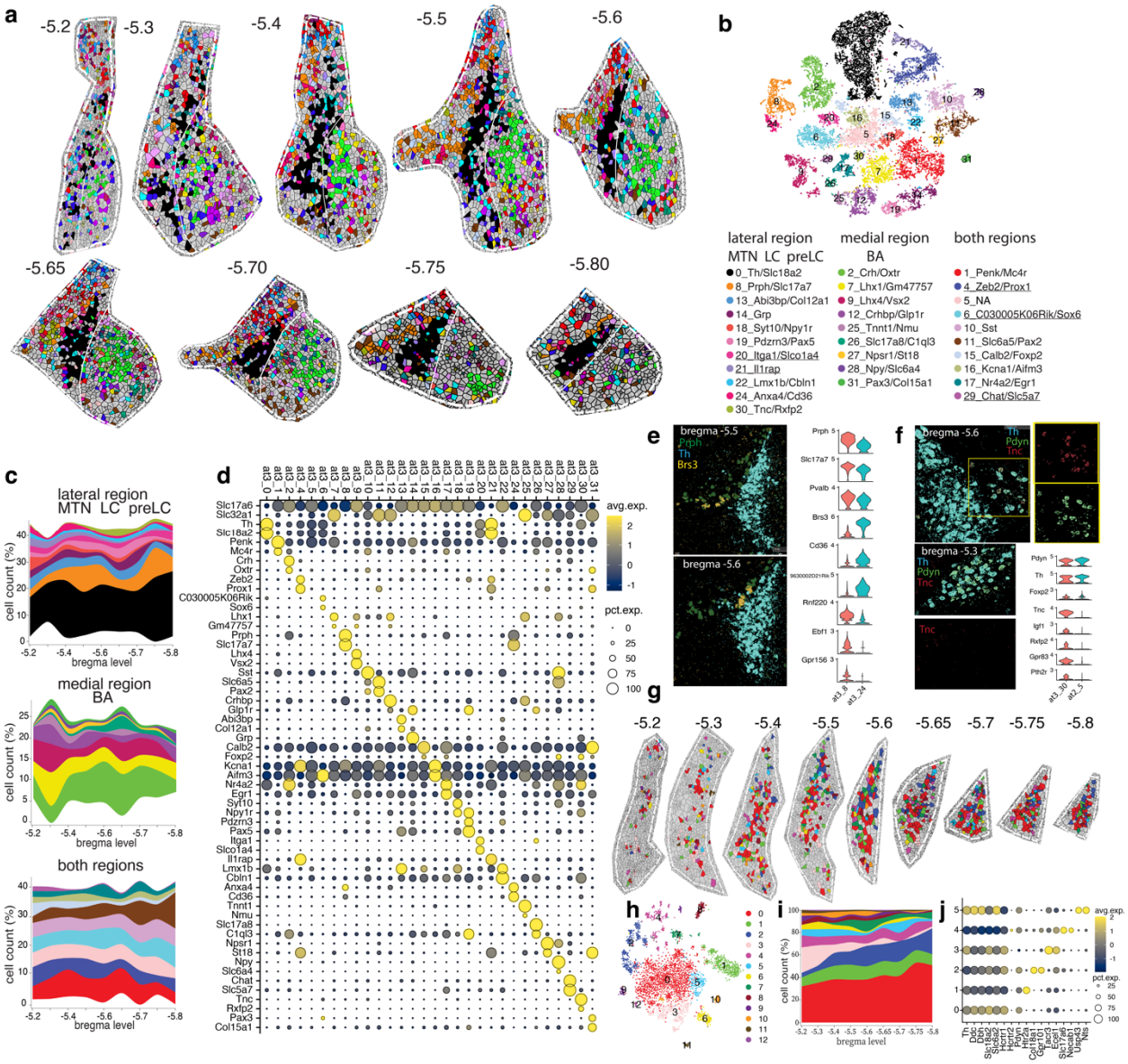
a
-5.2
-5.3
-5.4
-5.5
-5.6
-5.65
-5.70
-5.75
-5.80
b
lateral region
MTN LC preLC
medial region
BA
both regions
0_Th/Slc18a2
8_Prph/Slc17a7
13_Abi3bp/Col12a1
14_Grp
18_Syt10/Npy1r
19_Pdzrn3/Pax5
20_Itga1/Slco1a4
21_Il1rap
22_Lmx1b/Cbln1
24_Anxa4/Cd36
30_Tnc/Rxfp2
2_Crh/Oxtr
7_Lhx1/Gm47757
9_Lhx4/Vsx2
12_Crhbp/Glp1r
25_Tnnt1/Nmu
26_Slc17a8/C1ql3
27_Npsr1/St18
28_Npy/Slc6a4
31_Pax3/Col15a1
1_Penk/Mc4r
4_Zeb2/Prox1
5_NA
6_C030005K06Rik/Sox6
10_Sst
11_Slc6a5/Pax2
15_Calb2/Foxp2
16_Kcna1/Aifm3
17_Nr4a2/Egr1
29_Chat/Slc5a7
c
lateral region
MTN LC preLC
medial region
BA
both regions
cell count (%)
bregma level
d
avg.exp.
pct.exp.
e
bregma -5.5
Prph
Th
Brs3
bregma -5.6
f
bregma -5.6
Th
Pdyn
Tnc
bregma -5.3
g
-5.2
-5.3
-5.4
-5.5
-5.6
-5.65
-5.7
-5.75
-5.8
h
i
j

Figure 5

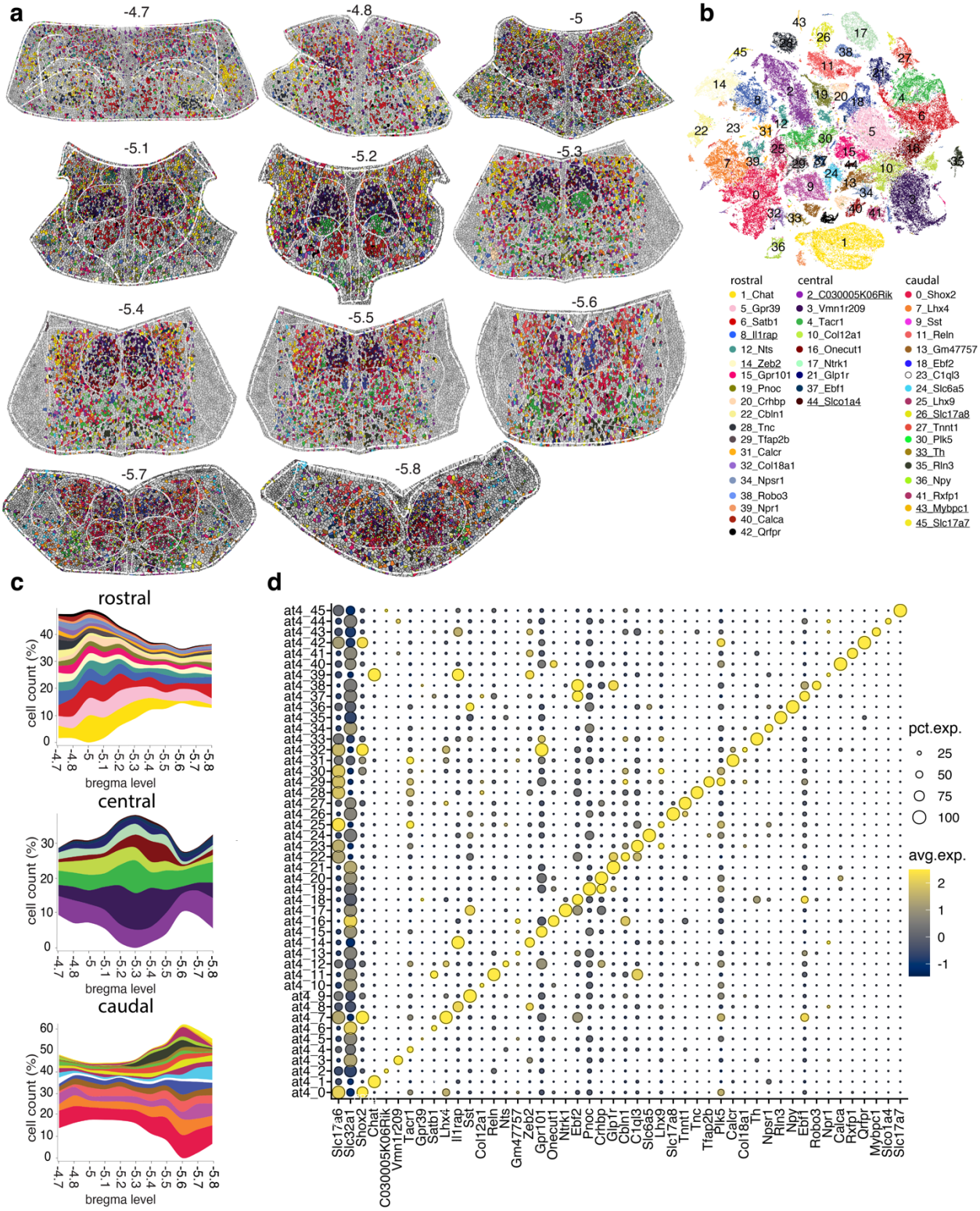
a
-4.7
-4.8
-5
-5.1
-5.2
-5.3
-5.4
-5.5
-5.6
-5.7
-5.8
b
rostral
1_Chat
5_Gpr39
6_Satb1
8_Il1rap
12_Nts
14_Zeb2
15_Gpr101
19_Pnoc
20_Crhbp
22_Cbln1
28_Tnc
29_Tfap2b
31_Calcr
32_Col18a1
34_Npsr1
38_Robo3
39_Npr1
40_Calca
42_Qrfpr
central
2_C030005K06Rik
3_Vmn1r209
4_Tacr1
10_Col12a1
16_Onecut1
17_Ntrk1
21_Glp1r
37_Ebf1
44_Slco1a4
caudal
0_Shox2
7_Lhx4
9_Sst
11_Reln
13_Gm47757
18_Ebf2
23_C1ql3
24_Slc6a5
25_Lhx9
26_Slc17a8
27_Tnnt1
30_Plk5
33_Th
35_Rln3
36_Npy
41_Rxfp1
43_Mybpc1
45_Slc17a7
c
rostral
central
caudal
cell count (%)
bregma level
d
pct.exp.
25
50
75
100
avg.exp.
2
1
0
-1

Figure 6

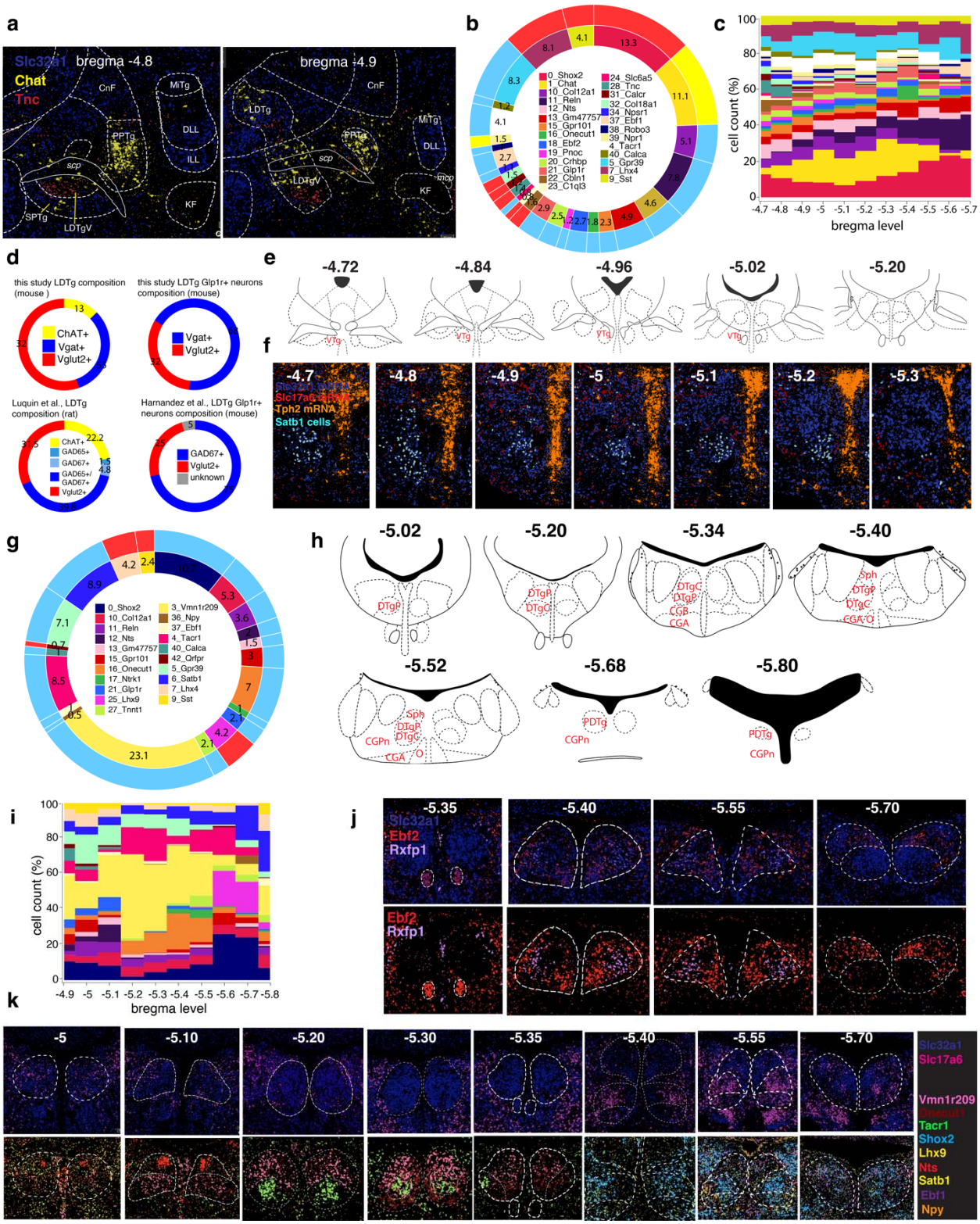
a
Slc32a1
Chat
Tnc
bregma -4.8
bregma -4.9
CnF
MiTg
PPTg
DLL
ILL
scp
KF
SPTg
LDTgV
LDTg
mcp
b
0_Shox2
1_Chat
10_Col12a1
11_Reln
12_Nts
13_Gm47757
15_Gpr101
16_Onecut1
18_Ebf2
19_Pnoc
20_Crhbp
21_Glp1r
22_Cbln1
23_C1ql3
24_Slc6a5
26_Tnc
31_Calcr
32_Col18a1
34_Npsr1
37_Ebf1
38_Robo3
39_Npr1
4_Tacr1
40_Calca
5_Gpr39
7_Lhx4
9_Sst
c
cell count (%)
bregma level
d
this study LDTg composition (mouse)
this study LDTg Glp1r+ neurons composition (mouse)
ChAT+
Vgat+
Vglut2+
Vgat+
Vglut2+
Luquin et al., LDTg composition (rat)
Harnandez et al., LDTg Glp1r+ neurons composition (mouse)
ChAT+
GAD65+
GAD67+
GAD65+/ GAD67+
Vglut2+
GAD67+
Vglut2+
unknown
e
-4.72
-4.84
-4.96
-5.02
-5.20
VTg
f
-4.7
-4.8
-4.9
-5
-5.1
-5.2
-5.3
Slc17a6 mRNA
Tph2 mRNA
Satb1 cells
g
0_Shox2
10_Col12a1
11_Reln
12_Nts
13_Gm47757
15_Gpr101
16_Onecut1
17_Ntrk1
21_Glp1r
25_Lhx9
27_Tnnt1
3_Vmn1r209
36_Npy
37_Ebf1
4_Tacr1
40_Calca
42_Qrfpr
5_Gpr39
6_Satb1
7_Lhx4
9_Sst
h
-5.02
-5.20
-5.34
-5.40
-5.52
-5.68
-5.80
DTgP
DTgC
CGB
CGA
Sph
CGPn
PDTg
i
cell count (%)
bregma level
j
-5.35
-5.40
-5.55
-5.70
Slc32a1
Ebf2
Rxfp1
k
-5
-5.10
-5.20
-5.30
-5.35
-5.40
-5.55
-5.70
Slc32a1
Slc17a6
Vmn1r209
Onecut1
Tacr1
Shox2
Lhx9
Nts
Satb1
Ebf1
Npy

Figure 7

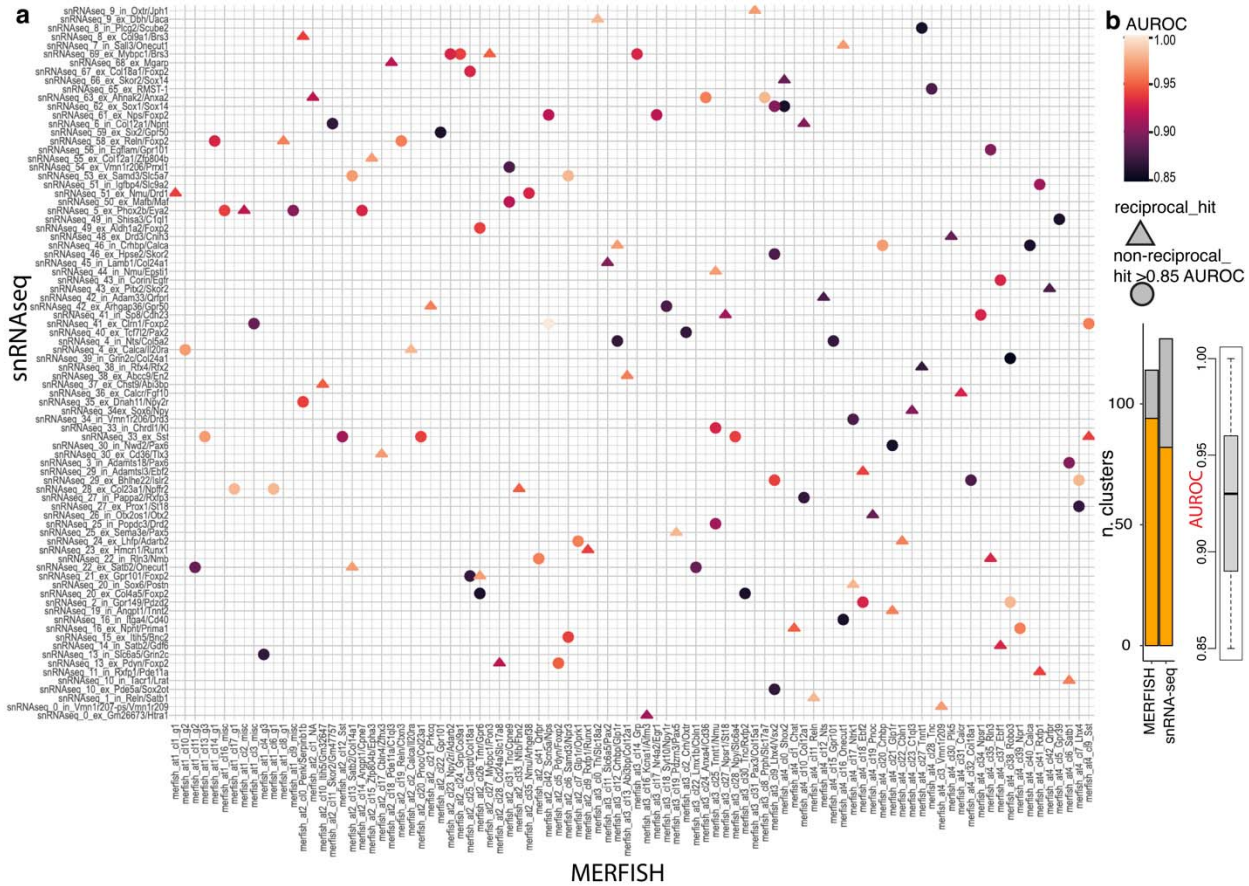

Figure 8

FIGURES LEGENDS

Table1. Brain nuclei abbreviations.

Fig1. snRNA-seq transcriptional profile of the dPnTg. a) Experimental workflow summarized in five main steps: brain dissections, nuclei isolation, snRNA-seq, sequencing, and bioinformatic analyses. **b**) Image illustrating the two dissection strategies relying on the visualization of PB (top) and Bar (bottom). **c)** t-SNE plot of 222,592 nuclei color-coded according to the legend in panel d. **d)** Donut plot representing the fraction (%) of each cell type identified. **e**) Dot plot of 35 cell marker genes that univocally identify each cell type. Three marker genes were plotted for all cell types except for CPE cells, where only the top two were used. **f**-**g**) t-SNE plots showing 47,756 nuclei from the "excitatory" group (f) and 30,771 nuclei from the "inhibitory" group (g) color-coded by cell cluster. The top marker genes that specify the identity of each “excitatory” or “inhibitory” cluster are in panels h and i, respectively. **h-i**) Dot plots illustrating the expression level of the top marker gene for the "excitatory" (h) and "inhibitory" (i) neuronal groups. All differentially expressed genes in the dot plot have an average log fold-change >0.25 and an adjusted p-value <0.01. Test used: *Wilcoxon Rank Sum two-sided Bonferroni-corrected Test*. lPBN/ mPBN parabrachial nucleus lateral/ medial divisions; Bar, Barrington's nucleus; scp, superior cerebellar peduncle; t-SNE, t-distributed Stochastic Neighbor Embedding; OPC, oligodendrocyte progenitor cell; PVM, perivascular macrophages; VSMC, vascular smooth muscle cells; CPE cells, choroid plexus epithelial cells; VLMC1/2, vascular and leptomeningeal

cell type 1/2, Diff.OPC, immature oligodendrocytes; NA, no marker detected; CONT, glia contamination.

Fig2. MERFISH transcriptional profile of the dPnTg a) Experimental workflow summarized in five main steps: brain dissection, MERFISH assay, signal deconvolution, bioinformatic analyses, and data visualization. In total, 7 animals were used, of which 4 represent a complete series of 10 serial coronal sections. **b**) t-SNE plot of 685,289 cells color-coded according to the legend in panel c. **c**) Donut plot depicting the fraction (%) of each cell type identified. **d**) Dot plot of 17 cell markers (y-axis) that univocally identify each cell type (x-axis). For each cell type, two markers were plotted, except for VLMC types I and II, where one marker was used. **e**-**f**) t-SNE of 231,103 cells from the "excitatory" group (e) and 110,332 cells from the "inhibitory" group (f) color-coded by cell cluster. The top two marker genes specify the identity of each cluster as per panels g and h, respectively. **g**-**h**) Dot plot of the expression level of the top marker gene for the "excitatory" (g) and "inhibitory" (h) neuronal clusters. All differentially expressed genes in the dot plot have an average log fold-change >0.25 and an adjusted p-value <0.01. Test used: *Wilcoxon Rank Sum two-sided Bonferroni-corrected Test*. Source Data is provided as a Source Data file. t-SNE, t-distributed Stochastic Neighbor Embedding; OPC, oligodendrocyte progenitor cell; PVM, perivascular macrophages; VSMC, vascular smooth muscle cells; CPE cells, choroid plexus epithelial cells; VLMC1/2, vascular and leptomeningeal cell type 1/2, Diff.OPC, immature oligodendrocytes; NA, no marker detected; CONT, glia contamination.
.

Fig3. Spatially-resolved neuronal atlas of the KF a) Overlay of Franklin-Paxinos atlas anatomic boundaries on MERFISH image depicting *Slc32a1*, *Chat*, *Tfap2b,* and *Calca* transcripts. **b**) Voronoi plots depicting KF cells across 3 bregma levels. Glia/ non-neuronal cells are in grey. **c**) t-SNE plot of 4,554 neurons from the KF. **d**) Donut plot showing the fraction (%) of each neuronal cluster of the KF. **e**) Stacked area chart showing each cluster's cell frequency (*cluster trajectory*) across three bregma levels. **f**) Dot plot showing the top 3 markers for each cluster. Red boxes indicate the five groups. Bold characters indicate KF clusters; other clusters are from neighboring regions. Clusters displayed by the Voronoi, t-SNE, donut plot, and stacked area chart are color-coded according to the legend in panel f. **g**) Heatmap depicting the Pearson's *r* correlation coefficient of the average expression of 315 genes for all possible combinations of the PB cluster at2_2, KF clusters at1_6, at1_10, and at1_11. **h**) Dot Plot of marker genes specific for PB cluster at2_2, all PB clusters except at2_2, KF clusters at1_6, at1_10, and at1_11. **i**) MERFISH images depicting *Calca*, *Prph*, *Col11a1*, *Pou6f2*, and *Chst9* transcripts in the KF at bregma levels -4.8 and -4.9. Green, red, and orange arrows represent high Calca (*Calca*+++/*Pou6f2,* KF cluster at1_10), medium Calca (*Calca*++/ *Chst9,* KF cluster at1_11), and low Calca (*Calca*+/*Col11a1,* KF cluster at1_6) neuronal clusters, respectively. **j**) Donut plot depicting the fraction of *Calca*+ neuronal clusters (clusters at1_6, at1_10, and at1_11) at bregma level -4.8 and -4.9 of the KF. The cluster percentage in plots refers to the images in panel i. All differentially expressed genes in the dot plot have an average log fold-change >0.25 and an adjusted p-value <0.01. Test used: *Wilcoxon Rank Sum two-sided Bonferroni-corrected Test*.

Fig4. Spatially-resolved neuronal atlas of the PB. a) Voronoi plots depicting PB cells across nine sequential MERFISH sections from -4.95 to -5.70 bregma level. Glia/ non-neuronal cells are in grey. **b**) t-SNE plot of 79,413 neurons. **c**) Stacked area charts showing each cluster's cell frequency (*cluster trajectory*) across all nine bregma levels. Clusters displayed by the Voronoi, t-SNE, and stacked area chart are color-coded according to the legend in panel b. Clusters underlined in the legend represent external-to-the-PB neuron types/ glia contamination. **d**) Dot plot of the top 2 markers for each cluster. **e**) Voronoi plots representing neurons from PB cluster

at2_2 across ten sequential coronal sections from bregma level -4.95 to -5.75. Other PB neuronal clusters and glia/ non-neuronal cells are in grey. **f**) t-SNE plot representing 4,504 neurons. **g**) Dot plot depicting the *Calca* gene and the top marker for each *Calca*+ subcluster. **h**) Stacked area chart showing the *cluster trajectory* across the ten sequential MERFISH sections in panel e. Clusters displayed by the Voronoi, t-SNE, and stacked area chart are color-coded according to the legend in panel f. **i**) Left: MERFISH image of *Slc32a1*, *Calca,* and *Slc6a2* transcripts in the PB complex at bregma level -5.15. Right: enlarged view of the *Calca*+ cluster 4. **j**) Left: MERFISH image of *Slc32a1*, *Calca,* and *Qrfpr* transcripts in the PB complex at bregma level -4.95. Right: enlarged view of the *Calca*+ cluster 8. In panels g-h, only clusters composed of >100 cells were included. All differentially expressed genes in the dot plot have an average log fold-change >0.25 and an adjusted p-value <0.01. Test used: *Wilcoxon Rank Sum two-sided Bonferroni-corrected Test;* NA, no marker detected.

Fig5. Spatially-resolved neuronal atlas of the MTN, pre-LC, LC, and Bar. a) Voronoi plots depicting cells of a ROI that includes MTN, pre-LC, LC, and Bar across nine sequential sections, from -5.2 to -5.8 bregma level. Glia/ non-neuronal cells are in grey. **b**) t-SNE plot of 22,358 neurons. **c**) Stacked area chart showing each cluster's cell frequency (*cluster trajectory*) across all 9 MERFISH sections. Clusters displayed by the Voronoi, t-SNE, and stacked area chart are color-coded according to the legend in panel b. Clusters underlined in the legend represent external-to-the-ROI neuron types/ glia contamination. **d**) Dot plot of the top two markers for each cluster. **e**) Left: MERFISH image showing the spatial distribution of *Prph*, *Th,* and *Brs3* at bregma levels -5.5 and -5.6. Right: violin plots depicting the average expression level (y-axis) of 9 genes in clusters at3_8 and at3_24 (x-axis). **f**) Left: MERFISH image showing the spatial distribution for *Th*, *Pdyn,* and *Tnc* in bregma levels -5.6 and -5.3 in the pre-LC (top) and LPBD (bottom). Right: violin plots depicting the expression level (y-axis) of eight genes in clusters at3_30 (pre-LC) and at2_5 (LPBD) (x-axis). **g**) Voronoi plots depicting LC noradrenergic neurons across nine sequential MERFISH sections from -5.2 to -5.8 bregma level. Other ROI's neuronal clusters and glia/ non-neuronal cells are in grey. **h**) t-SNE plot of 4,074 noradrenergic neurons **i**) Stacked area chart showing each cluster's cell frequency (*cluster trajectory*) across nine sequential MERFISH sections in panel g. Clusters displayed by the Voronoi, t-SNE, and stacked area chart are color-coded according to the legend in panel h. **j**) Dot plot depicting *Th*, *Ddc*, *Dbh*, *Slc18a2*, *Slc6a2, Hcrtr1,* and *Hcrtr2* genes and the top 2 marker genes for each subcluster. In panels i-j, only clusters composed of >200 cells were included. All differentially expressed genes in the dot plot have an average log fold-change >0.25 and an adjusted p-value <0.01. Test used: *Wilcoxon Rank Sum two-sided Bonferroni-corrected Test;* NA, no marker detected.

Fig6. Spatially-resolved neuronal atlas of LDTg, DTg, VTg, Sph, NI, CGA, CGB, and CGPn. a) Voronoi plots depicting cells of a ROI that includes LDTg, DTg, VTg, Sph, NI, CGA, CGB, and CGPn across 11 sequential sections from -4.7 to -5.8 bregma level. Glia/ non-neuronal cells are in grey. **b**) t-SNE plot of 120,182 neurons. **c**) Stacked area charts showing each cluster's cell frequency (*cluster trajectory*) across all 11 MERFISH sections. Clusters displayed by the Voronoi, t-SNE, and stacked area chart are color-coded according to the legend in panel b. Clusters underlined in the legend represent external-to-the-ROI neuron types/ glia contamination. **d**) Dot plot of the top marker for each cluster. All differentially expressed genes in the dot plot have an average log fold-change >0.25 and an adjusted p-value <0.01. Test used: *Wilcoxon Rank Sum two-sided Bonferroni-corrected Test*. Source Data are provided as Source Data files; NA, no marker detected.

Fig7. In-depth characterization of the LDTg, VTg, DTg, and Sph. a) Overlay of Franklin-Paxinos atlas anatomic boundaries on MERFISH image depicting *Slc32a1*, *Chat*, and *Tnc*

transcripts. **b**) Donut plots: the inner plot shows the overall contribution (%) of each cluster to the total LDTg/ LDTgV neurons; the outer plot classifies the clusters as glutamatergic (red), GABAergic (light blue) and cholinergic (yellow). **c**) Stacked area charts of the LDTg/ LDTgV cluster trajectory. Clusters are color-coded according to the legend in panel b. **d**) Left: donut plot showing the LDTg cell partition in glutamatergic (red), GABAergic (blue), and cholinergic (yellow) in this study and as reported by Luquin et al. Right: estimation of *Glp1r+*/*Slc32a1+* and *Glp1+r*/*Slc17a6+* cells in mouse LDTg by this study and as reported by Hernandez et al. **e**) Schematic from the Paxinos atlas showing the VTg anatomical location. **f**) MERFISH image showing cluster at4_6 (VTg neurons; cyan polygons) along with *Slc32a1*, *Slc17a6,* and *Tph2* transcripts. **g**) Donut plots: the inner plot shows the overall contribution (%) of each cluster to the total DTg neurons; the outer plot classifies the clusters as glutamatergic (red) and GABAergic (light blue). **h**) Schematic from the Franklin-Paxinos atlas showing the DTg, Sph, NI, CGA, and CGB anatomical location from -5.02 to -5.8 bregma level. For panels e and h, abbreviations refer to Table 1. **i**) Stacked area charts of the DTg cluster trajectory. Clusters are color-coded according to the legend in panel g. **j**) Overlay of Franklin-Paxinos atlas anatomic boundaries on MERFISH images depicting *Slc32a1, Ebf2,* and *Rfxfp1* (top) and *Ebf2* and *Rfxp1* marker genes (bottom) in the Sph. **k**) Overlay of Franklin-Paxinos atlas anatomic boundaries on MERFISH images depicting *Slc32a1* and *Slc17a6* (top) and nine marker genes (bottom) in the DTg across the same rostrocaudal levels. Legend is on the right side of both panels. In panels (b) and (g), only clusters contributing >0.5 % to the overall neuronal population were plotted. Source Data are provided as Source Data files.

Fig8. Cluster correspondence between mouse snRNA-seq and MERFISH data. a) Heatmap depicting the cluster correspondence between snRNA-seq and MERFISH data of the dPnTg. Legend defining the AUROC score and the “match type” (reciprocal vs non-reciprocal) is on the right side of panel a. **b**) Left: stacked bar plot showing the number of clusters with a match (orange) over the total clusters (grey) identified by MERFISH (atlases 1-4) and snRNA-seq approaches. Right: boxplot showing the AUROC scores distribution. Highlighted in black is the median. Source Data is provided as a Source Data file. AUROC, area under the receiver operator characteristic curve; NA, no marker detected; CONT, glia contamination.

SUPPLEMENTARY FIGURES AND LEGENDS

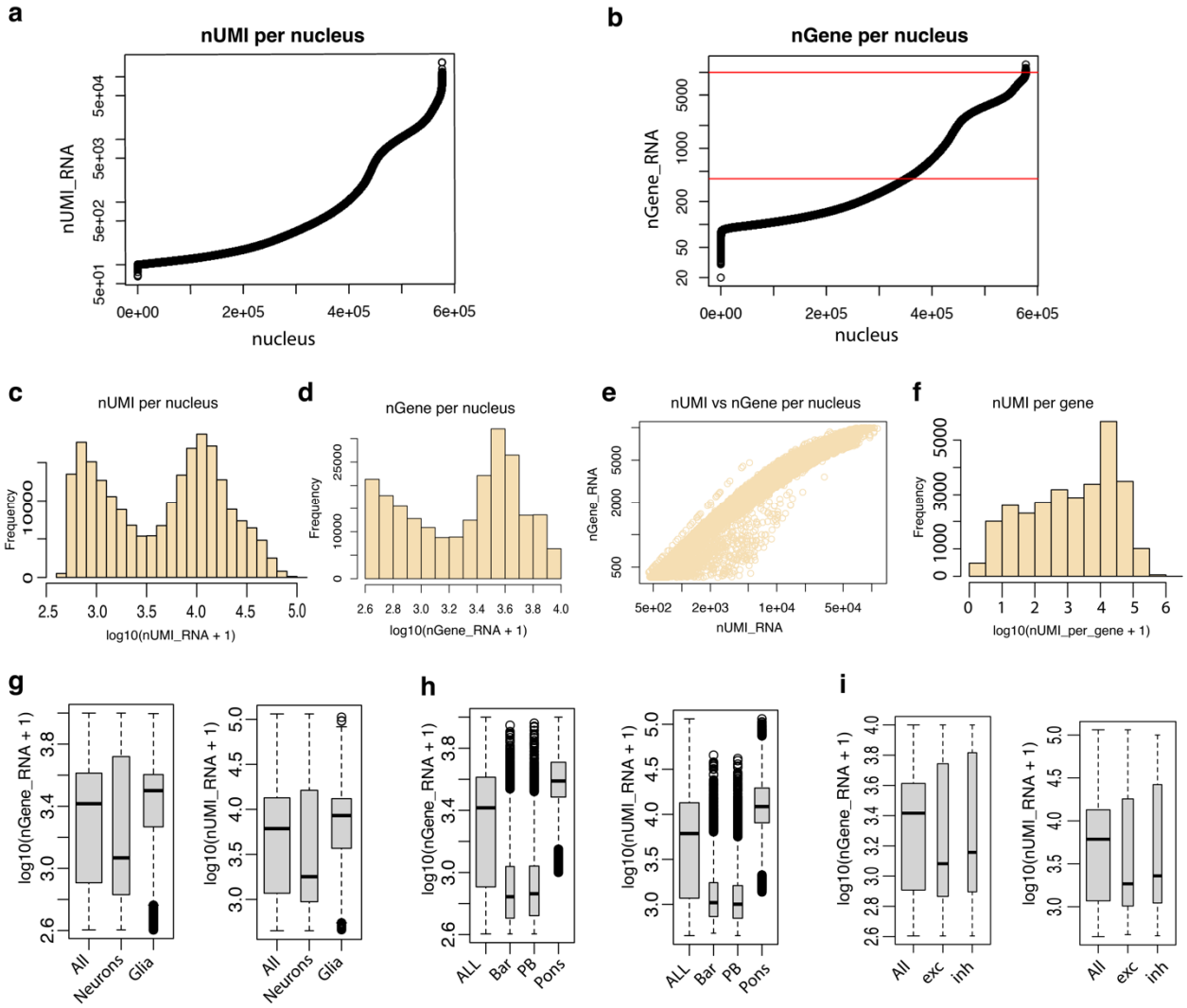

SFigure 1

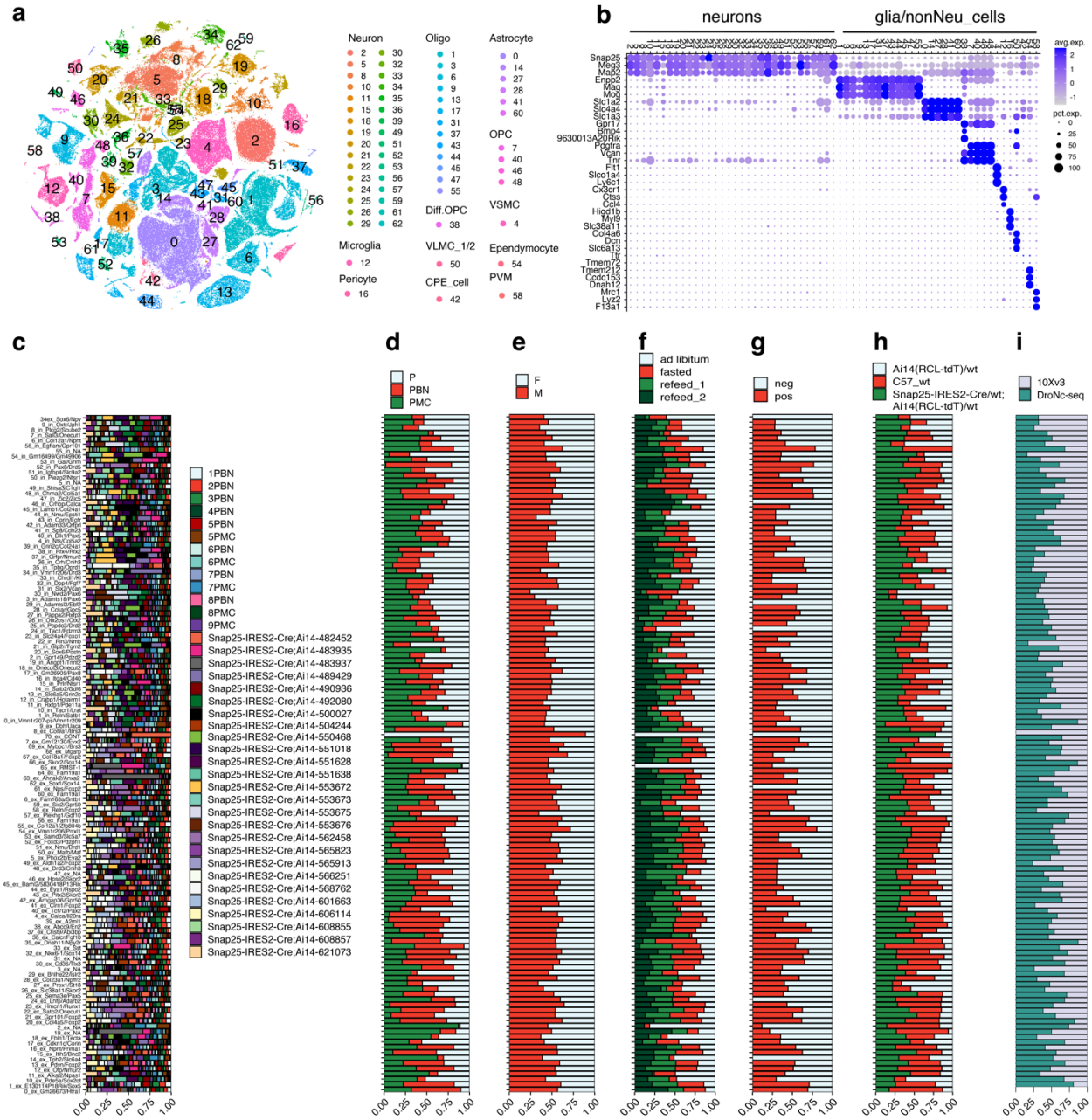
a
Neuron
Oligo
Astrocyte
OPC
Diff.OPC
VSMC
Microglia
VLMC_1/2
Ependymocyte
Pericyte
CPE_cell
PVM
b
neurons
glia/nonNeu_cells
avg.exp.
pct.exp.
c
d
P
PBN
PMC
e
F
M
f
ad libitum
fasted
refeed_1
refeed_2
g
neg
pos
h
Ai14(RCL-tdT)/wt
C57_wt
Snap25-IRES2-Cre/wt;
Ai14(RCL-tdT)/wt
i
10Xv3
DroNc-seq

SFigure 2

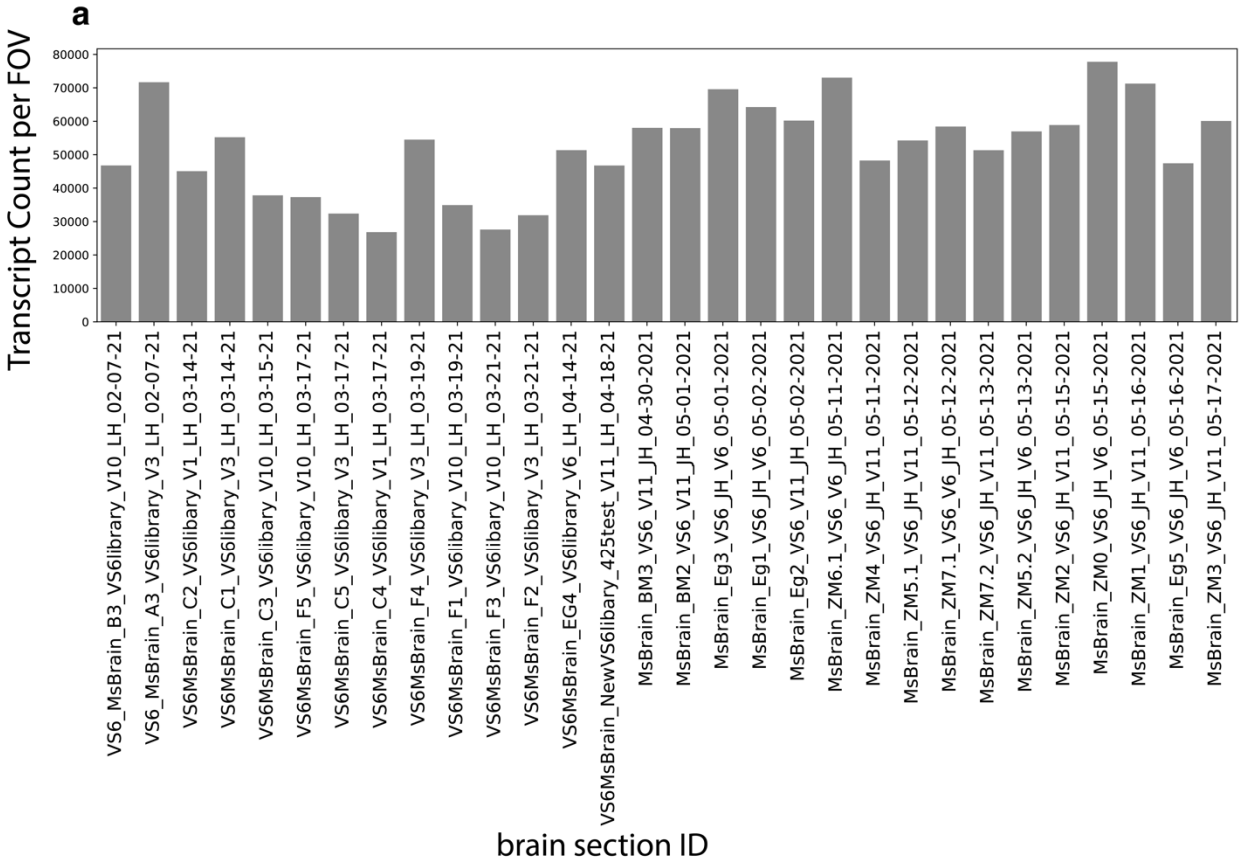
a
Transcript Count per FOV
80000
70000
60000
50000
40000
30000
20000
10000
0
VS6_MsBrain_B3_VS6library_V10_LH_02-07-21
VS6_MsBrain_A3_VS6library_V3_LH_02-07-21
VS6MsBrain_C2_VS6library_V1_LH_03-14-21
VS6MsBrain_C1_VS6library_V3_LH_03-14-21
VS6MsBrain_C3_VS6library_V10_LH_03-15-21
VS6MsBrain_F5_VS6library_V10_LH_03-17-21
VS6MsBrain_C5_VS6library_V3_LH_03-17-21
VS6MsBrain_C4_VS6library_V1_LH_03-17-21
VS6MsBrain_F4_VS6library_V3_LH_03-19-21
VS6MsBrain_F1_VS6library_V10_LH_03-19-21
VS6MsBrain_F3_VS6library_V10_LH_03-21-21
VS6MsBrain_F2_VS6library_V3_LH_03-21-21
VS6MsBrain_EG4_VS6library_V6_LH_04-14-21
VS6MsBrain_NewVS6libary_425test_V11_LH_04-18-21
MsBrain_BM3_VS6_V11_JH_04-30-2021
MsBrain_BM2_VS6_V11_JH_05-01-2021
MsBrain_Eg3_VS6_JH_V6_05-01-2021
MsBrain_Eg1_VS6_JH_V6_05-02-2021
MsBrain_Eg2_VS6_V11_JH_05-02-2021
MsBrain_ZM6.1_VS6_V6_JH_05-11-2021
MsBrain_ZM4_VS6_JH_V11_05-11-2021
MsBrain_ZM5.1_VS6_JH_V11_05-12-2021
MsBrain_ZM7.1_VS6_V6_JH_05-12-2021
MsBrain_ZM7.2_VS6_JH_V11_05-13-2021
MsBrain_ZM5.2_VS6_JH_V6_05-13-2021
MsBrain_ZM2_VS6_JH_V11_05-15-2021
MsBrain_ZM0_VS6_JH_V6_05-15-2021
MsBrain_ZM1_VS6_JH_V11_05-16-2021
MsBrain_Eg5_VS6_JH_V6_05-16-2021
MsBrain_ZM3_VS6_JH_V11_05-17-2021
brain section ID

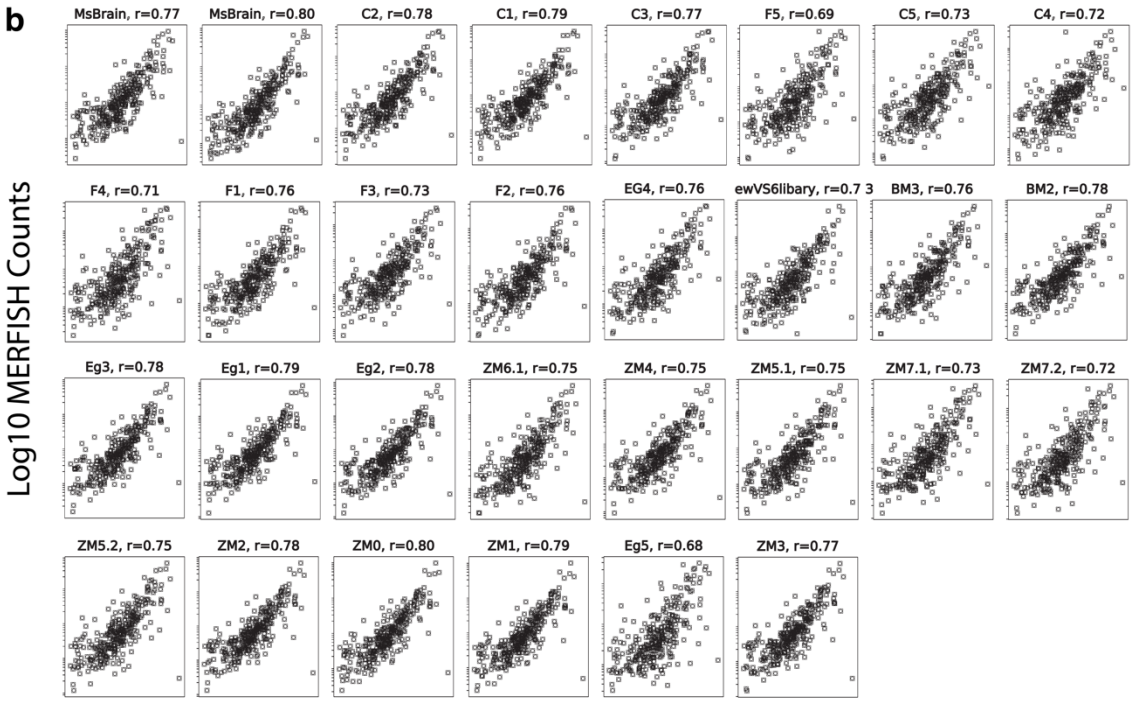
b
Log10 MERFISH Counts
MsBrain, r=0.77
MsBrain, r=0.80
C2, r=0.78
C1, r=0.79
C3, r=0.77
F5, r=0.69
C5, r=0.73
C4, r=0.72
F4, r=0.71
F1, r=0.76
F3, r=0.73
F2, r=0.76
EG4, r=0.76
ewVS6libary, r=0.7 3
BM3, r=0.76
BM2, r=0.78
Eg3, r=0.78
Eg1, r=0.79
Eg2, r=0.78
ZM6.1, r=0.75
ZM4, r=0.75
ZM5.1, r=0.75
ZM7.1, r=0.73
ZM7.2, r=0.72
ZM5.2, r=0.75
ZM2, r=0.78
ZM0, r=0.80
ZM1, r=0.79
Eg5, r=0.68
ZM3, r=0.77

SFigure 3

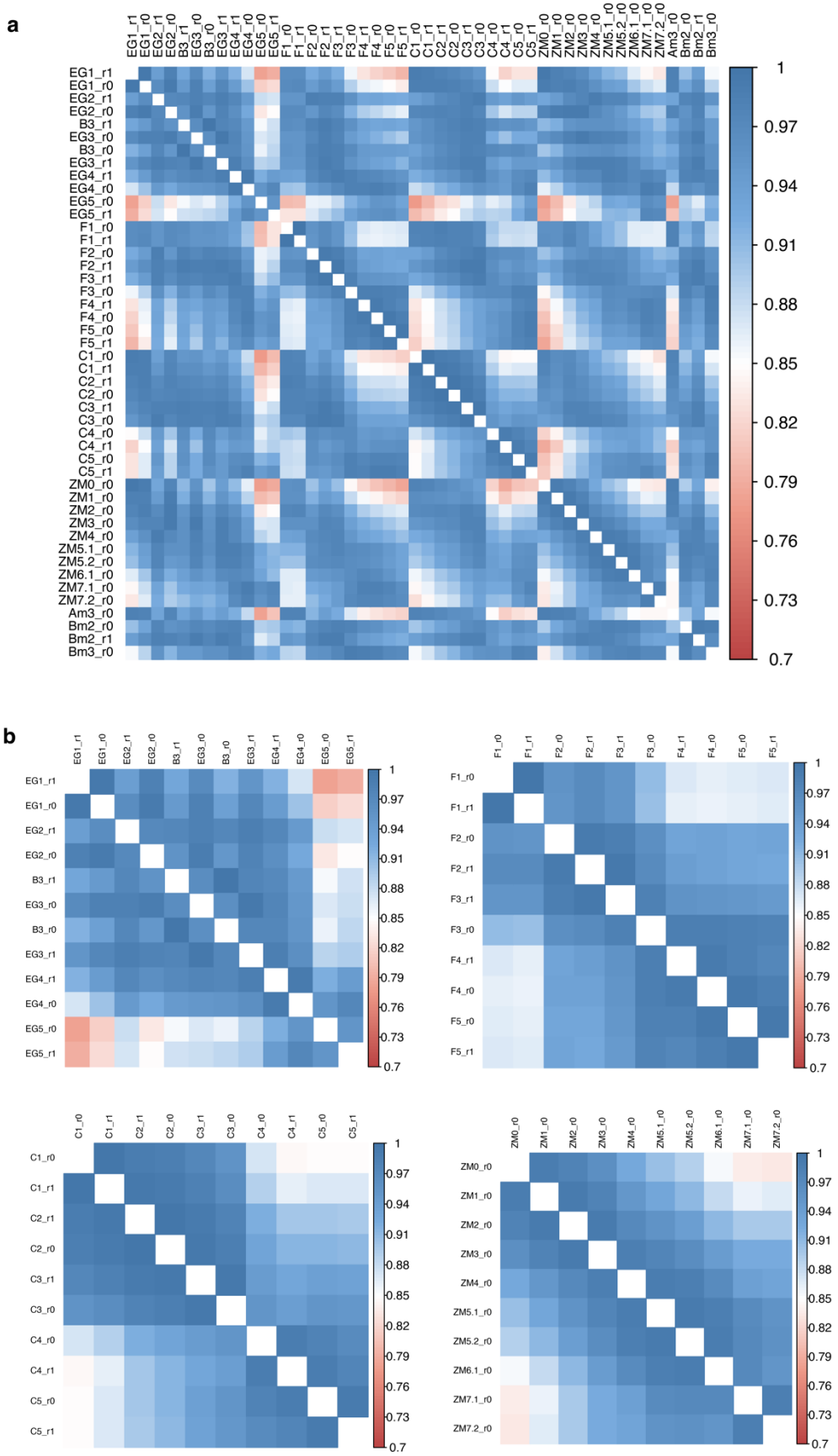
a
EG1_r1
EG1_r0
EG2_r1
EG2_r0
B3_r1
EG3_r0
B3_r0
EG3_r1
EG4_r1
EG4_r0
EG5_r0
EG5_r1
F1_r0
F1_r1
F2_r0
F2_r1
F3_r1
F3_r0
F4_r1
F4_r0
F5_r0
F5_r1
C1_r0
C1_r1
C2_r1
C2_r0
C3_r1
C3_r0
C4_r0
C4_r1
C5_r0
C5_r1
ZM0_r0
ZM1_r0
ZM2_r0
ZM3_r0
ZM4_r0
ZM5.1_r0
ZM5.2_r0
ZM6.1_r0
ZM7.1_r0
ZM7.2_r0
Am3_r0
Bm2_r0
Bm2_r1
Bm3_r0
1
0.97
0.94
0.91
0.88
0.85
0.82
0.79
0.76
0.73
0.7
b

9 **SFigure 4**

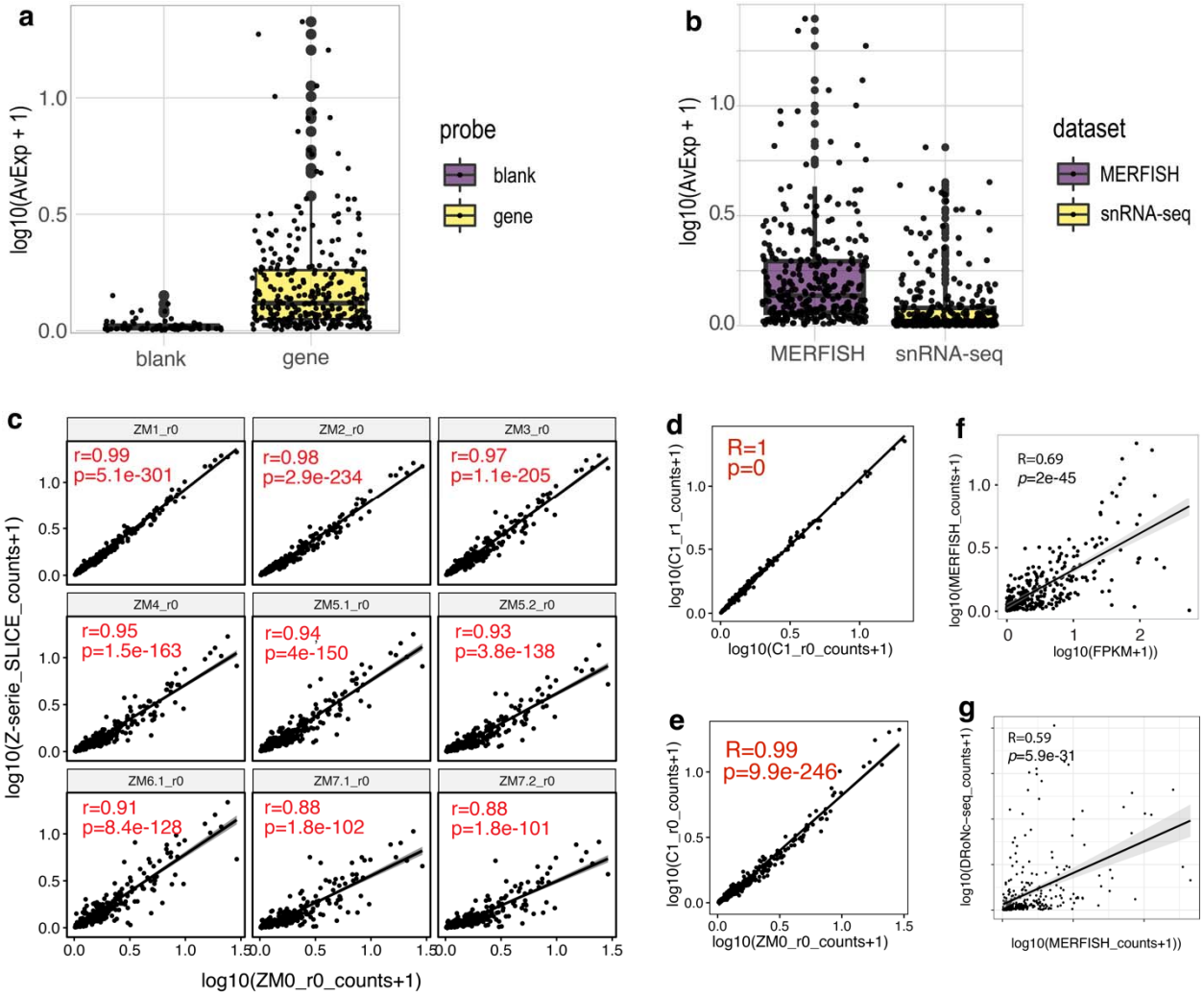
a
log10(AvExp + 1)
blank
gene
probe
blank
gene
b
log10(AvExp + 1)
MERFISH
snRNA-seq
dataset
MERFISH
snRNA-seq
c
ZM1_r0
r=0.99
p=5.1e-301
ZM2_r0
r=0.98
p=2.9e-234
ZM3_r0
r=0.97
p=1.1e-205
ZM4_r0
r=0.95
p=1.5e-163
ZM5.1_r0
r=0.94
p=4e-150
ZM5.2_r0
r=0.93
p=3.8e-138
ZM6.1_r0
r=0.91
p=8.4e-128
ZM7.1_r0
r=0.88
p=1.8e-102
ZM7.2_r0
r=0.88
p=1.8e-101
log10(Z-serie_SLICE_counts+1)
log10(ZM0_r0_counts+1)
d
R=1
p=0
log10(C1_r1_counts+1)
log10(C1_r0_counts+1)
e
R=0.99
p=9.9e-246
log10(C1_r0_counts+1)
log10(ZM0_r0_counts+1)
f
R=0.69
p=2e-45
log10(MERFISH_counts+1)
log10(FPKM+1))
g
R=0.59
p=5.9e-31
log10(DRoNc-seq_counts+1)
log10(MERFISH_counts+1))

SFigure 5

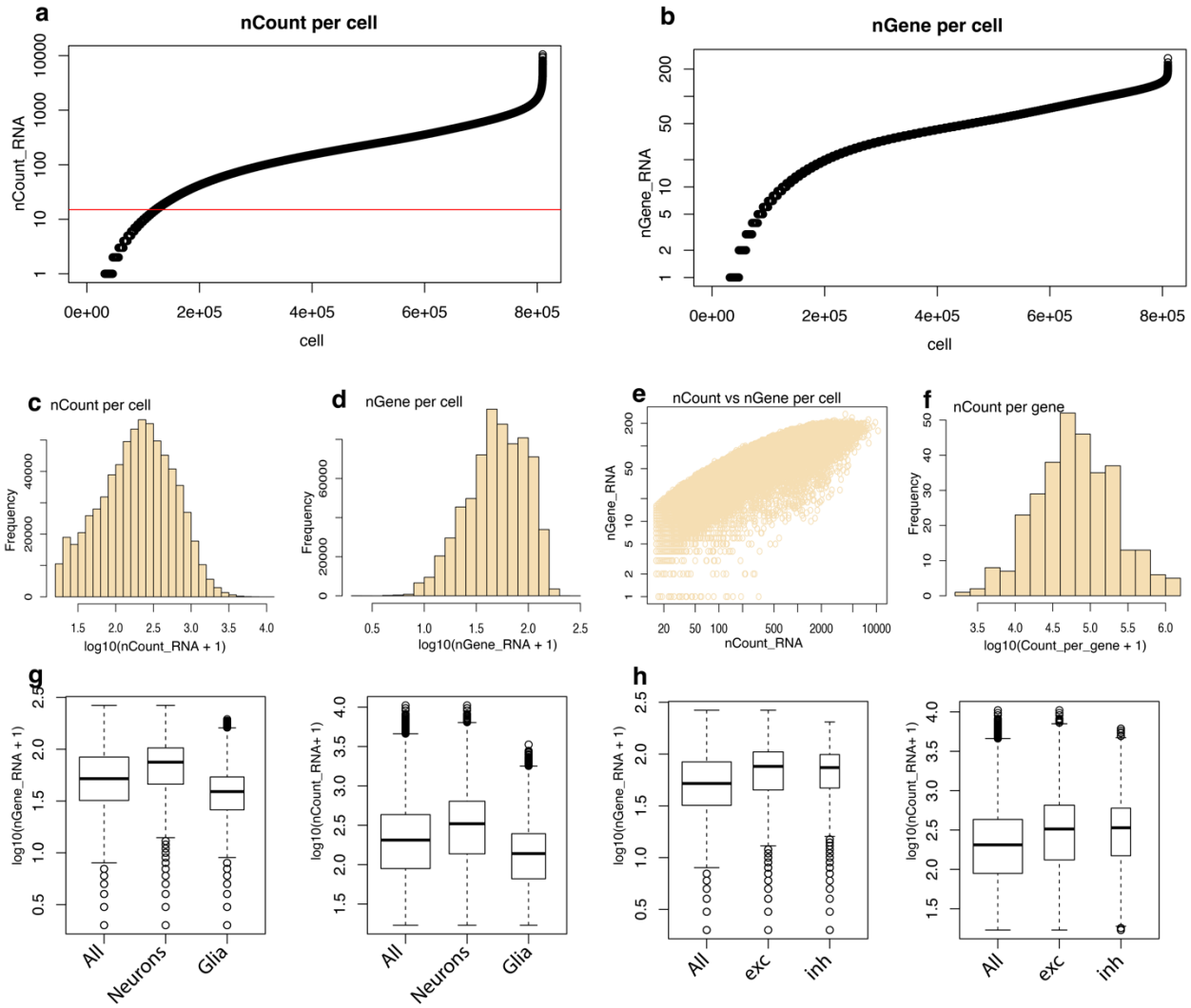
a
nCount per cell
nCount_RNA
cell
b
nGene per cell
nGene_RNA
cell
c
nCount per cell
Frequency
log10(nCount_RNA + 1)
d
nGene per cell
Frequency
log10(nGene_RNA + 1)
e
nCount vs nGene per cell
nGene_RNA
nCount_RNA
f
nCount per gene
Frequency
log10(Count_per_gene + 1)
g
log10(nGene_RNA + 1)
All
Neurons
Glia
log10(nCount_RNA+ 1)
All
Neurons
Glia
h
log10(nGene_RNA + 1)
All
exc
inh
log10(nCount_RNA+ 1)
All
exc
inh

SFigure 6

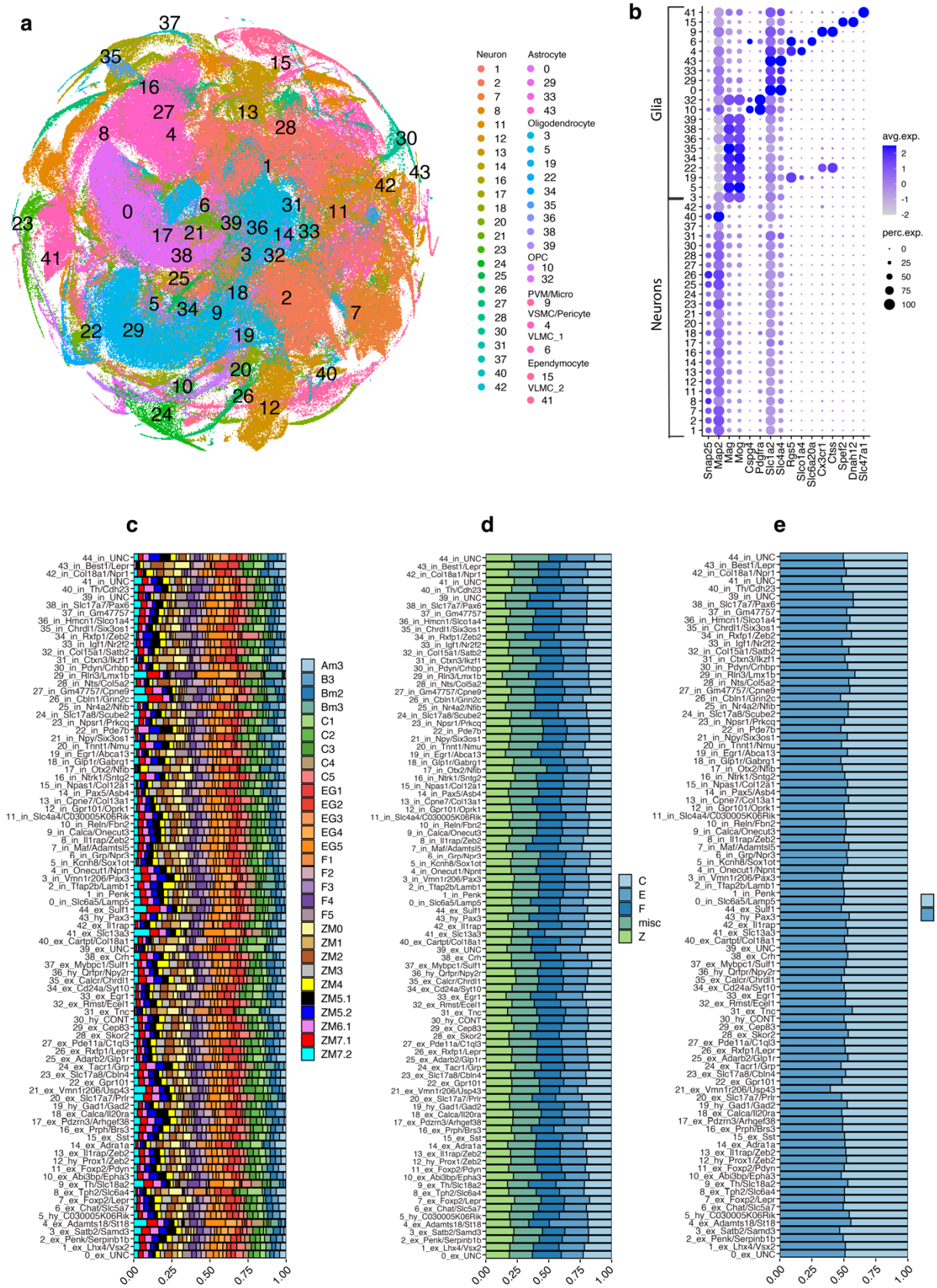
a
Neuron
Astrocyte
Oligodendrocyte
OPC
PVM/Micro
VSMC/Pericyte
VLMC_1
Ependymocyte
VLMC_2
b
Glia
Neurons
avg.exp.
perc.exp.
Snap25
Map2
Mag
Mog
Cspg4
Pdgfra
Slc1a2
Slc4a4
Rgs5
Slco1a4
Slc6a20a
Cxcr1
Ccr1
Spef2
Dnah12
Slc47a1
c
d
e
Am3
B3
Bm2
Bm3
C1
C2
C3
C4
C5
EG1
EG2
EG3
EG4
EG5
F1
F2
F3
F4
F5
ZM0
ZM1
ZM2
ZM3
ZM4
ZM5.1
ZM5.2
ZM6.1
ZM7.1
ZM7.2
C
E
F
misc
Z
M
F
0.00
0.25
0.50
0.75
1.00

SFigure 7

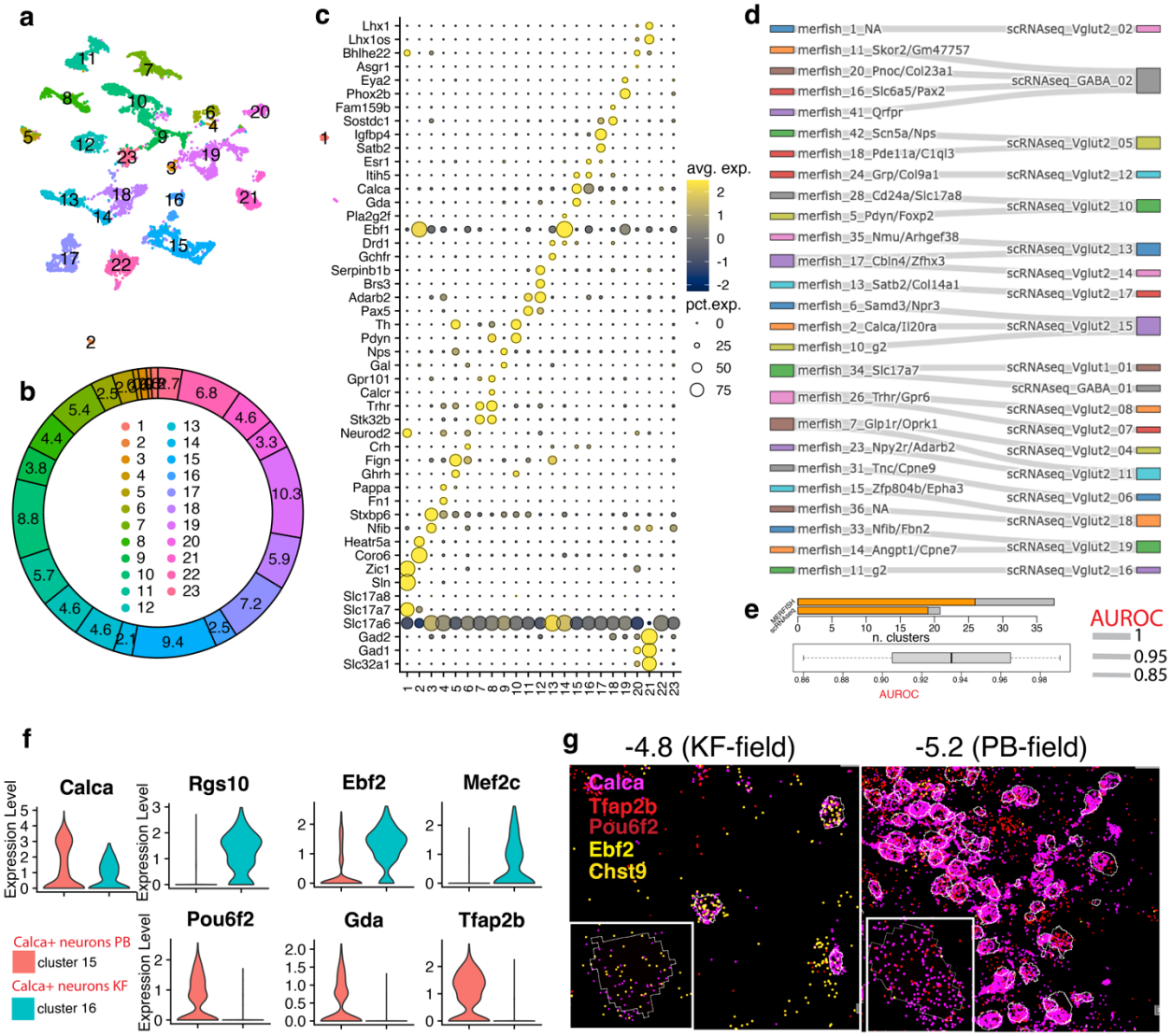
a
b
c
d
e
f
g
avg. exp.
pct.exp.
n. clusters
AUROC
merfish_1_NA
merfish_11_Skor2/Gm47757
merfish_20_Pnoc/Col23a1
merfish_16_Slc6a5/Pax2
merfish_41_Qrfpr
merfish_42_Scn5a/Nps
merfish_18_Pde11a/C1ql3
merfish_24_Grp/Col9a1
merfish_28_Cd24a/Slc17a8
merfish_5_Pdyn/Foxp2
merfish_35_Nmu/Arhgef38
merfish_17_Cbln4/Zfhx3
merfish_13_Satb2/Col14a1
merfish_6_Samd3/Npr3
merfish_2_Calca/Il20ra
merfish_10_g2
merfish_34_Slc17a7
merfish_26_Trhr/Gpr6
merfish_7_Glp1r/Oprk1
merfish_23_Npy2r/Adarb2
merfish_31_Tnc/Cpne9
merfish_15_Zfp804b/Epha3
merfish_36_NA
merfish_33_Nfib/Fbn2
merfish_14_Angpt1/Cpne7
merfish_11_g2
scRNAseq_Vglut2_02
scRNAseq_GABA_02
scRNAseq_Vglut2_05
scRNAseq_Vglut2_12
scRNAseq_Vglut2_10
scRNAseq_Vglut2_13
scRNAseq_Vglut2_14
scRNAseq_Vglut2_17
scRNAseq_Vglut2_15
scRNAseq_Vglut1_01
scRNAseq_GABA_01
scRNAseq_Vglut2_08
scRNAseq_Vglut2_07
scRNAseq_Vglut2_04
scRNAseq_Vglut2_11
scRNAseq_Vglut2_06
scRNAseq_Vglut2_18
scRNAseq_Vglut2_19
scRNAseq_Vglut2_16
Calca
Rgs10
Ebf2
Mef2c
Pou6f2
Gda
Tfap2b
Expression Level
Calca+ neurons PB
cluster 15
Calca+ neurons KF
cluster 16
-4.8 (KF-field)
-5.2 (PB-field)
Calca
Tfap2b
Pou6f2
Ebf2
Chst9

SFigure 8

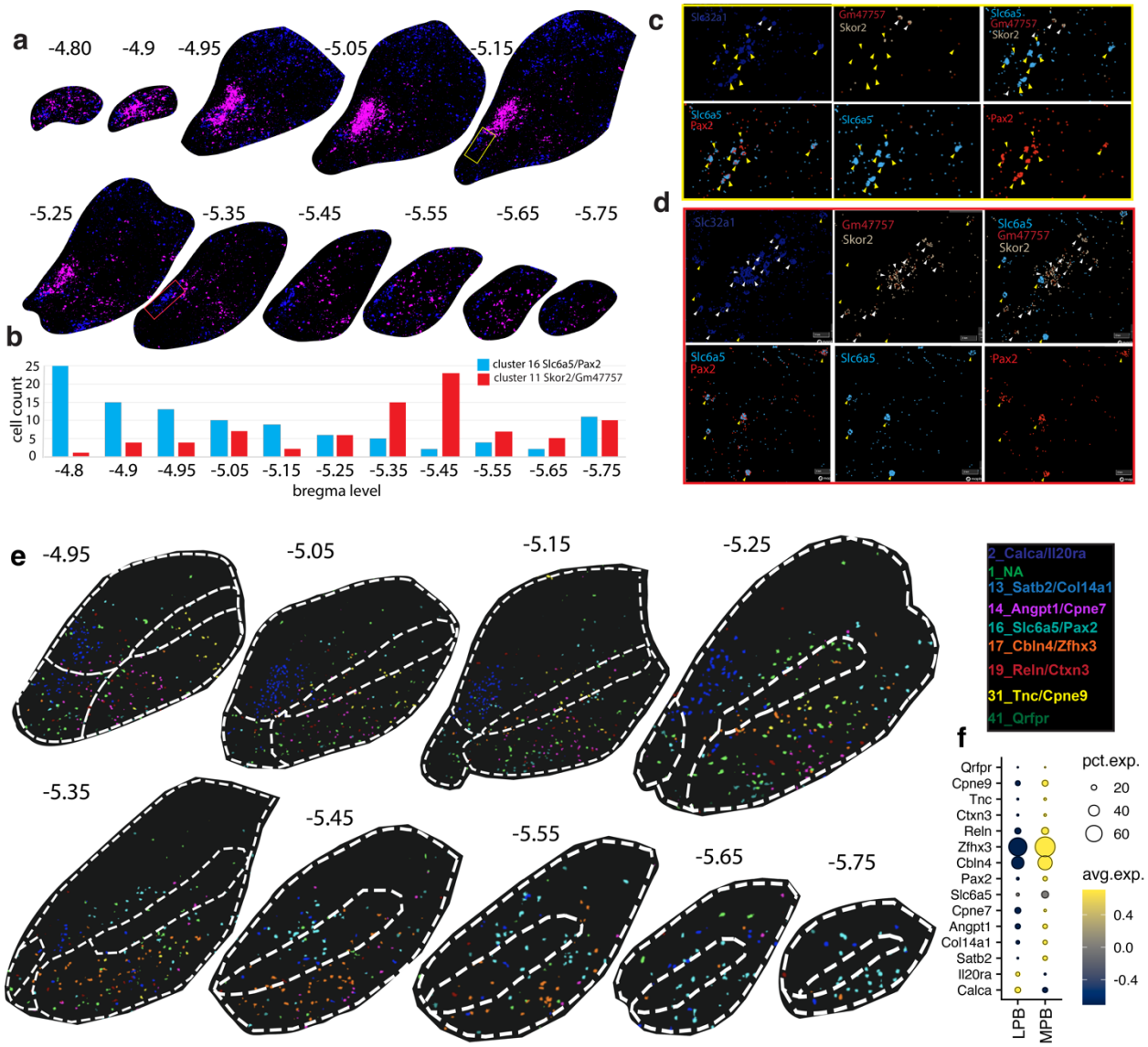
a
-4.80
-4.9
-4.95
-5.05
-5.15
-5.25
-5.35
-5.45
-5.55
-5.65
-5.75
b
cell count
cluster 16 Slc6a5/Pax2
cluster 11 Skor2/Gm47757
bregma level
c
d
Slc32a1
Gm47757
Skor2
Slc6a5
Pax2
e
2_Calca/Il20ra
1_NA
13_Satb2/Col14a1
14_Angpt1/Cpne7
16_Slc6a5/Pax2
17_Cbln4/Zfhx3
19_Reln/Ctxn3
31_Tnc/Cpne9
41_Qrfpr
f
Qrfpr
Cpne9
Tnc
Ctxn3
Reln
Zfhx3
Cbln4
Pax2
Slc6a5
Cpne7
Angpt1
Col14a1
Satb2
Il20ra
Calca
LPB
MPB
pct.exp.
avg.exp.

SFigure 9

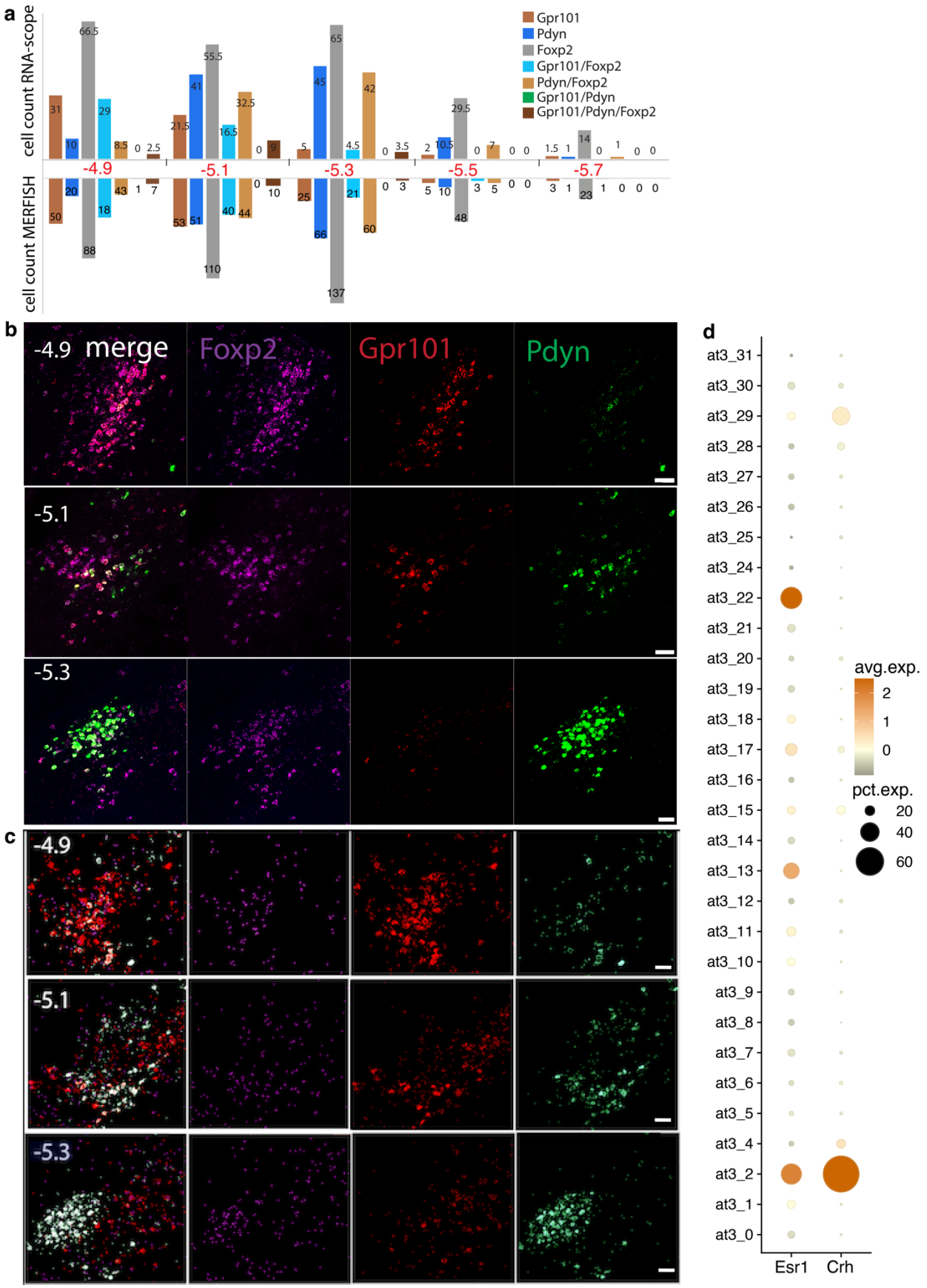

17 **SFigure 10**

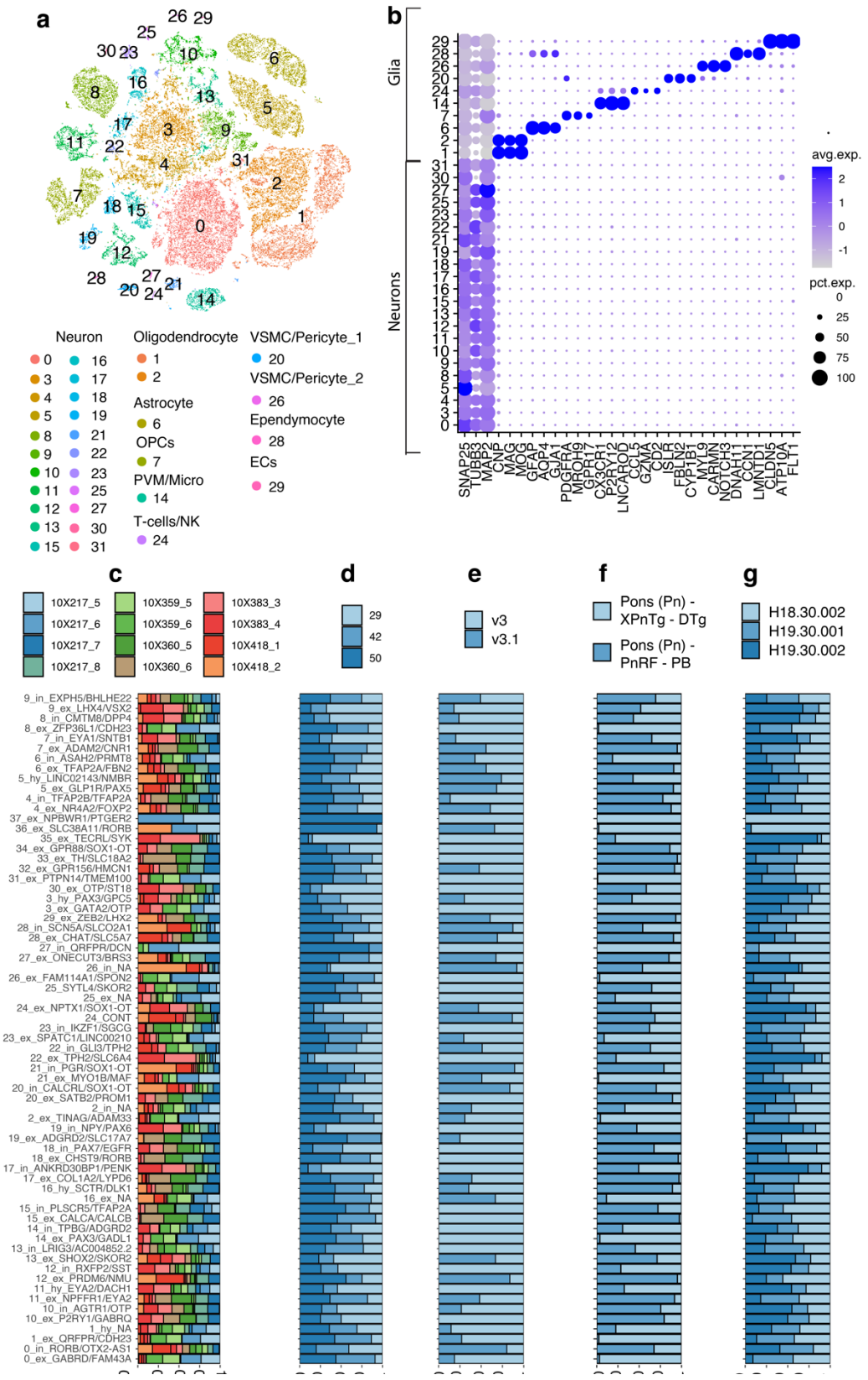
a
b
Glia
Neurons
avg.exp.
pct.exp.
Neuron
Oligodendrocyte
VSMC/Pericyte_1
VSMC/Pericyte_2
Astrocyte
Ependymocyte
OPCs
ECs
PVM/Micro
T-cells/NK
c
d
e
f
g
10X217_5
10X217_6
10X217_7
10X217_8
10X359_5
10X359_6
10X360_5
10X360_6
10X383_3
10X383_4
10X418_1
10X418_2
v3
v3.1
Pons (Pn) - XPnTg - DTg
Pons (Pn) - PnRF - PB
H18.30.002
H19.30.001
H19.30.002

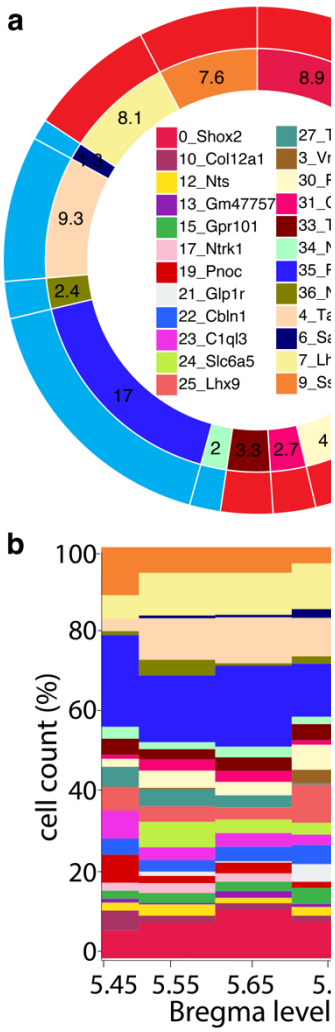
a
b
cell count (%)
Bregma level

SFigure 11

SFigure 12

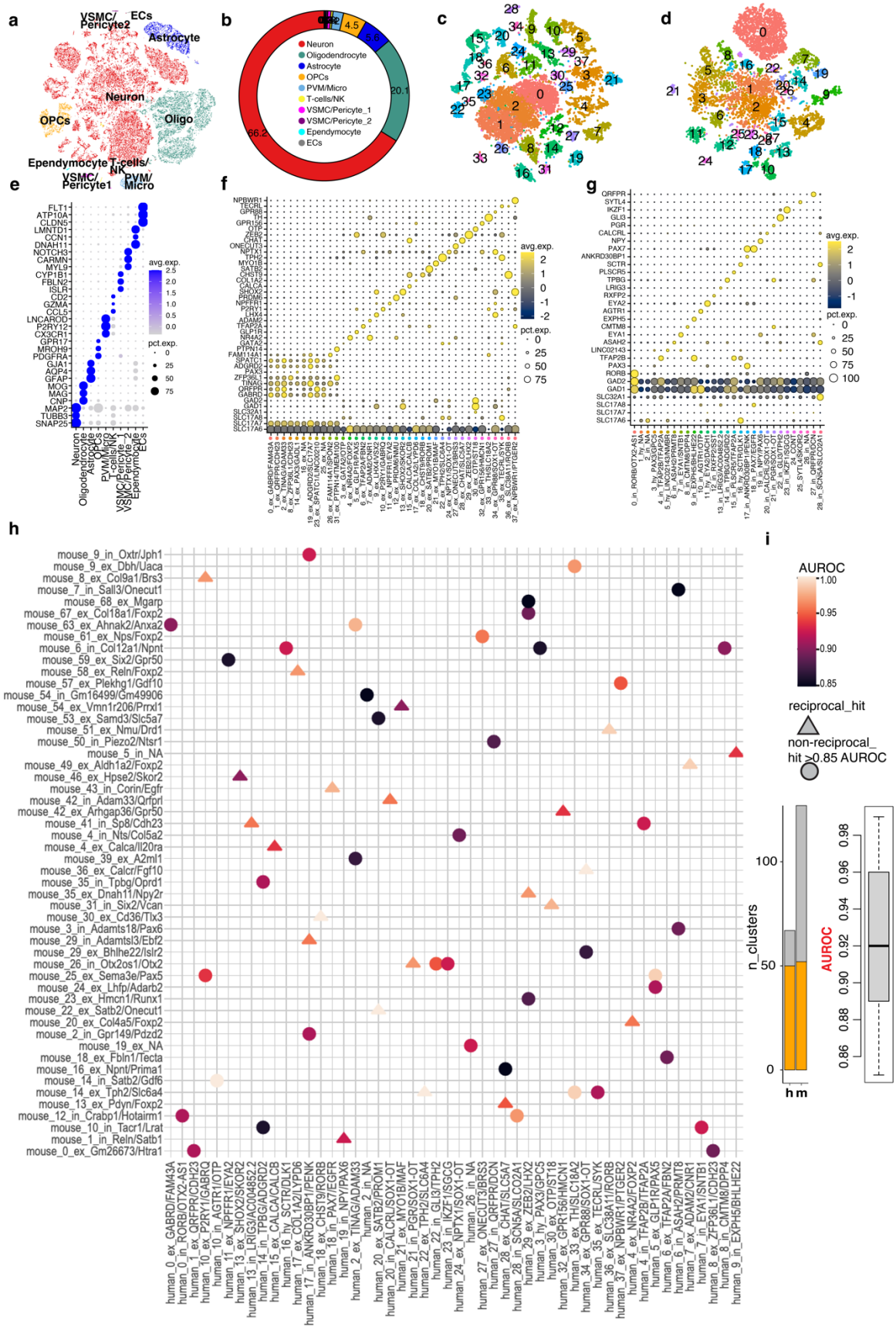

22 **SFigure 13**

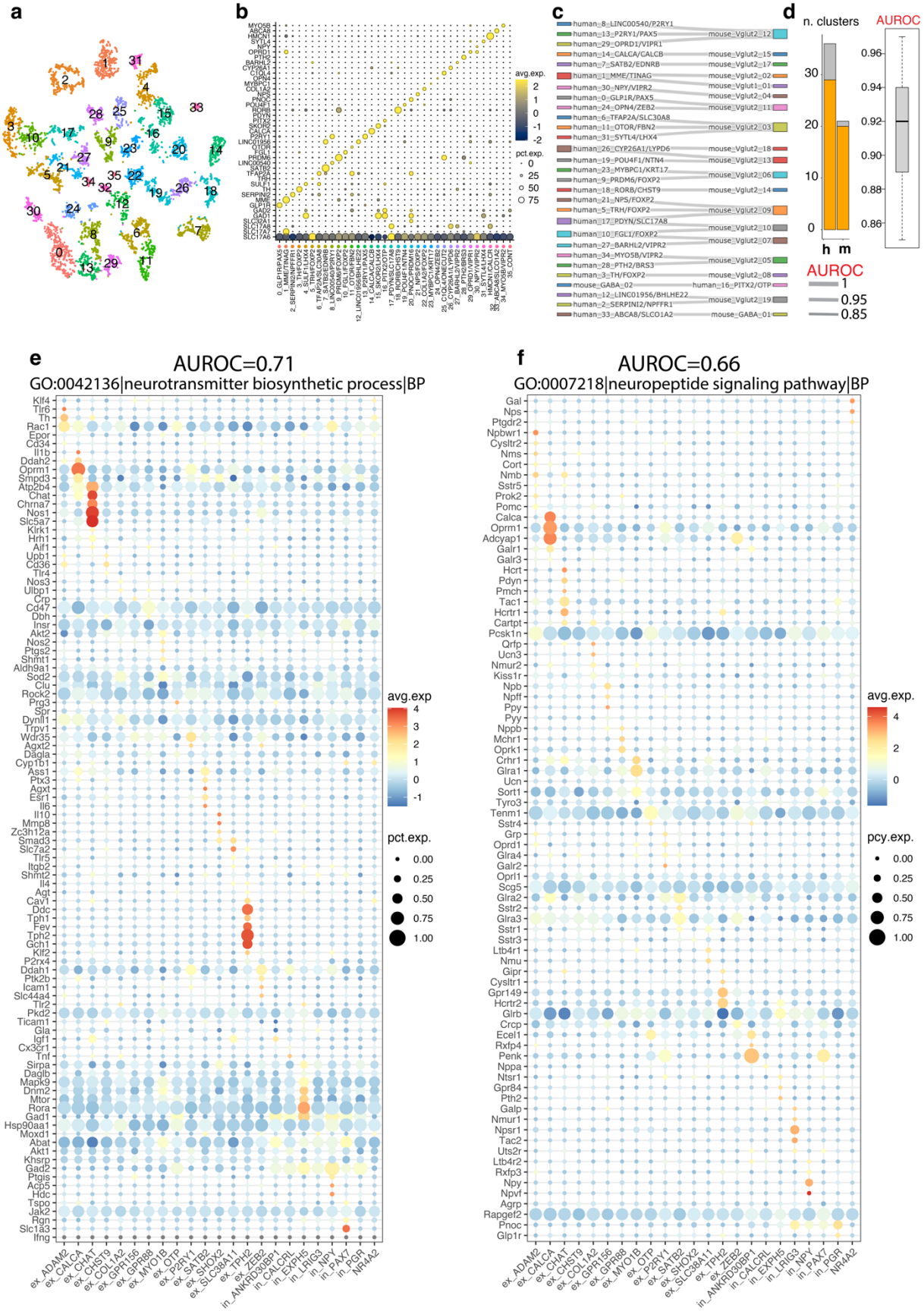

23 **SFigure 14**

SFig1. Data distribution and QC plots of snRNA-seq dataset a-b) Scatter plots showing the distribution, plotted in crescent order, of nUMI (**a**) and nGene (**b**) for all nuclei in the snRNA-seq dataset before filtering was applied. The two red lines indicate the thresholds set to filter out potential empty/ low-quality droplets (nGene <400) or doublets (nGene >10000). **c**) Bar plot of nUMI per nucleus. **d**) Bar plot of nGene per nucleus. **e**) Scatter plot of nUMI versus nGene. **f**) Bar plot of nUMI per gene. **g**) Box plot displaying the distribution of nGene (left) and nUMI (right) in "all nuclei", "neurons", "and glia/ non-neuronal" cells. **h**) Box plot displaying the distribution of nGene (left) and nUMI (right) in all nuclei of the "merged", "PB", "Bar", and "Pons" datasets. **i**) Box plot displaying the distribution of nGene (left) and nUMI (right) in "all nuclei", "excitatory", and "inhibitory" neurons. Highlighted in black is the median of the distribution. Black circles indicate outliers. Bar, Barrington's nucleus; PB, Parabrachial Nucleus; "exc", excitatory neurons; "inh" inhibitory neurons; "All" all nuclei; nUMIs, number of unique molecular identifiers; nGene, number of unique gene counts.

SFig2. Seurat clustering of the dPnTg nuclei profiled by snRNA-seq. a) t-SNE plot of 222,592 nuclei color-coded by annotated cell cluster. The legend on the right assigns each cluster a color and a cell type. **b**) Dot plot of 35 marker genes used to distinguish all main cell types belonging to "glia/non-neuronal cells" and "neurons" groups. 3 markers were plotted for all cell types except for CPE cells, where only two markers were used. **c-i**) Bar plot representing the contribution, expressed as % of nuclei (x-axis), of each experimental batch (c), dissection strategy (d), gender (e), feeding regime (f), CO2 treatment (g), mouse strain (h), and snRNA-seq technology (i) to each neuronal cluster (y-axis). All differentially expressed genes in the dot plot have an average log fold-change >0.25 and an adjusted p-value <0.01. Test used: *Wilcoxon Rank Sum two-sided Bonferroni-corrected Test*. Bar, Barrington's nucleus; PB, parabrachial nucleus; M, male; F, female; OPC, oligodendrocyte precursor cells; PVM, perivascular macrophages; VSMC, vascular smooth muscle cells; VLMCs, vascular and leptomeningeal cells; CPE, choroid plexus epithelial cells; t-SNE, t-distributed stochastic neighbor embedding; Diff.OPC, immature oligodendrocytes; NA, no marker detected; CONT, glia contamination.

SFig3. Transcript count per FOV and correlation between the average gene expression of 315 genes in MERFISH versus mouse brain bulk RNA-seq datasets. a) Bar plot showing the total Transcript Count per FOV (y-axis) across each MERSCOPE slide (x-axis) of the 315 MERFISH-assessed genes. **b**) Scatter plots representing the Pearson's *r* correlation coefficient of the average gene expression of 315 MERFISH-assessed genes between the whole mouse brain bulk RNA-seq and each MERSCOPE slide. For whole brain bulk RNA-seq, the average expression is reported as log10 FPKM, whereas for MERFISH, as log10 raw counts. All bar and scatter plots in panels a and b, respectively, except those representing BM3, Am3, and Z-series, refer to 2 coronal sections placed on the same slide and processed together. FOV, field of view; FPKM, Fragments per kilobase of transcript per million mapped fragments

SFig4. Correlation plots of the average expression of 315 genes between MERFISH sections. a) Correlation plot of the average expression of 315 genes among 46 MERFISH sections. **b**) Correlation plots of the average expression of 315 genes among 42 MERFISH sections grouped in 4 series of 10 sequential sections (except E-series, which includes 12 sections). Each series represents an experimental batch (i.e., a mouse). For all plots, a color-coded legend indicates Pearson's *r* correlation coefficient between two sections. The white diagonal represents the correlation between identic sections corresponding to 1.

SFig5. Specificity, sensitivity, and reproducibility of MERFISH assay. a) Box plot of the average expression level of 315 MERFISH-assessed genes (specific signal) versus 60

scrambled probes (non-specific signal). **b**) Box plot displaying the average expression level of 315 genes assessed by snRNA-seq versus MERFISH technology**. c**) Scatter plots representing the Pearson's *r* correlation coefficient calculated on the average expression of 315 genes between the section ZM0_r0 and the other nine sequential sections of the Z-series. **d**-**e**) Scatter plots representing the Pearson's *r* correlation coefficient calculated on the average expression of 315 genes between two sequential sections of the C-series (d) and two sections from two different series representing the same bregma level (e). **f-g**) Scatter plots representing Spearman's rho correlation coefficient of the average expression of 315 genes in MERFISH versus bulk RNA-seq from the whole mouse brain (f) and snRNA-seq from this study (g).

SFig6. Data distribution and QC plots of MERFISH dataset a-**b**) Scatter plots showing the distribution, plotted in crescent order, of nCount (a) and nGene (b) for all cells in the MERFISH dataset before filtering was applied. The red line corresponds to the threshold to eliminate potential low-quality cells or segmentation artifacts (nCount >15). **c**) Bar plot of nCount per cell. **d**) Bar plot of nGene per cell. **e**) Scatter plot of nCount versus nGene per cell. **f**) Bar plot of nCount per gene. **g**) Box plot of the distribution of nGene (left) and nCount (right) in "all cells", "neurons", and "glia/non-neuronal cells". **h**) Box plots of the distribution of nGene (left) and nCount (right) in "all cells", "excitatory", and "inhibitory" neurons. Highlighted in black is the median of the distribution. Black circles indicate outliers. "exc", excitatory; "inh", inhibitory; "All" all cells; nCount, number of raw counts; nGene, number of unique gene counts.

SFig7. Seurat clustering of all dPnTg cells profiled by MERFISH. a) t-SNE plot of 685,289 cells color-coded by annotated cell cluster. **b**) Dot plot of 16 cell markers used to differentiate all main cell types belonging to "neurons" and "glia/non-neuronal cells" classes. For all cell types, two markers were plotted except for VLMC type I and type II, where only one marker was plotted. **c-e**) Bar plot representing the contribution, expressed as % of cells (x-axis), of each experimental batch (c), series (d), and gender (e) to each neuronal cluster (y-axis). All batches, except the section Am3 and those from the Z series, refer to two coronal sections on a slide processed together. A series represents a mouse. All differentially expressed genes in the dot plot have an average log fold-change >0.25 and an adjusted p-value <0.01. Test used: *Wilcoxon Rank Sum two-sided Bonferroni-corrected Test*. t-SNE, t-distributed Stochastic Neighbor Embedding; OPC, oligodendrocyte progenitor cell; PVM/Micro, perivascular macrophages/ microglia; VSMC, vascular smooth muscle cells; VLMC, vascular and leptomeningeal cell; misc, miscellaneous; M, male; F, female; NA, no marker detected; CONT, glia contamination.

SFig8. Seurat clustering of PB/KF neurons from Pauli et al. dataset and correspondence with MERFISH atlas 2 (PB atlas). a) UMAP plot of 8,439 putative PB/KF neurons whose transcriptome was profiled by scRNA-seq. **b**) Donut plot depicting the fraction (%) of each neuronal cluster /total neurons. Color-coded legend is in the middle of the plot. **c**) Dot plot of the expression level of each neuronal cluster's top 2 marker genes. **d**) Sankey plot depicting the cluster correspondence between MERFISH atlas 2 (PB) and scRNA-seq dataset from Pauli et al. The thickness of the line reflects the AUROC score. **e**) Top: stacked bar plot showing the number of clusters with a match (orange) over the total clusters (grey) identified by MERFISH and scRNA-seq approaches. Bottom: boxplot showing the AUROC scores distribution. Highlighted in black is the median. Black circles indicate outliers. **f**) Violin plots showing the expression level of 7 genes in cluster 15 (PB) versus 16 (KF) of the Pauli et al. dataset. **g**) MERFISH images showing the expression level of 5 genes at -4.8 (KF-field) and -5.2 (PB-field) bregma levels. All differentially expressed genes in the dot plot have an average log fold-change >0.25 and an adjusted p-value <0.01. Test used: *Wilcoxon Rank Sum two-sided Bonferroni-corrected Test*. UMAP, Uniform Manifold Approximation and Projection; AUROC,

area under the receiver operator characteristic curve; NA, no marker detected; CONT, glia contamination.

SFig9. In-depth characterization of the MPB. a) MERFISH images showing the distribution of *Calca* and *Slc32a1* across the entire PB complex. *Calca* is in magenta, and *Slc32a1* is in blue. **b**) Bar plot of the frequency distribution of clusters at2_11 (red) and at2_16 (cyan) indicated as absolute cell count (y-axis) across bregma levels from -4.8 to -5.75 (x-axis). **c-d**) Representative images of two sampled areas from panel (a) highlighted in yellow (c) and red(d) where clusters at2_16 (yellow arrows) and at2_11 (white arrows) are prevalent on their counterpart, respectively. Quantification and images of all levels are reported in STable 14. **e**) MERFISH image showing only clusters residing in the MPB and cluster at2_2 in the LPBE as reference. Legend is in the top right corner. **f**) Dot plot depicting the average expression level of the top marker for the MPB clusters and the cluster at2_2 as control. All differentially expressed genes in the dot plot have an average log fold-change >0.25 and an adjusted p-value <0.01. Test used: *Wilcoxon Rank Sum two-sided Bonferroni-corrected Test*. Source Data are provided as Source Data files.

SFig10. MERFISH-detected clusters, at2_5 (*Foxp2+/Pdyn+*) and at2_26 (*Foxp2+/Gpr101+*), confirmed by *in situ* RNA-scope. a) Bar plots depicting the cell counts (y-axis) of 7 gene combinations (as per legend) relative to panels (b) and (c) across 3 sequential levels (x-axis). Quantification and images of all levels, including -those not reported in panels (b) and (c), are in STable 16-17. **b-c**) RNA-scope (b) and MERFISH (c) assays probing *Foxp2*, *Pdyn,* and *Gpr101* transcripts at bregma levels -4.9, -5.1, and -5.3 are shown as single channels and overlay images. They are quantified in panel a. Scale bars: 20 µm (bottom right). **d**) Dot plot of *Esr1* and *Crh* gene expression in MERFISH atlas 3. All differentially expressed genes in the dot plot have an average log fold-change >0.25 and an adjusted p-value <0.01. Test used: *Wilcoxon Rank Sum two-sided Bonferroni-corrected Test*. Source Data are provided as Source Data files.

SFig11. In-depth characterization of the NI, CGA, and CGB. a) Donut plots: inner plot shows the overall contribution (%) of each cluster to the total NI, CGA, and CGB neurons; the outer plot classifies the clusters as glutamatergic (red) and GABAergic (light blue). **b**) Stacked area charts of the NI, CGA, and CGB *cluster trajectories.* Clusters are color-coded according to the legend in panel a. **c**) Right side: MERFISH images show cluster at4_35 NI neurons (cyan polygons) along its marker gene, *Rln3* (magenta spots). Left side: images depicting *Slc32a1*, *Slc17a6*, and *Rln3* transcripts across the same bregma levels. In panel (a), only clusters contributing >0.5 % to the overall neuronal population were plotted. Source Data are provided as Source Data files.

SFig12. Seurat clustering of all dPnTg human nuclei profiled by snRNA-seq from Siletti et al. dataset a) t-SNE plot of 50,250 nuclei color-coded by annotated cell cluster. **b**) Dot plot of 30 marker genes used to differentiate “neurons” and “glia/non-neuronal cells”. For each cell type, 3 markers were plotted. **c-g**) Stacked bar plots representing the contribution, expressed as % of nuclei (x-axis), of the experimental batch (c) age (d), library construction chemistry (e), dissection strategy (f), and donor (g) covariates to each neuronal cluster (y-axis). All differentially expressed genes in the dot plot have an average log fold-change >0.25 and an adjusted p-value <0.01. Test used: *Wilcoxon Rank Sum two-sided Bonferroni-corrected Test*. t-SNE, t-distributed Stochastic Neighbor. Embedding; OPC, oligodendrocyte progenitor cell; PVM/Micro, perivascular macrophages/ microglia; VSMC, vascular smooth muscle cells; NK, natural killer cell; ECs, endothelial cells NA, no marker detected; CONT, glia contamination.

Fig13. snRNA-seq transcriptional profile of the human dPnTg and cluster correspondence between human snRNA-seq and mouse snRNA-seq datasets. a) t-SNE plot of 50,250 nuclei. **b**) Donut plot depicting each cell type's fraction (%) identified. Color-coded legend for panels a and b is in panel b. **c-d**) t-SNE plots of 17,995 neuronal nuclei from the "excitatory" group (c) and 11,871 neuronal nuclei from the "inhibitory" group (d) color-coded by cell cluster according to legends in panels f and g, respectively. **e**) Dot plot of 30 cell markers (y-axis) that univocally identify each cell type (x-axis). For each cell type, 3 markers were plotted. **f-g**) Dot plots displaying the expression level of the top marker gene for the "excitatory" (f) and "inhibitory" (g) neuronal clusters. The top 2 marker genes specify the identity of each cluster. **h**) Heatmap depicting the cluster correspondence between human snRNA-seq and mouse snRNA-seq datasets in the dPnTg. Legend defining the AUROC score and the "match type" (reciprocal vs non-reciprocal) is on the right side of panel h. **i**) Left: stacked bar plot showing the number of clusters with a match (orange) over the total clusters (grey) identified by snRNA-seq in humans and mice. Right: boxplot showing the AUROC scores distribution. Highlighted in black is the median. Black circles indicate outliers. All differentially expressed genes in the dot plot have an average log fold-change >0.25 and an adjusted p-value <0.01. Test used: *Wilcoxon Rank Sum two-sided Bonferroni-corrected Test*. Source Data is provided as a Source Data file. t-SNE, t-distributed Stochastic Neighbor Embedding; OPC, oligodendrocyte progenitor cell; PVM/Micro, perivascular macrophages /microglia; VSMC, vascular smooth muscle cell; NK, natural killer cell; ECs, endothelial cells; AUROC, area under the receiver operator characteristic curve, h, *homo sapiens*; m, *mus musculus* NA, no marker detected; CONT, glia contamination.

SFig14. A subset of GO gene sets moderately contributes to cell-type replicability. a) t-SNE plot of 6,638 neuronal nuclei derived exclusively from human PB dissections. **b)** Dot plots displaying each cluster's top marker gene expression level. **c**) Sankey plot depicting the cluster correspondence between the mouse PB atlas from Pauli et al. and the human PB atlas from Siletti et al. The thickness of the line reflects the AUROC score. **d**) Left: stacked bar plot showing the number of clusters with a match (orange) over the total clusters (grey) identified in human and mouse PB atlases. Right: boxplot showing the AUROC scores distribution. Highlighted in black is the median. Black circles indicate outliers. **e-f**) Dot plot depicting two examples of GO hits related to "neurotransmitters" and "neuropeptides" classes. The size of the dots indicates the number of cells expressing a gene in a cell type. The color reflects the average expression in z-score. The gene expression is first averaged and scaled in each of the two datasets (human and mouse), and then a final value is obtained by averaging across datasets. In both panels, matches are defined by a joint label that uses one of the two top marker genes from human clusters NA, no marker detected; CONT, glia contamination.

SUPPLEMENTARY TABLES

STable_1. DE analysis related to "all nuclei" from the snRNA-seq mouse dataset of the dPnTg.

STable_2. DE analysis related to "excitatory" neurons from the snRNA-seq mouse dataset of the dPnTg.

STable_3. DE analysis related to "inhibitory" neurons from the snRNA-seq mouse dataset of the dPnTg.

STable_4. MERFISH gene panel. Data table listing the 315 target genes assessed in MERFISH assay. Reported in the table is the following information: gene name, the type of cell targeted (neuron or glia/ non-neuronal cells), the FPKM from mouse brain bulk RNA-seq (see methods), transcript ID, target regions, isoform length, sufficient target regions, gene targetability.

STable_5. DE analysis related to “all cells” from the MERFISH mouse dataset of the dPnTg.
STable_6. DE analysis related to “excitatory” neurons from the MERFISH mouse dataset of the dPnTg.
STable_7. DE analysis related to “inhibitory” neurons from the MERFISH mouse dataset of the dPnTg.
Stable_8. Spatial localization of “excitatory” neurons from the MERFISH mouse dataset of the dPnTg. Data table reporting the spatial location of the “excitatory” MERFISH clusters according to the Franklin-Paxinos brain atlas. The table shows the following information: percentage of cells per cluster/total cells, number of cells of each cluster, cluster ID, top 5 markers of each cluster, anatomical location of each cluster, and their inclusion in the downstream analyses.
STable_9. Spatial localization of “inhibitory” neurons from the MERFISH mouse dataset of the dPnTg. Data table reporting the spatial location of the “inhibitory” MERFISH clusters according to the Franklin-Paxinos brain atlas. The table shows the following information: percentage of cells per cluster/total cells, number of cells of each cluster, cluster ID, top 5 markers of each cluster, anatomical location of each cluster, and their inclusion in the downstream analyses.
Stable_10. DE analysis related to neurons from the MERFISH atlas 1.
STable_11. DE analysis performed between clusters at1_10, at1_11, and at1_6 (as a negative control, *Calca*-) from the MERFISH atlas 1 and cluster at2_2 from the MERFISH atlas 2.
STable_12. DE analysis expression related to PB neurons of the Pauli et al. dataset.
STable_13. MetaNeighbor output from the comparison of all clusters from MERFISH atlas 2_ plus clusters at1_10 and at1_11 from atlas_1 versus scRNA-seq atlas from Pauli et al. of the mouse PB.
STable_14. DE analysis performed between clusters 15 and 16 of the PB's Pauli et al. scRNA-seq atlas.
STable_15. DE analysis related to neurons from the MERFISH atlas 2.
STable_16. Cell frequency of MERFISH atlas 2 clusters at2_11 (*Skor2*/*Gm47757*) and at2_16 (*Slc6a5*/*Pax2*) estimated across 11 coronal sections, from -4.8 to -5.75 bregma level. In the Excel sheet, there are the cell count and the MERFISH images relative to two gene expression combinations (i.e., *Skor2/Gm47757*, *Slc6a5/Pax2*) across 11 coronal sections from -4.8 to -5.75 bregma levels.
STable_17. Data table displaying the anatomical location of each cluster in MERFISH atlas 2 across 10 coronal sections, from -4.95 to -5.7 bregma level. The anatomical locations of the MERFISH atlas 2 clusters have been established according to the Franklin-Paxinos brain atlas. Abbreviations are in Fig 1A.
STable_18. Triple RNA scope for *Foxp2*/*Gpr101*/*Pdyn* in the PB complex. In the main Excel sheet, there is the cell count relative to the 7 possible gene expression combinations (i.e., *Foxp2*, *Gpr101*, *Pdyn*, *Foxp2*/*Gpr101*, *Foxp2*/*Pdyn*, *Gpr101*/*Pdyn*, *Foxp2*/*Gpr101*/*Pdyn*) across 5 bregma levels (-4.9, -5.1, -5.3, -5.5, -5.7) for a total two mouse brains. In the Excel sheets named “STable 18 A-E” are the cell counts and the images relative to each of the 5 bregma levels for two mouse brains.
STable_19. MERFISH detection of *Foxp2*/*Gpr101*/*Pdyn* in the PB complex. In the main Excel sheet, there is the cell count relative to the 7 possible gene expression combinations (i.e., *Foxp2*, *Gpr101*, *Pdyn*, *Foxp2*/*Gpr101*, *Foxp2*/*Pdyn*, *Gpr101*/*Pdyn*, *Foxp2*/*Gpr101*/*Pdyn*) across 5 bregma levels (-4.9, -5.1, -5.3, -5.5, -5.7) for a total two mouse brains. In the Excel sheets named “STable 19 A-E” are the cell counts and the images relative to each of the 5 bregma levels for two mouse brains.

STable_20. DE related to re-clustering analysis of the MERFISH atlas 2 cluster at2_2 (Calca/Il20ra).
STable_21. DE analysis related to the MERFISH atlas 3.
STable_22. DE analysis performed between clusters at3_8 and at3_24 of the MERFISH atlas 3.
STable_23. DE analysis performed between clusters at3_30 of the MERFISH atlas 3 and at2_5 of the MERFISH atlas 2.
STable_24. DE related to re-clustering analysis of the MERFISH atlas 3 cluster at3_0 (Th/Slc18a2).
STable_25. DE analysis related to the MERFISH atlas 4.
STable_26. MetaNeighbor output from the comparison of MERFISH atlases 1-4 versus snRNA-seq dataset of the mouse dPnTg.
STable_27. DE analysis related to “all nuclei” from the snRNA-seq human dataset of the dPnTg from Siletti et al.
STable_28. DE analysis related to “excitatory” neurons from the snRNA-seq human dataset of the dPnTg from Siletti et al.
STable_29. DE analysis related to “inhibitory” neurons from the snRNA-seq human dataset of the dPnTg from Siletti et al.
STable_30. MetaNeighbor output from the comparison of the human dPnTg (snRNA-seq from Siletti et al.) versus the mouse PnTg (snRNA-seq).
STable_31. MetaNeighbor GO analysis performed only on “reciprocal” matches from the output of STable 30.
STable_32. DE analysis related to neurons from only anatomical dissection of the human PB from Siletti et al.
STable_33. MetaNeighbor output from the comparison of the human PB dataset (snRNA-seq from Siletti et al.) versus the mouse PB dataset (scRNA-seq from Pauli et al.)
STable_34. Cartesian coordinates (x, y) define an ROI's boundaries that contain the entire dPnTg.
STable_35. Data table including the average expression reported as FPKM for all gene isoforms detected in a whole mouse brain bulk RNA-seq dataset.
STable_36. Data table containing the KEY ID used to correspond to the gene isoform used to design the MERFISH probe-set to the one in the whole mouse brain bulk RNA-seq dataset.